Functional Validation of Candidate Osteosarcoma Genes Identified via *Sleeping Beauty* Mutagenesis

A DISSERTATION
SUBMITTED TO THE FACULTY OF THE GRADUATE SCHOOL OF THE
UNIVERSITY OF MINNESOTA
BY

Branden Andrew Smeester

IN PARTIAL FULFILLMENT OF THE REQUIREMENTS FOR THE DEGREE OF
DOCTOR OF PHILOSOPHY

Advisor: Branden S. Moriarity

Co-advisor: David A. Largaespada

May 2020

ACKNOWLEDGEMENTS

It's hard to put into words the immense gratitude I owe to all those who I have encountered along the way during my scientific career thus far. Looking back, each step of my journey was truly filled with a mix of serendipity, good timing, helpful guidance, and persistence through all its ups and downs. I owe a great many thanks to a number of individuals who helped me along the way to completing a PhD: To my graduate advisors Dr. Branden Moriarity and Dr. David Largaespada for their guidance in helping me become an independent scientist. To my first scientific mentors Dr. Alvin Beitz (and committee chair) and Dr. Phil Portoghese who offered me opportunities to become involved in scientific research through joining their labs. To my informal graduate advisor Dr. James McCarthy for his willingness to listen and consistent drip of wisdom. To my other thesis committee members Dr. Logan Spector and Dr. Kim Mansky who were individuals I could always count on for advice and good conversation. To dear old colleagues and friends Elaine O'Brien, Josh Parker, Don Ariyakumar, and Mary Lunzer for giving me a strong technical foundation prior to even attempting graduate work. To Dr. Kyle Williams and Dr. Bryant Keller for the five-year long coffee break, advice, and lasting friendship. Lastly, to the many undergraduates, technicians, and other graduate students who I have worked with over the years in the Moriarity and Largaespada labs. You are the backbone of all that I have been able to accomplish and I am eternally grateful for your assistance over the years.

DEDICATION

This thesis is dedicated to my wife Kate. We did it.

TABLE OF CONTENTS

LIST OF TABLES

LIST OF FIGURES

THESIS STATEMENT

PURPOSE

The work presented throughout this thesis sought to functionally, mechanistically, and therapeutically investigate a number of top candidate gene targets and associated signalling pathways in osteosarcoma (OSA) that were originally identified using the *Sleeping Beauty* (*SB*) transposon system. Chapter 1 begins with a current overview of OSA biology, metastasis, therapeutic treatments, and mechanisms of pain. Chapter 2 focuses on how new candidate OSA genes were identified using the *SB* system. Subsequent chapters (3-5) are dedicated to the functional and mechanistic characterization of three top candidate genes (*SEMA4C*, *CSF1R*, and *ZNF217*) with the explicit goal of characterizing their biology in the context of OSA and ultimately exploiting their therapeutic potential.

MAJOR FINDINGS

In brief, 1) SEMA4C was found to be implicated in promoting OSA growth and metastasis. Cellular transformation associated with these cancer phenotypes could be reversed via administration of a monoclonal antibody against SEMA4C *in vitro*; 2) Active CSF1R was found to be involved in OSA growth and metastatic burden in part through enhanced ERK signalling which could be disrupted through small molecule CSF1R kinase blockade; 3) ZNF217 was found to accelerate OSA progression, growth, and metastasis through regulation of PI3K-AKT signalling, which could be therapeutically blocked via an AKT inhibitor.

CHAPTER 1

Osteosarcomagenesis – Biology, Development, Metastasis and Mechanisms of Pain

Branden A. Smeester[1,2,3], Branden S. Moriarity[1,2,3] and Alvin J. Beitz[4*]

[1]Department of Pediatrics, University of Minnesota, Minneapolis, Minnesota, USA
[2]Center for Genome Engineering, University of Minnesota, Minneapolis, Minnesota, USA
[3]Masonic Cancer Center, University of Minnesota, Minneapolis, Minnesota, USA
[4]Department of Veterinary and Biomedical Sciences, University of Minnesota, Minneapolis, MN, USA

A published version of this chapter is available below:

Smeester BA, Moriarity BS, Beitz AJ. Osteosarcomagenesis – Biology, Development, Metastasis and Mechanisms of Pain. InTech “Osteosarcoma - Biology, Behavior and Mechanisms", ISBN: 978-953-51-4915-6. 2017.

Conception and design: BAS, BSM, AJB
Writing, review and revisions: BAS, BSM, AJB
Study oversight: BAS, BSM, AJB

Summary

Osteosarcoma is the most common primary cancer of the bone and third most common cancer in children and adolescents with approximately 900 new cases annually (400 pediatric cases) in the United States. A major facet of osteosarcoma is its high level of genomic instability, in particular chromosomal instability, which is the result of increased or decreased chromosome number in a cell. Furthermore, pain is the most common symptomatic feature of osteosarcoma that lacks effective therapy. Pain in osteosarcoma is relatively more complicated than many other painful conditions requiring a more thorough understanding of its etiology, pathobiology, and neurobiology to allow the development of better therapies for reducing pain in osteosarcoma patients. Studies are underway to define the diverse modalities of presentation, growth, development, metastases and nociception in osteosarcoma. New data from human studies in combination with data from studies incorporating transgenic mouse models of osteosarcoma are providing valuable insights into the mechanisms underlying the development of both the tumor and the tumor-induced pain. This will undoubtedly lead to improved prognoses as well as significantly decreased pain in the future.

Introduction

Osteosarcoma is the most common malignant bone tumor found in children and adolescents and is associated with many complications including metastases and intractable cancer pain (Smeester, Al-Gizawiy, & Beitz, 2012; Smeester, Lunzer, Akgun, Beitz, & Portoghese, 2014). Typically, the prevalence of osteosarcoma shows a strong relationship with skeletal growth and thus, the main incidence peak occurs in the second decade of life and generally is associated with a highly defined phenotype. Osteosarcoma also occurs in elderly adults in the sixth and seventh decades of life and is often preceded by certain genetic predispositions (Franchi, 2012). Osteosarcomas predominately form in the metaphyses of the long bones in the major growth centers such as the distal femur, proximal tibia and proximal humerus. Osteosarcomas are quite aggressive locally, but often produce early, lethal systemic metastases (Raymond & Jaffe, 2009). Chest CTs have been estimated to miss nearly 25% of metastatic nodules found during thoracotomy and up to 14% of metastases are not nodular in shape, which complicates the metastatic picture in many patients (Ciccarese et al., 2015). With no known precursor to osteosarcoma, treatment options are extremely limited. Adjuvant chemotherapy and surgical resection are standard therapies, but treatment efficacy still remains poor for over one-third of osteosarcoma patients (Gelderblom et al., 2011; Tsubaki et al., 2012). Although our understanding of the mechanisms underlying tumor development, tumor progression and metastasis is improving (Al-Salihi et al., 2007; Copeland &

Jenkins, 2010; Kim, Lewis, & Nadel, 2011; Sueyoshi et al., 2012; Tarkkanen et al., 1995), the complex nature of the bone tumor microenvironment presents unique challenges in identifying novel drug targets and treatment strategies.

The most common presenting symptom of osteosarcoma is pain, particularly with activity. Osteosarcoma pain can start in adolescence, leading to hospitalization, reduced survival and poor quality of life. Pain in osteosarcoma is unique because of unpredictable and recurrent episodes of acute pain due to vaso-occlusive crises (VOC), in addition to chronic pain experienced by a majority of adult patients on a daily basis (Ballas, Gupta, & Adams-Graves, 2012). As detection and survival among cancer patients have improved, pain has become an increasing challenge, because traditional therapies are often only partially effective (Falk & Dickenson, 2014). In this regard, treatment of osteosarcoma pain is complicated because long-term treatment choices remain limited and generally involve opioids, which impose liabilities of their own including constipation, mast cell activation, addiction and respiratory depression (Kohli et al., 2010). Moreover, significantly larger doses of opioids are required to treat pain in osteosarcoma as compared to other acute and chronic pain conditions. Pain can be life-long in osteosarcoma and may therefore influence cognitive function and lead to depression and anxiety, which can in turn promote the perception of pain (Ballas et al., 2012). In general, treatment of chronic pain remains unsatisfactory, perhaps due to the diverse pathobiology in different diseases. Therefore, it is critical to understand the mechanisms specific to the genesis of osteosarcoma-related pain to develop targeted therapies.

Normal bone development

Bone is a readily adaptive, mineralized tissue that performs diverse functions including enabling locomotion, storing nutrients such as phosphate and calcium and protecting soft tissues among many others. Despite its static appearance, osteoclasts and osteoblasts, two major cell types abundant throughout bone tissue are constantly remodelling bone. Osteoblasts are the resident bone-producing cells of the body. Osteoblasts are derived from a lineage of cells arising from a mesenchymal origin (Long, 2012), while osteoclasts arise from a hematopoietic lineage (Yavropoulou & Yovos, 2008). The remodelling of bone is a tightly coupled process. From a physiological perspective, distinct differentiation and maturation pathways of these two cell types allows for uninterrupted maintenance of bone homeostasis (Sims & Martin, 2014). The differentiation process of osteoblasts is often divided in specific stages: mesenchymal progenitors, preosteoblasts, and osteoblasts. Similarly, this process also occurs in osteoclastogenesis where cells of myeloid origin differentiate into one of four cell types, one being osteoclasts (Yavropoulou & Yovos, 2008). While differentiation stages are useful for cellular identification, the maturation process is not well understood. Often, the identities of cells during each stage are characterized by expression of various molecular markers highly associated with osteoblast development. Markers of cells from mesenchymal origin are not well defined and are still a matter of intense debate. Similarly, preosteoblast markers are also difficult to identify. These cells are highly

heterogeneous in their expression patterns, as this stage can encompass various cell types during maturation into osteoblasts, bone-lining cells or osteocytes. However, two common transcription factors, Runt-Related Transcription Factor 2 *(RUNX2)* and later *OSTERIX* (also known as *SP7*) are expressed during maturation and are highly associated with maturation of the preosteoblast lineage (Fakhry, Hamade, Badran, Buchet, & Magne, 2013), while Hematopoietic Transcription Factor *(PU.1)*, Microphthalmia-Associated Transcription Factor *(MITF)* and *c-FOS* are associated with osteoclast precursors (Yavropoulou & Yovos, 2008).

Tumorigenesis

There is currently no known origin to osteosarcoma, however, much research has pointed to osteoblasts as the progenitor cell type. The single most shared feature of all osteosarcomas histologically is the presence of osteoid matrix, secreted by malignant cells in the growing tumor. In addition, the presence and quantity of this matrix does not define the disease, as osteosarcomas may be composed of many tissue types including chondroblastic, fibroblastic and osteoblastic (Quist et al., 2015). Osteosarcoma has been shown to be associated with loss of key tumor suppressor genes such as Tumor Protein P53 (*TP53)* and Retinoblastoma 1 *(RB1)* (Walkley et al., 2008) and alterations in *p53* are associated with reduced event-free survival (Tsuchiya et al., 2000). Moreover, sporadic osteosarcomas are highly associated with mutations in the *RB* gene. Additionally, germline mutations in the *p53* gene predisposes patients

with Li-Fraumeni syndrome (LFS) to osteosarcoma (Porter et al., 1992) with an incidence of up to 12% (Siddiqui et al., 2005).

Chromosomal abnormalities

Despite its well-defined phenotypic characteristics, genetically speaking, osteosarcoma is chaotic and disordered. It is often associated with massive chromosomal rearrangements, cytogenetic aberrations and numerous mutations (Moriarity et al., 2015). Numerous cytogenetic and molecular studies of osteosarcoma have been conducted in recent years yielding interesting results, but often with conflicting findings (Ragland, Bell, Lopez, & Siegal, 2002). Many of these studies have limited prognostic and diagnostic value and fail to understand the driving events necessary for osteosarcoma development. However, the overall infrequency of this disease makes elucidating these factors all the more challenging. It has been apparent since early studies that osteosarcomas have a significant propensity towards aneuploidy with over 96% of high-grade cases being hyperploid (Ragland et al., 2002). Furthermore, cytogenetic analyses have provided evidence for enormous variation in karyotypic alterations. A major facet of osteosarcoma is its high level of genomic instability, in particular chromosomal instability (CIN). CIN can contribute to tumor initiation and progression through altering expression of proto-oncogenes or tumor suppressor genes. The rate of gain or loss of entire chromosomes or sections is significant in the pathogenesis of osteosarcoma resulting in numerous aberrations and wide variability between cells and tumors (Martin, Squire, & Zielenska, 2012).

Oncogene/tumor suppressor gene dysfunction

The search for specific drivers of osteosarcoma development have stemmed from the early cytogenetic and molecular findings. Initial genetic studies sought to identify important genes involved in cancers although not necessary specific to osteosarcoma. These early studies have implicated a number of important tumor suppressors, oncogenes and growth factors that are implicated in other sarcomas and carcinomas as well (Ragland et al., 2002). As stated earlier, perhaps the best two characterized examples of this are the tumor suppressor gene *TP53* and the retinoblastoma *RB1* gene. The location of *TP53* on chromosome 17p13 is an area frequently altered in osteosarcomas and is readily apparent in cytogenetic analyses. Alterations in the *TP53* gene have significant effects on the downstream signaling targets, many of which are normally involved in cell cycle control and apoptosis. Gene rearrangements, point mutations, epigenetic modification (Mu, Brynien, & Weiss, 2015; Mu et al., 2014), and/or allelic loss can presumably lead to inactivation of normal *TP53* function and these aberrations have been associated with the development of osteosarcoma. In a recent study that characterized the genomic landscape of osteosarcoma via whole genome sequencing (WGS), the majority of *TP53* inactivation in osteosarcoma was found to be due to translocations (Chen et al., 2014). Furthermore, this study highlights the fact that *TP53* mutation is highly prevalent in osteosarcoma, with >90% of all tumors containing a mutation in at least one allele, and upwards of 80% containing mutations in both alleles. In

addition to the *TP53* gene, associations between osteosarcoma and *RB1* are well recognized as well, especially in patients with hereditary retinoblastoma of which osteosarcoma incidence is 1000 times higher than in the general population. Loss of heterozygosity and/or sporadic alterations in the *RB1* gene is apparent in >60% of osteosarcoma cases and these genetic changes have significant prognostic value (Sadikovic et al., 2008). As only these prototypical cancer genes and a few others have been definitively implicated in osteosarcoma, there is a pressing need to identify more genes and pathways governing its development and metastasis to better treat osteosarcoma patients and their associated pain.

Axonal guidance genes in osteosarcoma

Recently, a new pathway has been identified using the Sleeping Beauty mutagenesis system in mice implicating axon guidance genes such as Semaphorin-4D *(SEMA4D)* in osteosarcoma (Moriarity et al., 2015). During normal bone homeostasis, osteoclasts express high levels of *Sema4d*, whereas osteoblasts do not. Instead, osteoblasts express its cognate receptor and co-receptor, Plexin B1 (*Plxnb1)* and Erb-B2 Receptor Tyrosine Kinase 2 *(Erbb2)*, respectively. Thus, it is possible that misexpression of *SEMA4D* and MET proto-oncogene, receptor tyrosine kinase (*MET)* in osteoblasts might give rise to a subset of osteosarcomas. Similarly, the tumorigenic properties induced by overexpression of *SEMA4D* in human osteosarcoma cells are dependent on MET and ERBB2 levels, which has been reported (Swiercz, Worzfeld, &

Offermanns, 2008). Previous studies in osteosarcoma showed that high levels of *ERBB2* are associated with a good outcome and that overexpression of *MET* can directly transform osteoblasts into osteosarcomas (Akatsuka et al., 2002; Patane et al., 2006). The fact that *SEMA4D* is a cell surface receptor makes it an attractive candidate for novel therapies. This will be addressed later in the chapter.

Metastasis

Approximately 20-30% of osteosarcoma patients have overt metastases at diagnosis and about 40% of patients will develop lung metastases during the course of treatment (Kager et al., 2003; Kansara & Thomas, 2007; Meyers et al., 1993). Analysis of clinical outcomes of patients without overt metastasis at diagnosis prior to the advent of chemotherapy demonstrated >90% of patients developed lung metastasis 6-36 months after surgical resection, indicating the majority of seemingly non-metastatic patients actually have micro-metastatic disease at diagnosis (Chen et al., 2014). While it is largely believed that the implementation of chemotherapy eradicates these developing micro-metastases in many cases, these data highlight the fact that metastasis is the most important factor associated with poor outcome in osteosarcoma (Allison et al., 2012). Recent work from Moriarity and colleagues identified many genes that promote osteosarcoma development and metastasis through a forward genetic screen in mice using the *SB* transposon-based mutagenesis system. Both classes of genes (oncogenes and tumor suppressors) may be critical for development of

detectable metastases present at diagnosis and/or the ability of latent micro-metastases to develop to a detectable level. Subsets of genes identified via the SB screen were only present in the metastatic lesions, while others were found both in primary tumors and metastases. Among those genes identified were Phosphatase And Tensin Homolog *(Pten),* Glycogen Synthase Kinase 3 Beta (*Gsk3b*), Synaptosome Associated Protein 23kDa *(Snap23)*, Mitogen-Activated Protein Kinase Kinase Kinase Kinase 3 *(Map4k3)*, Rho GTPase Activating Protein 35 *(Arhgap35 (Grlf1))*, Rho/Rac Guanine Nucleotide Exchange Factor 18 *(Arhgef18)*, Axin 1 *(Axin1)*, Raf-1 Proto-Oncogene, Serine/Threonine Kinase *(Raf1)* and Ubiquitin Associated Protein 2 Like *(Ubap2l)*. Interestingly, these have been implicated in metastasis of other cancers which supports the conclusion that these genes are central to osteosarcoma metastasis (Moriarity et al., 2015). Additionally, bone metastases are also highly painful. The ability for osteosarcoma to successfully metastasize relies in part on its ability to exploit many mechanisms of normal bone remodeling (Sottnik, Hall, Zhang, & Keller, 2012). Two such examples of this are the Wnt family of proteins and bone morphogenetic proteins (BMPs), both of which are critical in bone development and are implicated in cancer pain (Nguyen, Scott, Dry, & James, 2014; Y. K. Zhang et al., 2013). The evolving physiologic and pathological roles of the Wnt/β-catenin signaling pathway may offer attractive therapeutic targets for novel antagonists and inhibitors for patients with primary and metastatic osteosarcoma. Likewise, BMPs are responsible for numerous osteoinductive cellular processes including bone growth, differentiation and matrix maintenance (Nguyen et al.,

2014). *In vitro* examination in numerous osteosarcoma cell lines revealed highly abundant expression of BMPs in virtually all lines tested (Anderson et al., 1995; Hara et al., 1996; Ogose, Motoyama, Hotta, Watanabe, & Takahashi, 1995). Moreover, BMP expression has been found to correlate with metastasis in osteosarcoma (Arihiro & Inai, 2001), while overexpression of BMP-9 reduces invasion and migration properties of osteosarcoma cells (Lv et al., 2013). Conversely, analysis of 47 human osteosarcoma found no correlations between BMP expression and prognostic outcomes (Sulzbacher, Birner, Trieb, Pichlbauer, & Lang, 2002). Furthermore, BMPs have also been shown to induce bone formation in human osteosarcoma cells (Wang et al., 2013). As mentioned earlier, osteosarcomas can present with mixed cell lineages and differentiation patterns (Quist et al., 2015). These studies and others suggest that perhaps BMPs may be expressed at differing levels depending on the cellular state and their presence may offer an attractive therapeutic option for the treatment of osteosarcoma. While the significance of BMP signaling in osteosarcomagenesis is not yet fully understood, current research suggests BMPs may play an important role.

Characteristics of pain in osteosarcoma

Cancer-induced bone pain is a complex pain state involving a combination of background, spontaneous, and incident (movement-evoked) pain (Falk & Dickenson, 2014; Portenoy & Hagen, 1990). Regional pain alone or in combination with a palpable mass are the two main reasons that osteosarcoma

patients consult a doctor. Patients with osteosarcoma of the jaws typically present with pain, swelling, ulceration or neurological deficit (J. H. Bennett, Thomas, Evans, & Speight, 2000), but again pain is a major symptom causing these patients to seek medical attention. Currently only about half of patients with cancer-induced bone pain experience temporary relief from conventional therapies (Meuser et al., 2001), which stresses the need for the development of more effective treatments. The following table summarizes some of the types of pain experienced by bone cancer patients and animal models of bone cancer pain (Table 1).

Peripheral and central mechanisms of pain in osteosarcoma

While our knowledge of the mechanisms of bone cancer pain is ever expanding, part of our failure to adequately manage osteosarcoma and other forms of bone cancer pain is an inadequate understanding of the etiology and mechanisms involved. Cancer-induced bone pain is a mixed-mechanism pain state exhibiting elements of inflammatory, neuropathic and ischemic pain, but with distinctive effects on the tissues and nerves in the periphery, as well as unique biochemical changes within the spinal cord (Falk & Dickenson, 2014; Zhu et al., 2015).

Peripheral mechanisms

As summarized by Falk and colleagues, the biology of cancer-induced bone pain involves a complex interplay among the tumor cells, peripheral nerves,

and cells of the bone (Falk & Dickenson, 2014). The tumor cells trigger a number of nociceptive and immune responses that ultimately recruit inflammatory cells including macrophages, neutrophils, and T cells to the bone resulting in release of a plethora of endogenous chemicals acting on bone cells, cancer cells and importantly on primary afferent nerve fibers (P. W. Mantyh, Clohisy, Koltzenburg, & Hunt, 2002; Ueno & Oh-ishi, 2002). Thus, tumor and tumor-associated cells in the cancer microenvironment may release various peripheral mediators. These include adenosine triphosphate (ATP), formaldehyde, protons, proteases, endothelin, bradykinin, tumor necrosis factor (TNF) and nerve growth factor (NGF), that result in the activation and/or sensitization of peripheral and central neurons (Lam, 2016; Shor et al., 2015). The complexity of this neuroimmune and inflammatory effect on cancer pain has been recently reviewed (Brown & Ramirez, 2015). Ultimately this cascade of events leads to the activation and sensitization of nociceptors, the degradation of bone, and subsequent increased tumor growth (Falk & Dickenson, 2014). Furthermore, studies have shown that cancer cells in the bone induce a highly disorganized sprouting of sensory and sympathetic fibers, leading to the formation of small neuromas. These disorganized bundles of nerve fibers are thought to contribute to episodes of breakthrough pain or even movement-induced pain (Jimenez-Andrade, Ghilardi, Castaneda-Corral, Kuskowski, & Mantyh, 2011; W. G. Mantyh et al., 2010). In addition to changes in nerve fibers, bone tumors in mice have also been shown to be associated with changes in both blood vessels and lymphatics, which may

facilitate metastasis and which interestingly, can be altered by acupuncture treatment (Smeester et al., 2013).

Central mechanisms

Both the spinal cord dorsal horn and dorsal root ganglia undergo unique changes induced by bone tumors suggesting that the peripheral alterations drive central alterations. Some of the bone tumor-induced changes observed in spinal glial and neurons are distinct, but many are reflective of changes seen with other chronic pain states. Thus, tumors are associated with increased expression of dynorphin with accompanying spinal astrocyte hypertrophy and upregulation of galanin and AF3 (Falk & Dickenson, 2014; Smeester et al., 2013). Clearly, the recent identification of a vast number of mediators and receptors that contribute to bone cancer-related pain, as well as more detailed knowledge of the peripheral and central mechanisms underlying the development of bone tumor nociception will provide novel therapeutic targets for treating patients with osteosarcoma pain. Subsets of these targets are discussed in more detail below.

Treatment of osteosarcoma

From the discussion above, it is clear that due to the complex nature of osteosarcoma pathobiology and the neurobiologic mechanisms that underlie the development of bone cancer pain, it may be necessary to target multiple receptors, mediators and genes to adequately treat osteosarcomas and

osteosarcoma-associated pain. Below we review some of the established and novel targets for the treatment of osteosarcoma and its associated pain.

Immunomodulation

Semaphorins

VX15/2503 (Vaccinex, Inc.) is a highly novel, immunomodulatory monoclonal antibody that specifically targets *SEMA4D* (CD100), a receptor and soluble protein from the semaphorin family known to be involved in immune modulation (Evans et al., 2015) and regulation of normal bone formation (Negishi-Koga et al., 2011). Initial interest in this monoclonal antibody was rooted in results indicating that immune cell-dependent interactions were in fact responsible for its anti-tumor activity (Evans et al., 2015). Early preclinical studies have determined that high concentrations of *SEMA4D* are expressed at the invasive border of many human cancers and that this border restricts the anti-tumor cell infiltrate from effectively combating the growing tumor. Treatment with anti-*SEMA4D* restores the inhibited immune response leading to reduced tumor burden and delayed growth in animal models. Furthermore, anti-*SEMA4D* blockade results in phase I clinical trials of 42 adult patients with advanced solid tumors have been well tolerated with many exhibiting stable disease over various treatment regimens. Antibody therapy targeting *SEMA4D* has also been shown to reduce tumor growth in a xenograft model of soft tissue sarcoma (STS) when combined with antibody therapy for Vascular Endothelial Growth Factor (VEGF) (H. Zhou, Binmadi, Yang, Proia, & Basile, 2012).

Intracellular signaling pathway inhibitors

Hedgehog (Hh)

While encompassing diverse functions such as tissue homeostasis and embryonic development, Hedgehog (Hh) signaling is highly complex and not completely understood (Briscoe & Therond, 2013). Signaling through its receptor Patched-1 (PTCH), Smoothened is activated and promotes subsequent downstream signaling pathway of the Hedgehog (Hh) pathway (Lum & Beachy, 2004). This activation has been implicated in many cancers including osteosarcoma where aberrant activation increases cell proliferation, but can be reduced through inhibition of the signaling (Paget et al., 2012). Hedgehog inhibitors have been successfully tested in clinical trials of other cancers such as chondrosarcoma (Campbell et al., 2014; Tiet et al., 2006), carcinoma (Von Hoff et al., 2009) and medulloblastoma (Rudin et al., 2009) providing solid evidence for consideration as a novel therapeutic in osteosarcoma.

Mammalian target of rapamycin (mTOR)

The Mammalian Target of Rapamycin (mTOR) is a protein kinase that regulates cell survival and proliferation (Zarogoulidis et al., 2014). Due to its diverse functions, mTOR is implicated in many cancers making it an attractive target in treating tumors, including osteosarcoma. In one recent study, activated mTOR was visualized in osteosarcoma and the staining positively correlated to metastasis and necrosis (Q. Zhou et al., 2010). Targeted inhibition of the

signaling pathway of mTOR has been shown to reduce metastatic behaviour in a mouse model of osteosarcoma (Wan, Mendoza, Khanna, & Helman, 2005) as well as human xenograft models (Houghton et al., 2008). Current and future clinical trials using mTOR inhibitors may prove therapeutically fruitful in the treatment of osteosarcoma (Mu, Isaac, Schott, Huard, & Weiss, 2013).

Tyrosine kinase receptors

Human epidermal growth factor receptor 2 (HER2)

HER2 is a member of the human epidermal growth factor receptor family. Located on chromosome 17, activation and overexpression has been implicated in a number of cancers including osteosarcoma. *HER2* is overexpressed in ~40% of osteosarcomas and has been found to occur more frequently in metastatic patients (Ando et al., 2013). Expression was also found to correlate with decreased tumor necrosis and event-free survival (Gorlick et al., 1999). Chimeric antigen receptor (CAR) modified T cells have been shown to kill *HER2*-positive osteosarcoma cells in xenograph and metastatic mouse models (Ahmed et al., 2009).

Vascular endothelial growth factor (VEGF)

VEGF expression has been shown to involved in osteosarcoma (Hassan et al., 2012), correlated with overall survival (Abdeen et al., 2009) and implicated in metastatic development (Ando et al., 2013). A recent paper by Zhou and colleagues found anti-VEGF strategies to be anti-angiogenic in osteosarcoma (H.

Zhou et al., 2012). Interestingly, *SEMA4D* blockade enhanced the anti-cancer activity of anti-VEGF treatment that provide a viable adjunct to *VEGF* therapy alone. While discussed above, development of a highly novel monoclonal antibody to *SEMA4D* is underway and may provide further insight into targeting *VEGF*-resistant tumors as well as associated malignancies.

Treatment of osteosarcoma pain

With a growing population of patients receiving inadequate treatment for intractable bone cancer pain, new targets need to be considered to better address this largely unmet clinical need for improving their quality of life. In general, while there are a variety of methods that are used to treat bone cancer pain, including bisphosphonates, radiation therapy, chemotherapy, hormone therapy and surgery, the clinical treatment of bone cancer pain still focuses on the three-step program. This program was established by the World Health Organization and includes NSAIDs and narcotics as therapeutic treatment options. However, as we learn more about the mechanisms responsible for cancer pain and the genetic basis for the development of osteosarcomas, there are several areas that offer hope for the development of novel treatments for bone cancer pain. It is important to point out that bone cancer pain can be treated by both systemic and local administration of drugs as well as alternative medical approaches. The obvious advantage of peripheral targets is the reduced potential for CNS side effects, such as the sedation and nausea that often accompany opiate analgesics.

Cytokines

Pain is a complex trait and thus, the influence of genetics on pain sensitivity and the efficacy of analgesics is an ongoing challenge. A recent study found that polymorphisms in the Interleukin 1 Beta (IL-1β) family have a significant influence on cytokine serum levels and maximum pain intensity in cancer patients, as well as affecting cancer proliferation (Oliveira et al., 2014). IL-1β has been shown to be expressed in astrocytes and microglia and in nociceptive dorsal root ganglion neurons (Copray et al., 2001) and thus may represent a target for the treatment of cancer pain.

TRPV1 receptors

TRP channels were first identified in Drosophilia (Montell, 2011) and TRPV1 denotes the transient receptor potential channel family number 1 and was the first mammalian TRP channel to be cloned (Caterina et al., 1997). Capsaicin and other TRPV1 agonists selectively stimulate nociceptive neurons and thus while it induces pain, it is possible to treat pain by boosting algesic pathways (Fattori, Hohmann, Rossaneis, Pinho-Ribeiro, & Verri, 2016). In this regard the use of the TRPV1 agonist, resiniferatoxin (RTX) to block cancer pain has recently been reviewed (Iadarola & Gonnella, 2013). In human cancer patients, RTX was given by intrathecal injection into the lumbar cistern and all patients experienced substantial analgesia without significant side effects. In addition, a recent study has shown that cancer cells undergo numerous

metabolic changes that include increased glutamine catabolism and over-expression of the enzyme glutaminase, which mediates glutaminolysis. This produces large pools of intracellular glutamate (Fazzari, Linher-Melville, & Singh, 2016). This is coupled to an up-regulation of the plasma membrane antiporter, system x_c^-. System x_c^- is an amino acid antiporter that typically mediates the exchange of extracellular l-cystine and intracellular l-glutamate across the cellular plasma membrane. The exchange-mediated export of l-glutamate is particularly important within the nervous system, since it represents a non-vesicular route of release through which glutamate can participate in either neuronal signaling or in excitotoxic pathology. With respect to osteosarcomas, the excess glutamate is released directly from the cancer cells and can act on peripheral glutamate receptors located on nerve fibers. It is known that glutamate receptors can modulate peripheral TRPV1 receptors [78]. Thus, the released glutamate converges on peripheral afferent nerve terminals to transmit nociceptive signals through TRPV1. Activation of TRPV1 receptors can ultimately initiate central sensitization in response to tumor-released glutamate (Fazzari et al., 2016). Thus, using RTX to block peripheral TRPV1 channels would block this excess glutamate effect on TRPV1 and reduce both tumor-induced peripheral and central sensitization.

Opioid receptors

Three members of the opioid receptor family were cloned in the early 1990s, including the delta-opioid receptor (DOR1), the mu-opioid receptor

(MOR1) and the kappa-opioid receptor (KOR1) (Przewlocki & Przewlocka, 2001). These three receptors and their corresponding peptide systems are significantly implicated in antinociceptive processes. Opiates have long been the mainstay of treatment for chronic bone cancer pain. However, there is increasing pressure to ensure that prescribing opioid analgesics is minimized to reduce not only the risk of dependence and illicit diversion, but also the potential harms associated with tolerance, side effects and complications, since opioid doses required for bone cancer patients are associated with adverse side effects further diminishing their quality of life (Remeniuk et al., 2015). This has often led to opiate under-dosing (Varilla, Schneiderman, & Keefe, 2015). It is important to note that while opioids are routinely used to treat tumor-induced bone pain, Parreca's lab has shown that sustained morphine use increases pain, osteolysis, bone loss, and spontaneous fracture, as well as markers of neuronal damage in DRG cells and the expression of pro-inflammatory cytokines in a rodent model of bone cancer (King et al., 2007). More recent studies indicate that morphine contributes to chemo-resistance via expanding the population of cancer stem cells, promotes tumor angiogenesis and promotes tumor growth, thereby revealing a novel role of morphine and providing some new guidelines for the clinical use of morphine (Bimonte et al., 2015; Niu et al., 2015). It is also worth noting that treatment guidelines tend to consider morphine and morphine-like opioids comparable and interchangeable in the treatment of chronic cancer pain, but individual responses can vary. A recent clinical trial found that while there were no significant analgesic differences among morphine, oxycodone, transdermal fentanyl or

buprenorphine, the dose escalation was greater with fentanyl and switches and discontinuations were more frequent with morphine (Corli et al., 2016). Interestingly, this study identified groups of patients that were non-responders to opiate treatment ranging from 11.5% (morphine) to 14.4% (buprenorphine). Thus, subsets of patients that do not respond to opiates are found in the general population and like non-responders for acupuncture analgesia (discussed below), these patients should be considered for alternative treatments. Finally, cannabis may be used both to treat chronic cancer pain and importantly to significantly reduce opiate usage. Thus, a 2011 clinical trial that examined the administration of vaporized plant cannabis in chronic cancer pain patients on a daily regimen of morphine or oxycodone reported that inhaled cannabis augments the analgesic effect of opioids (Johnson et al., 2010).

Complementary/alternative therapies

While acupuncture has been around for thousands of years, only recently has it been evolving as a promising approach to relieve chronic cancer pain (Dhanani, Caruso, & Carinci, 2011; Stone & Johnstone, 2010). A recent study has shown that acupuncture and related therapies are effective in reducing pain, fatigue, and in improving quality of life when compared with conventional intervention alone among cancer patients (Lau et al., 2016). On the other hand, a subgroup analysis of 5 randomised controlled trials (RCTs) that evaluated acupuncture's effect on cancer pain, did not include cancer-induced bone pain, because none of the studies made any reference to bone pain (Paley, Johnson,

Tashani, & Bagnall, 2015). At this point in time there is not convincing evidence that acupuncture significantly reduces cancer pain in the human literature. That being said there are several studies using animal models of cancer bone pain that suggest that acupuncture can reduce bone tumor-induced pain including osteosarcoma-induced pain (Ryu, Baek, Park, & Seo, 2014; Smeester et al., 2012; R. X. Zhang et al., 2007). The animal data suggest that electroacupuncture can alleviate bone cancer pain, at least in part by suppressing IL-1β expression and by altering nerve innervation and the vasculature of osteosarcoma. However, the acupuncture treatment schedule can affect tumor growth and therefore the sequence of acupuncture treatment must be determined carefully (Smeester et al., 2013). Clearly, more clinical research is required to address whether acupuncture can reproducibly reduce pain in human osteosarcoma patients without unwanted tumor-related consequences.

Conclusion

Despite advances in our knowledge of osteosarcoma biology, development, metastasis and its associated pain, the current treatment options have not changed over the last four decades and continue to rely on tumor resection and non-specific combination chemotherapy, which results in a dismal 5-year survival rate of 0-29% for patients with clinically detectable metastases (Allison et al., 2012; Jaffe, Puri, & Gelderblom, 2013). Additionally, severe lack of knowledge regarding osteosarcoma metastasis hinders advancement of clinical treatment in pediatric patients. With limited human samples available, animal

models hold promise for further understanding of the biology, pathways, and treatment options for osteosarcoma patients. While each model has its specific limitations, the collective insight into the genetics has proven extremely fruitful. With the advent of novel genetic engineering approaches, future studies will be instrumental in better modelling of the disease and uncovering new and valuable information. While conventional chemotherapy and surgical resection remain mainstays, in combination with new approaches will lead to highly novel treatments and prolonged if not remissive prognoses as well as significantly decreased pain for osteosarcoma patients in the future.

Table 1. Summary of some of the types of pain experienced by bone cancer patients and animal models of bone cancer pain.

Characteristics of pain	Pain phenotyping method	
	Subjects with OSA	**Mice with bone tumor**
Mechanical allodynia	Patients with cancer pain were evaluated for mechanical allodynia [52].	Paw withdrawal responses to von Frey monofilaments in bone cancer mice or rats [1, 53-55].
Heat hyperalgesia	Patients with cancer pain were evaluated for heat hyperalgesia [52].	Paw withdrawal latency and frequency in response to static heat stimuli in mice or rats [53, 54, 56].
Movement evoked pain	Use of a pain verbal rating scale during movement [57].	Count the number of spontaneous flinches of the hind limb in bone tumor mice [55].

CHAPTER 2

Cancer Gene Discovery Utilizing *Sleeping Beauty* Transposon Mutagenesis

Kelsie L. Becklin[1,2,3,4], Branden A. Smeester[1,2,3,4], Branden S. Moriarity[1,2,3]

[1]Department of Pediatrics, University of Minnesota, Minneapolis, Minnesota, USA
[2]Center for Genome Engineering, University of Minnesota, Minneapolis, Minnesota, USA
[3]Masonic Cancer Center, University of Minnesota, Minneapolis, Minnesota, USA
[4]College of Veterinary Medicine, University of Minnesota, Minneapolis, MN, USA

A published version of this chapter is available below:

Becklin KL, Smeester BA, Moriarity BS. Cancer Gene Discovery Utilizing Sleeping Beauty Transposon Mutagenesis. Methods Mol Biol. 2019;1907:161-170. doi: 10.1007/978-1-4939-8967-6_13.

Conception and design: KLB, BAS, BSM
Writing, review and revisions: KLB, BAS, BSM
Study oversight: KLB, BAS, BSM

Summary

Transposable elements are DNA sequences with the ability to move from one genomic location to another (Muñoz-López & García-Pérez, 2010). The movement of class II transposable elements have been functionally harnessed and separated into two distinct DNA transposon components: the terminal inverted repeat sequences that flank genetic cargo to be mobilized and a transposase enzyme capable of recognizing the terminal inverted repeat sequences and catalyzing the transposition reaction (Ammar, Izsvak, & Ivics, 2012). In particular, the *Sleeping Beauty* (SB) system was the first successful demonstration of transposon-based gene transfer in vertebrate species (Izsvak & Ivics, 2005). Over the years, several improvements have been made to *SB* technology and more recent studies have demonstrated the versatility of the system for many applications including insertional mutagenesis, gene transfer and transgenesis (Ammar et al., 2012; Izsvak & Ivics, 2005; Kool & Berns, 2009). These genetic engineering advances made available by *SB* both augment and advance large-scale efforts that have been directed towards identifying how genes and environmental factors influence human health in recent years (Wang, Jensen, & Zenklusen, 2016). In the age of personalized medicine, the versatility of *SB* provides numerous genetic engineering avenues for answering novel questions in basic and applied research. This chapter will discuss the use of *SB*-based insertional mutagenesis in mice for the efficient identification of candidate cancer genes across numerous types of cancers.

Introduction

While many factors ultimately play a role in cancer development, genetic alterations are largely involved early on in tumor development and its subsequent progression (Dupuy, 2010). Identifying these alterations that lead to cellular transformation aid in the understanding of underlying cellular processes and pathways that lead to cancer. The *SB* mutagenesis system is derived from the Tc1/mariner family of class II transposable elements which operate using a cut-and-paste mechanism (Plasterk, 1996). In its simplest form, this two-component system has an enzyme and a DNA element, termed transposase and transposon respectively (Moriarity & Largaespada, 2015). When both of these elements are expressed within the same cell, the transposase recognizes and binds to the specific inverted repeat/direct repeat (IR/DR) sequences that flank the transposon, subsequently catalyzing the excision of the transposon and its reintegration into a new genetic location (Ivics, Hackett, Plasterk, & Izsvak, 1997). The reintegration site can occur anywhere in the genome where there is a TA dinucleotide (Plasterk, 1996), a common sequence, giving *SB* the ability to effectively mutate every gene or genetic element at a variety of locations (Dupuy, 2010). The genetic cargo carried by the *SB* transposon used for cancer gene discovery includes splice acceptors with polyadenylation signals oriented in both directions of the transposon, effectively ending transcription independent of insertion orientation. This can also lead to the generation of truncated mutants with enhanced function, as has been demonstrated with EGFRIIV in hepatocellular carcinoma (Plasterk, 1996). In addition, the transposon contains a

promoter-splice donor element giving the transposon the ability to drive gene over expression when insertion occurs in the positive direction of gene transcription and prior to the gene coding sequences (Collier, Carlson, Ravimohan, Dupuy, & Largaespada, 2005). These features give the *SB* mutagenesis system the ability to identify potential tumor suppressor genes and oncogenes, many of which have been verified to date as such (Moriarity & Largaespada, 2015). Some of the reintegration sites that result in tumors happen more frequently than can be explained by chance and are commonly called common insertion sites (CIS) (Moriarity & Largaespada, 2015). Identification of these CIS leads to a list of potential genetic drivers of tumorigenesis, some of which may have not been previously reported. Briefly, identification of the CIS involves development of the mouse model, tumor collection, followed by high-throughput PCR and sequencing. Programs, such as TAPDANCE or Illumina sequencing (13 and 14) are commonly used to generate the CIS list, but discussion of such methods are beyond the scope of this chapter.

Materials

Genotyping

1. SDS Extraction Buffer: 20mM Tris-HCL, 1mM EDTA, 0.5% (w/v) SDS, Millipore water. To make 500mL add 10mL of 1M, pH 7.5 of Tris-HCl, 1mL of 0.5M, pH 8.0 of EDTA, 25mL of 10% w/v of SDS, and 464mL of Millipore water. Store at room temp indefinitely. (see note 1)

2. Tris-acetate-EDTA Electrophoresis buffer 1x (TAE): 40mM Tris base (pH 7.6), 20mM acetic acid, 1mM EDTA. To make 50x stock solution of TAE add 242g of Tris base in Millipore water, add 57.1mL acetic acid, and 100mL of 500mM EDTA (pH 8.0), add Millipore water until final volume is 1L. To make the working stock dilute the stock 50:1 with Millipore water. (see note 2)

Methods

Generation of transgenic animals

1. Obtain founder transgenic animals containing the following transgenes: multi-copy concatemer of a gain-of-function/loss of function transposon vector, tissue-specific (TSP) Cre line of choice, the conditional Rosa26-LSL-SB11 transposase line and transgenic animals containing the predisposing cancer background (PCB) of choice (optional) (see Figure 1 and note 3).
2. Typical breeding scheme is to breed the transposon containing mouse with the Cre/+ mice to generate transposon;TSP-Cre/+ animals.
3. Cross transposase-containing mice with the predisposing cancer background (PCB) animals to generate Rosa26-LSL-SB11; PCB animals.
4. Finally, cross transposon;TSP-Cre/+ mice to the Rosa26-LSL-SB11;PBC animals to generate transposon; TSP-Cre/+; Rosa26-LSL-SB11; PBC animals and controls.

5. Age the mice until tumor formation is detected or the animal shows ill health at which point they should be euthanized and tissue samples collected.

DNA extraction

1. Upon weaning the mice at 21 days collect a small portion of the tail, 0.5cm of tail is sufficient, for genotyping purposes. Place the tail overnight in a shaker at 55^{o}C in 500ul of SDS extraction buffer and 10µl of proteinase K.
2. Spin down the sample for 10 min at >12000 rpm on a standard tabletop centrifuge and transfer the lysate to a new tube for further extraction, discarding the remains of the tail.
3. Add 500µl of phenol:chloroform to the collected lysate (see notes 4 and 5)
4. Spin in tabletop centrifuge >12000 rpm for 5min.
5. Collect the aqueous top layer from the sample and place into a new tube (see note 6)
6. Add 350µl of isopropanol to the sample and invert the tube 5-7 times to precipitate genomic DNA.
7. Centrifuge the sample at >12000 rpm for 10min at 4^{o}C (see notes 7 and 8).
8. Remove all liquid from tube careful to not disturb the pellet.
9. Add 500µl of 70% ethanol to wash the pellet (see note 9).
10. Spin down for 5min at 4^{o}C at >12000 rpm.
11. Remove all liquid careful to not disturb the pellet

12. Air dry for 5-10min (see note 10).
13. Resuspend the sample in 200µl of Millipore water (see notes 11 and 12).
14. Quantify DNA samples using a spectrophotometer and dilute to a concentration of 100ng/µl.

PCR genotyping

1. To perform PCR genotyping, each sample will require; 25µl of 1.1 × ReddyMix Taq, 2µl of each primer diluted to a working stock of 10µMol, 19µl of DDW, and 200ng of your DNA sample (see note 13 and 14).
2. Run the PCR with an initial denaturation step at 95^{o}C for 2 min; 35 cycles of denaturing at 95^{o}C for 25 s, annealing at 55^{o}C for 35 s, and extension at 72^{o}C for 1.5 min; and a final extension step at 72^{o}C for 5 min. (see note 15)
3. Resolve PCR on a 1% TAE agarose gel.

Linker-mediated PCR (LM-PCR)

1. Upon necropsy a portion of the tumor should be snap frozen in liquid nitrogen and stored at -80^{o}C until genomic DNA extraction can be completed.
2. Genomic DNA should be extracted from collected tumors via the standard phenol:chloroform:isoamyl alcohol extraction as explained above for DNA extraction (section 4.2)

3. Anneal linkers by mixing in a 1.5mL Eppendorf tube 50µl of 10µMol of each BfaI Linker+ and Linker- (for left side of transposon) or NlaIII Linker+ and Linker- (for right side of transposon). Add 2µl of 5M NaCl and heat to 95^{o}C followed by a ramp down of 5^{o}C every one minute until 25^{o}C is reached (see Table 1 for a list of all primers and linkers used for LM-PCR).
4. Each tumor sample will undergo digestion with both BfaI and NlaIII (New England Biosciences; catalog numbers R0568S and R0125S) separately, allowing the DNA regions to the left and right side of the transposon to be cloned, respectively. Add 100ng of DNA to 0.5µl (5Units) of enzyme, 5µl of 10x CutSmart Buffer for a total volume of 50µl and incubate overnight at 37^{o}C (see note 16).
5. Heat inactivate the digestions at 80^{o}C for 20 min
6. To ligate the annealed linkers onto the digested genomic DNA fragments, mix 6µl of annealed linker with 8µl of digested DNA to the corresponding restriction enzyme, 4µl of 5x ligase buffer, and 2µl of T4 DNA ligase, for a total volume of 20µl. Incubate reaction overnight at 16^{o}C.
7. Purify the ligated DNA using Qiagen MinElute 96 UF Plates, following manufacturer's instructions with the exception of eluting in 40µl of Millipore water.
8. Digestion with BamHI will remove any remaining transposon concatemer array, which would otherwise be sequenced and waste sequence read depth. Use 22µl of the purified DNA from step 7, 5µl of 10x CutSmart

buffer, 0.5µl BamHI enzyme, and add Millipore water until total volume is 50µl. Incubate this reaction overnight at 37°C. (see note 17)

9. Purify the BamHI-digested DNA as in step 7 above.
10. A primary PCR must be performed using 2 × ReddyMix. For each reaction, you will use 12.5µL of 2x ReddyMix PCR Master Mix, 1.25µL of appropriate 1° IRDR primer (specific to the left or right side of the transposon), 1.25µL of 1° linker primer, 100ng Purified DNA, and Millipore water to a total reaction volume of 25µL. Perform PCR as follows: initial denaturation of 95°C for 2 min; 30 cycles of denaturing at 95°C for 25 s, annealing at 55°C for 35 s, and extension at 72°C for 1.5 min; and a final extension step at 72°C for 5 min.
11. Dilute the primary PCR to 1:75 in Millipore water and take 1µl of this dilution to use for the secondary PCR.
12. The secondary PCR is carried out with Long-Amp Taq (New England Biolabs). For each reaction, you will use 10µl of 5x Long-Amp Taq reaction buffer, 1.5µl of 10mM dNTPs, 2µl of appropriate 2° IRDR primer (either left or right), 2µl of 2° linker primer, 1µl of diluted PCR product, and Millipore water to a total reaction volume of 50µl. Perform PCR as follows: initial denaturation of 94°C for 30 sec; 35 cycles of denaturing at 94°C for 25 s, annealing at 53°C for 35 s, and extension at 65°C for 50 sec; and a final extension step at 65°C for 10 min.
13. Send in PCR product for next generation deep sequencing (see note 18.

14. Perform common insertion site analysis utilizing available bioinformatics software (see note 19).

Notes

1. SDS can come out of solution at low temperatures. It will appear as a white substance, which can be dissolved with warming.
2. All reagents must be DNase free to avoid degradation of the PCR amplicons.
3. A list of previously published screens and their predisposing backgrounds is available here (Moriarity & Largaespada, 2015).
4. Phenyl:chloroform is a biological hazard and steps 3-5 should be performed in a fume hood.
5. We have found that shaking the tube directly after addition of phenyl:chloroform vigorously for 1 min gave the best results. The solution after shaking will be a milky white color.
6. Care must be taken to not disturb the bottom layer or any precipitates that form on the interface of the two layers as this will decrease the quality of your purified genomic DNA.
7. The centrifuge must be maintained at 4^{o}C for the DNA to precipitate genomic DNA effectively.
8. You should see a small pellet after the sample has been spun down. If you do not see a pellet, add another 350µl of isopropanol to the sample and vigorously shake the sample for 30 sec and spin again.

9. Making fresh stocks of 70% ethanol frequently will ensure that your solution is properly diluted as ethanol evaporates faster than water and thus over time your solution may vary.
10. Air drying the pellet allows all remaining ethanol to evaporate as any remaining ethanol can decrease the quality of your sample.
11. Volume of resuspension can vary, for small pellets add as little as 75µl and for larger pellets up to 350µl for the initial resuspension.
12. After you have resuspended the pellet placing the sample into a 55^{o}C water bath for 15 min, followed by 30 seconds of vortexing, and a quick spin to collect sample in the bottom of the tube will ensure that the DNA is fully in solution.
13. All primers are diluted to a working stock of 10µMol. Amount of primer to add may vary slightly depending on what gene you are amplifying. If PCR results are not of high quality, conduct a PCR optimization with varying amounts of primers and DNA for your particular gene. Care must be taken to not contaminate primers as any DNA contamination will influence PCR results.
14. Controls should include a no DNA template to determine any contaminating DNA within reagents used.
15. PCR conditions given are for the T2/Onc transposon and SB11 transposase and a PCR optimization may be required for the TSP-Cre transgene as well as the PCB.

16. Using LM-PCR to clone the transposon junctions from both the left and right direct repeats involves two reactions for each sample. The primers, linkers, and restriction enzymes for each type of reaction (left and right) are different but the method for each is the same.
17. By digesting with an enzyme that cuts within the transposon that is within its original concatemer you will prevent the amplification of non-transposed transposons as the binding locations of the two primers will now be on separate strands of DNA and thus the only PCR product will be that of inserted transposons.
18. If you do run part of the PCR product on a 1% agarose gel you may see a smear or many distinct bands indicating the LM-PCR was successful.
19. There are many choices for statistical analysis on the sequencing samples such as TAPDANCE or Illumina sequencing (Brett et al., 2011).

Conclusion

With respect to this thesis, *SB* technology was an invaluable tool to identify novel genes that drive OSA and metastasis. Given the genetic heterogeneity and complexity of OSA (Kansara et al., 2014), there is a pressing need for the identification, functional validation, and therapeutic targeting of driver genes in OSA to overcome the severe treatment limitations that have not significantly improved OSA long-term survival rates in over 40 years. The subsequent chapters of this thesis build upon the findings of our seminal *SB* work in OSA and offer therapeutic solutions to overcome these current limitations.

Figure 1. Basic outline of *SB* screen breeding strategy. Generally, animals containing a tissue-specific Cre (TSP-Cre) and the multi-copy transposon concatamer are crossed with animals harboring the transposase and a predisposing cancer background (PCB) to generate cohorts of animals.

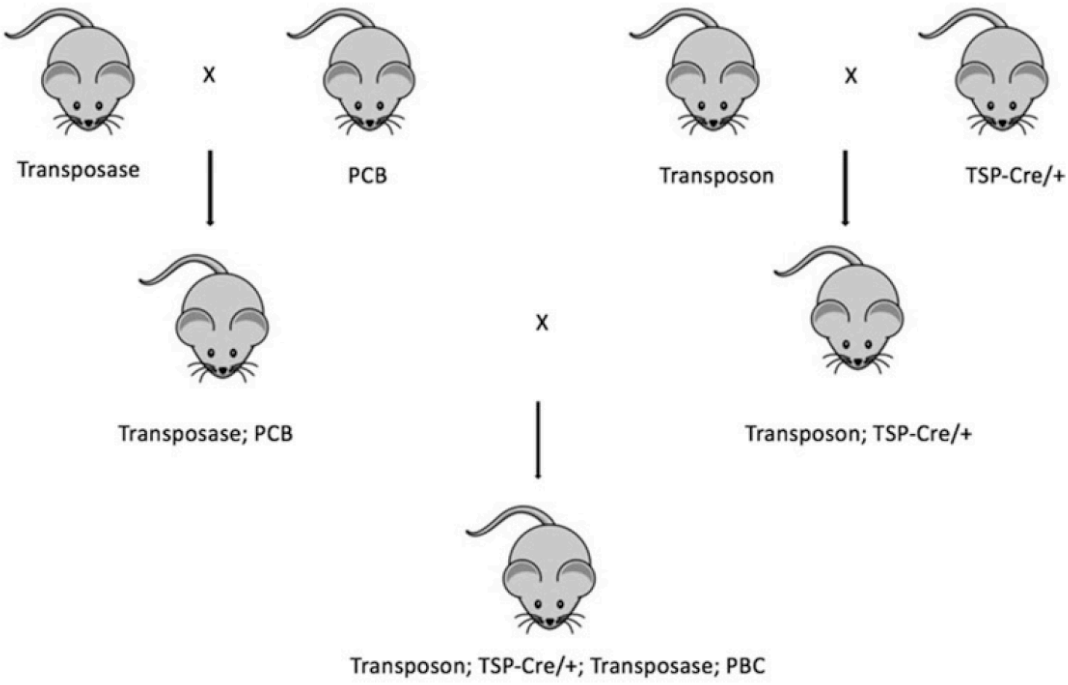
Transposase
X
PCB
Transposon
X
TSP-Cre/+
Transposase; PCB
X
Transposon; TSP-Cre/+
Transposon; TSP-Cre/+; Transposase; PBC

Table 1: List of all linkers and primers used for the linker-mediated PCR (LM-PCR).

PCR Primers	Primer Sequence
BfaI Linker+	GTAATACGACTCACTATAGGGCTCCGCTTAAGGGAC
BfaI Linker-	P-TAGTCCCTTAAGCGGAG-AM
NlaIII Linker+	GTAATACGACTCACTATAGGGCTCCGCTTAAGGGACCATG
NlaIII Linker-	P-GTCCCTTAAGCGGAGCC-AM
1° Splink IRDR Right	GCTTGTGGAAGGCTACTCGAAATGTTTGACCC
1° Splink IRDR Left	CTGGAATTTTCCAAGCTGTTTAAAGGCACAGTCAAC
1° Splink Linker	GTAATACGACTCACTATAGGGC
2° Splink IRDR Right (Illumina)	AATGATACGGCGACCACCGAGATCTACACTCTTTCCCTACACGACGCTCTTCCGATCT(N)^{10} AAGTGTATGTAAACTTCCGACTTCAA
2° Splink IRDR Left (Illumina)	AATGATACGGCGACCACCGAGATCTACACTCTTTCCCTACACGACGCTCTTCCGATCT(N)^{10} AGGTGTATGTAAACTTCCGACTTCAA
2° Linker (Illumina)	CAAGCAGAAGACGGCATACGAGCTCTTCCGATCTAGGGCTCCGCTTAAGGGAC

CHAPTER 3

SEMA4C is a novel target to limit osteosarcoma growth, progression, and metastasis

Branden A. Smeester[1,4,5], Nicholas J. Slipek[1,4,5], Emily J. Pomeroy[1,4,5], Heather E. Bomberger[2], Ghaidan A. Shamsan[2,5], Joseph J. Peterson[1,4,5], Margaret R. Crosby[1,4,5], Garrett M. Draper[1,4,5], Kelsie L. Becklin[1,4,5], Eric P. Rahrmann[6], James B. McCarthy[3,5], David J. Odde[2,5], David K. Wood[2], David A. Largaespada[1,4,5], Branden S. Moriarity[1,4,5]

[1]Department of Pediatrics, University of Minnesota
[2]Department of Biomedical Engineering, University of Minnesota
[3]Department of Laboratory Medicine and Pathology
[4]Center for Genome Engineering, University of Minnesota
[5]Masonic Cancer Center, University of Minnesota
[6]Cancer Research UK Cambridge Institute, University of Cambridge

A published version of this chapter is available below:

Smeester BA, Slipek NJ, Pomeroy EJ, Bomberger HE, Shamsan GA, Peterson JJ, Crosby MR, Draper GM, Becklin KL, Rahrmann EP, McCarthy JB, Odde DJ, Wood DK, Largaespada DA, Moriarity BS. SEMA4C is a novel target to limit osteosarcoma growth, progression, and metastasis. Oncogene. 2019 Oct 3. doi: 10.1038/s41388-019-1041-x.

Conception and design: BAS, DAL, BSM
Development and acquisition of data: BAS, NJS, EJP, HEB, GAS, MRC, JJP, GMD, KLB, EPR
Analysis and interpretation: BAS, NJS, DJO, DKW, JBM, DAL, BSM
Writing, review and revisions: BAS, NJS., EJP, HEB, GAS, MRC, JJP, GMD, KLB, EPR, JBM, DJ.O, DKW, DAL, BSM
Study oversight: BAS, DAL, BSM

Summary

Semaphorins, specifically type IV, are important regulators of axonal guidance and have been increasingly implicated in poor prognoses in a number of different solid cancers. In conjunction with their cognate PLXNB family receptors, type IV members have been increasingly shown to mediate oncogenic functions necessary for tumor development and malignant spread. In this study, we investigated the role of semaphorin 4C (SEMA4C) in osteosarcoma growth, progression, and metastasis. We investigated the expression and localization of SEMA4C in primary osteosarcoma patient tissues and its tumorigenic functions in these malignancies. We demonstrate that overexpression of SEMA4C promotes properties of cellular transformation, while RNAi knockdown of SEMA4C promotes adhesion and reduces cellular proliferation, colony formation, migration, wound healing, tumor growth, and lung metastasis. These phenotypic changes were accompanied by reductions in activated AKT signaling, G1 cell cycle delay, and decreases in expression of mesenchymal marker genes *SNAI1*, *SNAI2,* and *TWIST1*. Lastly, monoclonal antibody blockade of SEMA4C *in vitro* mirrored that of the genetic studies. Together, our results indicate a multi-dimensional oncogenic role for SEMA4C in metastatic osteosarcoma and more importantly that SEMA4C has actionable clinical potential.

Introduction

Osteosarcoma is a malignant, primarily pediatric tumor, of the growing long bones with peak incidence in the second decade of life (Morrow & Khanna, 2015). Derived from mesenchymal origins in the pre-osteoblastic lineage, osteosarcomas arise from the failure of osteoblasts to differentiate into mature bone-building cells (Yan, Lv, & Guo, 2016). Osteosarcomas are commonly typified by their heterogeneity, genomic instability, and frequency of systemic metastasis primarily to the lungs (Gianferante, Mirabello, & Savage, 2017; Rickel, Fang, & Tao, 2017). Despite advances in chemotherapy regimens and surgical resection, survival rates for patients with osteosarcoma have remained stagnant for more than four decades (Mirabello, Troisi, & Savage, 2009). The complex nature of osteosarcoma presents unique difficulties with respect to elucidating novel therapeutic targets and identifying treatment strategies that may prove most effective, particularly across individual patients. Given this, it is critically important to better understand not only the mechanisms specific to osteosarcoma development and progression, but most importantly metastasis, in order to develop better treatment options for patients with this devastating disease.

Semaphorins are a family of membrane-bound and soluble proteins that modulate a whole host of cellular functions including differentiation, cytoskeletal rearrangement, and motility (Alto & Terman, 2017). Interestingly, semaphorin family members have been reported to mediate many hallmarks of cancer including cellular proliferation, angiogenesis, and immune escape (Meyer, Fritz,

Pierdant-Mancera, & Bagnard, 2016; Tamagnone, 2012; Worzfeld & Offermanns, 2014). Recent evidence from studies of the SEMA4-PLXNB family of axonal guidance molecules in normal bone cells suggests that osteoclastic expression of SEMA4D inhibits osteoblastic bone formation through suppression of IGF1 signaling (Alto & Terman, 2017; Negishi-Koga et al., 2011), however, recent data from our lab suggests that high expression of SEMA4D is oncogenic in osteosarcoma (Moriarity et al., 2015). Given osteosarcomas retain mesenchymal-like characteristics (Abarrategi et al., 2016), this suggests the possibility of SEMA4 members signaling through similar pathways during osteosarcomagenesis as they do during normal bone development.

Furthermore, activation of downstream signaling processes that involve the MAP kinase/PI3K pathways through heterodimerization with other receptor tyrosine kinases (RTKs) such as MET (MET proto-oncogene, receptor tyrosine kinase) and/or ERBB2 (erb-b2 receptor tyrosine kinase 2) can potentiate many of the invasive cellular processes associated with solid cancers (Swiercz, Worzfeld, & Offermanns, 2008). SEMA4C, a type IV semaphorin, and its cognate receptor PLXNB2, have been recently characterized as oncogenic signaling partners in invasive breast cancer (Gurrapu, Pupo, Franzolin, Lanzetti, & Tamagnone, 2018), hepatocellular carcinoma (Lu et al., 2018), and glioma (Le et al., 2015). Moreover, SEMA4C has been shown to play diverse roles in the propagation of pain signaling (Paldy et al., 2017), as well as in the immune system during Th2-driven immune responses similar to other semaphorin IV family members (Xue et al., 2016).

Here, we studied SEMA4C's role in osteosarcoma growth and metastasis. We show that 1) SEMA4C is upregulated in a subset of osteosarcoma patient samples and cell lines; 2) high SEMA4C expression enhances properties of cellular transformation, mesenchymal marker expression, and that genetic knockdown conversely reduces those phenotypes/markers; 3) SEMA4C modulates osteosarcoma growth and lung metastasis and 4) targeted monoclonal antibody blockade of SEMA4C robustly reduces these phenotypes associated with high-level SEMA4C expression. Together, this study expands upon the current known functions of SEMA4C in a highly malignant pediatric solid cancer and suggests that antibody blockade of SEMA4C-PLXNB2 signaling may overcome the current hurdles for targeting pathways that ultimately lead to metastatic lung nodule formation and continued disease progression.

Materials and Methods

RNA sequencing data sets

SEMA4C expression levels were analyzed in normal human osteoblasts (NHOs) and two independent human osteosarcoma patient data sets (#1 and #2). Expression levels in NHOs and #1 were obtained from an existing data set (Moriarity et al., 2015). Expression levels in data set #2 were obtained from the Therapeutically Applicable Research to Generate Effective Treatments (TARGET) program (https://ocg.cancer.gov/programs/target/data-matrix) established by the National Cancer Institute's Office of Cancer Genomics; dbGaP accession phs000218.v21.p7.

Tissue microarray (TMA) samples and scoring

The osteosarcoma tissue microarray was purchased from Biomax (Osteosarcoma: OS804c) containing 40 samples in duplicate. Slides containing 4 μm thick formalin-fixed, paraffin-embedded sections of tumor tissue were deparaffinized and rehydrated. Antigen retrieval was performed in a steamer using 1 mM Tris base EDTA buffer, pH 9.0. After endogenous peroxidase blocking, a protein block was applied. Immunohistochemistry (IHC) for SEMA4C was performed using a rabbit anti-SEMA4C primary antibody (#AF6125, R & D Systems) on an autostainer (Dako). Detection was achieved using the Envision rabbit detection system (Dako) with diaminobenzidine (DAB) as the chromogen. Tissue sections were imaged on a Nikon E800M microscope at 40X magnification using a Nikon DSRi2 camera and Nikon Elements D Version 4 software. Slides were evaluated and scored as previously described (Rahrmann et al., 2013).

Cell culture

All osteosarcoma cell lines were purchased and obtained from the American Type Culture Collection (ATCC). Normal human osteoblasts (NHOs) and primary human umbilical vein cells (HUVECs) were purchased from Lonza. All cell lines were grown and maintained in accordance with standard cell culture techniques. Both HOS and MG-63 cells were grown in DMEM. G-292 cells were grown in McCoy's 5A. SJSA-1 cells were grown in RPMI-1640. NHOs were

grown in αMEM. Osteosarcoma cell line media was fortified with 10% fetal bovine serum (FBS) and 1X penicillin/streptomycin and NHO media was fortified with 20% FBS and 1X penicillin/streptomycin. HUVECs were cultured with EGM-2 bullet kit media (#cc-3162, Lonza) with 1X antibiotic-antimycotic (#15240062, Thermo Fisher) in cell culture flasks coated with 1% gelatin (#G1383, Sigma Aldrich).. All cell cultures were incubated in a water-jacketed incubator set at 5% carbon dioxide (CO_2) and at 37°C. All cell lines except NHO, G-292, and HUVECs were authenticated by the University of Arizona Genetics Core (UAGC) using short tandem repeat profiling. All cell lines were found to be free from mycoplasma.

Generation of shRNA knockdown and overexpression cell lines

Stable knockdown of SEMA4C was accomplished with pGIPZ lentiviral vectors expressing an shRNA against SEMA4C in conjunction with GFP and a puromycin selection marker (sh1 #V3LHS_394644, sh2 #V3LHS_413698, Open Biosystems). Control pGIPZ vector with non-targeting shRNA was used as a control (#RHS4346, Open Biosystems). Lentiviral particles were produced with 293T cells co-transfected with pGIPZ shRNAs, pMD2.G envelope (#12259, addgene) and psPAX2 (#12260, addgene) packaging vectors. Stable shRNA knockdown lines were established via puromycin selection at 1 μg/mL. Overexpression vectors were generated using the human *SEMA4C* cDNA sequence (#40035253, Dharmacon) and vectors/cell lines were established

using previously described methodology (Marko et al., 2016; Moriarity et al., 2014).

Anti-SEMA4C antibody treatment *in vitro*

Anti-SEMA4C or isotype control antibody was administered at 10 μg/mL and 15 μg/mL where indicated (#sc-136445, Santa Cruz Biotechnology).

RNA isolation and Quantitative RT-PCR

Total RNA was extracted from cell lines using the High Pure RNA Isolation Kit (Roche, Basel). 1 μg of extracted RNA was reverse transcribed into cDNA using the Transcriptor First Strand Synthesis kit (Roche). Quantitative RT-PCR was performed in triplicate using SYBR green mix (Qiagen) on an ABI 7500 machine (Applied Bio Systems). Primer sequences are available in Supp. Table 1. All measurements were calculated using the ΔΔCT method and expressed as fold change relative to respective control non-silencing shRNA line (shCON).

ELISA

Quantification of levels of soluble SEMA4C secreted in the conditioned media (72 hours) of indicated cell lines was performed via manufacturer's instructions (#MBS705730, MyBioSource).

Western blot

Protein was extracted from cultured cells in RIPA buffer containing a protease inhibitor (Roche) and phosphatase inhibitors (Sigma-Aldrich). Total protein was quantified using BCA (Thermo Fisher). Cell lysate was loaded and run on 4-12% Bis-Tris gels (Thermo Fisher) and transferred to PVDF membranes (Bio-Rad). Membranes were blocked in 5% nonfat dry milk for 1 hour (Bio-Rad) and incubated gently shaking overnight at 4°C in 1° antibody/PBS-T. Subsequently, membranes were washed and incubated in conjugated 2° antibodies for 1 hour. Blots were thoroughly washed following 2° incubation and developed using the WesternBright Quantum detection kit (Advansta) and the LICOR Odyssey (LICOR). A complete list of antibodies and other reagents utilized is available in Supp. Table 2. Densitometry was performed on all images. Bands were compared to each respective loading control, normalized to 1, and compared.

MTS cellular proliferation assay

Cellular proliferation assays were performed as previously described (Moriarity et al., 2015). Briefly, modified cells (1.2×10^3) were plated per well in 96-well plates. Cells were measured at 24, 48, 72, and 96 hours post plating. Absorbances at 490 nm and 650 nm were read using a SynergyMx (BioTek) fluorescence plate reader.

Transwell migration assay

Modified cells (2.5 x 10^4) were seeded in 500 μL of serum free media in the upper chamber of 8 μm inserts (Corning). The lower chamber was filled with 750 μL media fortified with 10% fetal bovine serum (FBS) as a chemo attractant. After 24 hours, non-migrating cells where removed with a cotton swab. Migrated cells located on the lower side of the chamber were fixed with crystal violet, air-dried, and photographed to quantify migration of cells. For anti-SEMA4C studies, cells were seeded into the top chamber with antibody following a 6-hour pre-treatment at indicated concentration.

Wound healing assay

Wound healing assays were performed as previously described (Marko et al., 2016). Briefly, 1 x 10^4 cells were plated into a removable 2-well silicone culture insert which generated a defined cell-free gap (ibidi). Cells were then incubated for 24 hours before inserts were removed and fresh cell culture media was added. Phase contrast images of the wounds were acquired every 10 minutes for 16-20 hours, which was sufficient for the cells to completely close the simulated wound gap. A custom-written image segmentation algorithm in MATLAB was used to measure wound distance over time and to calculate closure rate.

3D microfluidic cellular adhesion assay

Cellular adhesion assays were performed as previously described (Brett et al., 2018). Briefly, the microfluidic model was fabricated using standard soft

lithography of polydimethylsiloxane (PDMS) (#4019862, Ellsworth). Rat tail collagen I (#CD354249, Corning) was buffered with PBS and cell culture grade water to create a 6 mg/mL solution. Collagen was then loaded into the lower channel of the microfluidic model and allowed to nucleate at 37°C for at least 1 hour. The upper channel was coated with 1% gelatin solution for 30 minutes at room temperature. HUVECs were released using trypsin, resuspended in a 4% w/v dextran (#31392, Sigma Aldrich) solution in EGM-2 media at a concentration of approximately 1 x 10^6 cells per mL, and 50 μL of the cell solution was added to the inlet of the microfluidic model. HUVECs become confluent in the channel over 24-48 hours at 37°C. 5 x 10^4 green fluorescent protein (GFP)-expressing osteosarcoma cells were then added to the inlet of the model and allowed to adhere over 3 hours. Microfluidic models were imaged at 24 hours. Adhesion and invasion of osteosarcoma cells was quantified.

Soft agar colony formation assay

Modified cells (1 x 10^4) were seeded into a 0.35% agar solution placed on top of a 0.5% agar in six-well plates and allowed to incubate for 2-3 weeks. The resultant colonies were fixed, divided into four quadrants, and imaged using microscopy. Colonies were quantified via ImageJ v1.52a software using a standard colony quantification macro (Moriarity et al., 2015).

Flow cytometry

Cells were fixed with 2% paraformaldehyde (Electron Microscopy Sciences) and permeabilized with cold 90% methanol (Sigma). Cell cycle analysis was performed using PI/RNase Staining Buffer (BD Pharmingen). Cleaved caspase 3 (Asp175, clone D3E9) PE was purchased from Cell Signaling Technologies and cells were stained according to manufacturer's recommendations. Cells were analyzed on an LSR II or Fortessa digital flow cytometer (BD Biosciences) at the University of Minnesota Flow Cytometry Resource. Analysis was performed using FlowJo software.

Orthotopic osteosarcoma mouse model

All animal procedures were performed in accordance with protocols approved at the University of Minnesota in conjunction with the Institutional Animal Care and Use Committee (IACUC). Modified cells (2.5×10^5) were injected into the calcaneous of male and female 6-8-week-old immunocompromised mice (NOD Rag Gamma, Jackson Labs) (Khanna et al., 2000; Smeester, Al-Gizawiy, & Beitz, 2012; Smeester et al., 2013). Tumor volume was calculated via caliper measurements using the formula V = (W*W*L)/2 where V equals tumor volume, W equals tumor width and L equals tumor length (Faustino-Rocha et al., 2013).

Lung metastasis evaluation

Micrometastatic nodules were examined via H & E histology at 4X magnification. Quantification of nodule number and area was undertaken in 9

sections from four mice/group (shCON and shSEMA4C) at 4X using ImageJ v1.52a software.

Statistical analysis

All statistical analyses were performed using Prism v8 software (GraphPad). All data are presented as mean ± standard error of the mean (SEM). Two groups were compared using a two-tailed unpaired Student's t-test. Three or more groups were compared using a One-way ANOVA with Bonferroni's post hoc or Two-way ANOVA analyses were performed and followed with Bonferroni's post hoc testing. All statistical analyses are individually indicated where applied throughout. In all cases, $p < 0.05$ was considered statistically significant.

Results

SEMA4C is highly expressed in some osteosarcoma tissues and cell lines

In order to investigate the potential role of SEMA4C in osteosarcoma development and metastasis, we first examined *SEMA4C* mRNA expression in two available human osteosarcoma clinical data sets and in 3 normal human osteoblast control samples (Fig. 1A). Human osteosarcoma samples from both data sets had significantly higher *SEMA4C* expression when compared to normal human osteoblasts, (Fig. 1A; $*p < 0.05$). Next, we examined SEMA4C protein expression in a commercially available human osteosarcoma TMA (Figs. 1B and C). When all 40 sections were quantified, 32.5% had weak expression, 47.5%

had moderate expression, and 20.0% had strong expression of SEMA4C (Fig. 1B). Representative images of each staining pattern are shown in Fig. 1C. The majority of osteosarcoma tissue sections stained were greater than 75% SEMA4C positive (Supp. Fig. 1A) and had primarily cytoplasmic/membraneous staining localization (Supp. Fig. 1B). These results indicate that a subset of osteosarcoma patient tissues express high levels of SEMA4C. We next probed a number of commercially available osteosarcoma cell lines for SEMA4C and cognate receptor PLXNB2 expression via western blot and compared them to normal human osteoblasts (NHO). Relative to the NHOs, most osteosarcoma cell lines examined expressed detectable membrane-bound SEMA4C (Fig. 1D). Both MG-63 and G-292 cells had no detectable expression in Fig. 1D, but was minimally detectable in Fig. 2A at high exposures. Since SEMA4C is known to be shed from the extracellular membrane (Wei et al., 2017), we also analyzed cell culture media of indicated cell lines for the presence of soluble SEMA4C (Fig. 1E). Soluble SEMA4C was detectable in all lines including NHO, however, soluble SEMA4C was expressed at significantly elevated levels in U2OS, HOS, SJSA-1, and MG-63 osteosarcoma cell lines as compared to NHOs (Fig. 1E, $*p < 0.05$, $**p < 0.01$). These data indicate that SEMA4C is upregulated in a subset of osteosarcoma tissues and cell lines compared to normal osteoblasts.

Overexpression of *SEMA4C* promotes facets of cellular transformation in osteosarcoma cells

To understand the SEMA4C-PLXNB2 signaling axis in osteosarcoma, we overexpressed *SEMA4C* in endogenous low expressing MG-63 and G-292 osteosarcoma cell lines and confirmed by western blot (Fig. 2A). Overexpression of *SEMA4C* increased proliferation in both lines (Fig. 2B, *$p < 0.05$, ****$p < 0.0001$). In a soft agar colony formation assay, overexpression of *SEMA4C* promoted modest increases in colony formation in both lines (Fig. 2C, *$p < 0.05$, ****$p < 0.0001$). Interestingly, in a transwell migration assay, *SEMA4C*-overexpressing MG-63 cells had increased migration while G-292 cells displayed slightly reduced migration (Fig. 2D, ***$p < 0.001$, ****$p < 0.0001$). Representative images of the migration experiments are shown in Fig. 2E. Both MAPK and PI3K signaling were investigated following phenotypic assays. These changes in proliferation, migration, and colony formation were associated with increased activation of AKT signaling, but not ERK signaling (data not shown) (Fig. 2F). Lastly, overexpression of *SEMA4C* significantly promoted upregulation of mesenchymal markers *SNAI1*, *SNAI2*, and *TWIST1* in MG-63 cells, while all but *TWIST1* remained largely unchanged in G-292 (Fig. 2G, *$p < 0.05$, ****$p < 0.0001$). These data suggest that overexpression of SEMA4C promotes facets of cellular transformation and mesenchymal marker expression.

Knockdown of SEMA4C reduces cellular proliferation and colony formation

To complement our gain-of-function (GOF) studies and to elucidate the effects of knockdown of SEMA4C on cellular proliferation and anchorage-independent growth, we performed loss-of-function (LOF) experiments in two

endogenously high SEMA4C-expressing lines (See Figs. 1D and 1E). HOS and SJSA-1 osteosarcoma cell lines were transduced with shRNAs against SEMA4C (shSEMA4C or shS4C abbreviated) or non-silencing control (shCON) and stably selected with puromycin. Confirmation of optimal shRNA knockdown was evaluated via qRT-PCR (Fig. 3A, $^{**}p < 0.01$, $^{****}p < 0.0001$) and western blot (Fig. 3B). Following evaluation, shRNA #2 was chosen for both lines in all subsequent experiments. Knockdown of SEMA4C reduced cellular proliferation (Fig. 3C, $^{****}p < 0.0001$) and colony formation (Fig. 3D, $^{****}p < 0.0001$) in both lines. These reductions in 2D and 3D growth were accompanied by downregulation of activated AKT signaling (Fig. 3E). Lastly, silencing of SEMA4C was associated with G1 cell cycle delay in both lines (Fig. 3F, $^{*}p < 0.05$, $^{**}p < 0.01$). Silencing of SEMA4C did not induce cleaved CASP3 activity (Supp. Figs. 2A and 2B). Together, these data suggest SEMA4C modulates cellular growth and colony formation in osteosarcoma cell lines.

SEMA4C promotes cellular motility and loss of adhesion

Next, we examined the role of SEMA4C in cellular movement using migration chambers, wound healing assays, and 3D microfluidic chambers. Knockdown shSEMA4C lines displayed reduced cellular migration (Figs. 4A, $^{**}p < 0.01$, $^{****}p < 0.0001$). Representative migration images are shown in Fig. 4B. Following the migration assay, we evaluated cellular adhesion and invasion using 3D microfluidic chambers (Figs. 4C and 4D and Supp. Figs. 3A-D). Increased adhesion was observed in HOS, but not SJSA-1 cells (Fig. 4C, $^{*}p < 0.05$).

Representative images 24 hours post are depicted in Fig. 4D. No changes in invasion were observed in either HOS or SJSA-1 knockdown cells (data not shown). Similarly, SJSA-1 knockdown cells showed reduced wound closure rates while a non-significant trend towards reduced closure rates was observed in HOS (Fig. 4E, $p = 0.06$, $*p < 0.05$). Representative wound healing photographs are shown in Supp. Fig. 4A. These changes in cell motility were associated with reductions in expression of mesenchymal markers *SNAI1*, *SNAI2,* and *TWIST1* in both knockdown lines (Fig. 4F, $***p < 0.001$, $****p < 0.0001$). Together, these data suggest SEMA4C promotes cellular motility and loss of adhesion in osteosarcoma cell lines.

SEMA4C knockdown reduces tumor growth and development of lung metastases

Next, we evaluated the effects of SEMA4C knockdown on osteosarcoma tumor growth and lung metastasis in an orthotopic mouse model. Following injection of either shCON or shSEMA4C knockdown cells into the calcaneous of immunodeficient mice, tumors were allowed to form, and caliper measurements were taken beginning 10 days post-implantation and every 5 days for 30 days. Both HOS and SJSA-1 knockdown cell lines displayed reduced tumor growth (Fig. 5A, $*p < 0.05$, $***p < 0.001$, $****p < 0.0001$). Representative gross images of lungs from HOS shCON and shSEMA4C mice are shown in Fig. 5B. Visible macrometastatic nodules are indicated by white arrows. Whole cell lysates were made from representative control and knockdown tumors from each cell line.

SEMA4C knockdown was confirmed *in vivo* and activated AKT signaling was also reduced in SEMA4C knockdown tumors (Figs. 5C and 5D). These results mirrored that of our GOF and LOF *in vitro* studies in Fig. 2F and Fig. 3F respectively. Considering metastatic capacity is often associated with increased cell growth, motility, and anchorage-independence (Jiang et al., 2015; Mori et al., 2009), we investigated the effects of SEMA4C knockdown on lung nodule formation and size. When lung sections were examined, both SEMA4C knockdown lines had reduced numbers of micrometastatic nodules (Fig. 5E, ****$p < 0.0001$) and nodule area (Fig. 5F, ****$p < 0.0001$). Representative lung H & E images and high powered-insets are shown in Fig. 5G for both cell lines. Black arrows indicate micrometastases. Together, SEMA4C promotes tumor growth and lung metastasis formation in osteosarcoma.

Monoclonal antibody blockade of SEMA4C reduces tumorigenic properties of osteosarcoma cell lines

Lastly, we sought to evaluate the therapeutic potential of SEMA4C blockade using a commercially available monoclonal antibody raised against amino acids 400-510 of human SEMA4C. To evaluate the effects of blockade *in vitro*, we treated wild-type normal human osteoblasts (NHO), HOS, and SJSA-1 osteosarcoma cells with two concentrations of anti-SEMA4C or isotype control IgG and assayed its effects on cellular proliferation. Reduced cellular proliferation was observed following a 48-hour treatment in both osteosarcoma cell lines, but not NHOs (Fig. 6A, ****$p < 0.0001$). Similarly, treatment with anti-SEMA4C also

reduced migration in both osteosarcoma cell lines (Fig. 6B, ****$p < 0.0001$). Representative images are shown in Fig. 6C. Following treatment, G1 cell cycle delay was again observed similar to our genetic studies in both cell lines (Fig. 6D, *$p < 0.05$, **$p < 0.01$, ***$p < 0.001$, ****$p < 0.0001$). Our findings suggest that anti-SEMAC treatment may prove valuable for combating osteosarcoma tumor growth, progression, and ultimately lung metastasis through disruption of oncogenic SEMA4C signaling (Fig. 6E).

Discussion

Our studies provide several new insights into the functions of the semaphorin 4C (SEMA4C) signaling pathway promoting osteosarcoma progression and metastasis. SEMA4C has been shown to be highly expressed relative to control tissues and cell lines. Its heightened expression and signaling through its cognate receptor PLXNB2 correlates to patient outcomes in some solid cancers (Butti, Kumar, Nimma, & Kundu, 2018). Our results demonstrate high level cytoplasmic/membraneous SEMA4C expression in malignant primary patient tissues which suggests SEMA4C is targetable on the cell surface. Activation of PLXNB2 signaling by its ligand SEMA4C is likely to occur via autocrine mechanisms in co-expressing tumor cells and via paracrine signaling when PLXNB2 is stimulated from SEMA4C-producing cells in the microenvironment. Our study demonstrates that cultured normal osteoblasts and osteosarcoma cell lines indeed express both soluble SEMA4C and cognate receptor PLXNB2, but interestingly membrane-bound SEMA4C was only found to

be detectable in osteosarcoma cell lines *in vitro* as assessed by western blot. This data supports both autocrine and paracrine capabilities, but at an exaggerated level similar to previous findings in tumor-associated lymphatic endothelial cells and breast cancer (Gurrapu et al., 2018; Wei et al., 2017). These elevated levels suggest that osteosarcoma cells are also genetically and phenotypically distinct from that of their normal counterparts.

Accumulating evidence suggests that SEMA4C-PLXNB2 interactions can promote an oncogenic signaling axis. Recent reports from Gurrapu et al. and Le et al. established that SEMA4C-PLXNB2 signaling promotes cancer cell proliferation, migration, and tumorigenesis in breast and glioma tumor cells respectively (Gurrapu et al., 2018; Le et al., 2015). In our study, we demonstrated that SEMA4C directs both 2D and 3D growth *in vitro* as well as modulates invasive cell motility and adhesion in osteosarcoma. These phenotypes were associated with large perturbations in activated AKT signaling. In particular, genetic silencing of SEMA4C induced G1 cell cycle delay, which has been well-established and linked with changes in PI3K pathway signaling (García, Kumar, Marqués, Cortés, & Carrera, 2006). These *in vitro* findings were further substantiated by our mouse studies. We injected two SEMA4C knockdown cell lines into mice using a highly relevant orthotopic mouse model of osteosarcoma (Smeester et al., 2012; Smeester et al., 2013). SEMA4C knockdown tumor cells exhibited reduced tumor growth, micrometastatic nodule formation, and area. These data indicate a diverse role for SEMA4C in osteosarcoma growth, metastasis, and maintenance.

Among the family of SEMA4 members, several recent reports have demonstrated that SEMA4C also regulates EMT (Yang et al., 2015; Zhou et al., 2013). While this phenomenon has been well-established in cancers of epithelial origin (Roche, 2018), the precise and novel roles EMT factors play in a characteristically mesenchymal cancer such as osteosarcoma, remain to be determined. In agreement with other reports in controlling EMT (Yang et al., 2015; Zhou et al., 2013), our results suggest high level SEMA4C expression promotes invasive cell motility, is associated with mesenchymal marker expression, and can be reversed through genetic disruption. Excitingly, TWIST1 was significantly altered in both of our SEMA4C gain-of-function (GOF) and loss-of-function (LOF) studies. Research from Yin and colleagues suggests TWIST1 is associated with poor prognoses in osteosarcoma and can be used as a prognostic indicator of metastatic potency in patients (Yin, Liao, He, & Zhong, 2012). Moreover, in a study of 206 unique bone tumors, TWIST1 expression was one of three markers in a panel that afforded the most sensitive and specific diagnostic utility among varied bone tumor types (Horvai, Roy, Borys, & O'Donnell, 2012). TWIST1 is also essential for tumor initiation and maintaining a mesenchymal state in synovial sarcomas (Lee, Lee, Ham, Roh, & Kim, 2014). Reactivation of TWIST1 can also promote metastasis in other sarcomas such as Ewing's sarcoma (Choo, Wang, Newbury, Roberts, & Yang, 2018). The continued demonstration of the plasticity of TWIST1 and other mesenchymal markers in maintaining phenotypes associated with many aspects of osteosarcomagenesis, progression, and metastasis has led to the central belief

of skeletal cancer stem cells (Leder, Holland, & Michor, 2010; Poleszczuk & Enderling, 2016), of which have been just recently identified (Chan et al., 2018). High level expression of SEMA4C may help facilitate a hyper-mesenchymal state in osteosarcoma and/or even allow a plasticity that contributes to many of the phenotypes our study illustrates, including wound healing (Lamouille, Xu, & Derynck, 2014), cellular adhesion (Kumar, Das, & Sen, 2014), tumor growth, and metastasis (Ye & Weinberg, 2015).

The findings of our work may be highly relevant to the clinical setting. To date, metastases to the lungs remains the number one cause of osteosarcoma-related death (Meazza & Scanagatta, 2016). Our monoclonal antibody blockade studies support the concept of targeting SEMA4C therapeutically. Targeted blockade of SEMA4C-induced signaling appreciably slowed tumor cell proliferation and migration *in vitro*. These phenotypic changes were again accompanied by G1 cell cycle delay. Together, these data suggest a rationale for SEMA4C blockade as a potential novel treatment option for patients with metastatic osteosarcoma. Recent studies on SEMA4D, a type IV semaphorin member that can also signal through PLXNB2 (Deng et al., 2007), suggests high level expression restricts tumoricidal immune cells from entering the tumor microenvironment and blunts their activity, however, monoclonal antibody neutralization by an anti-Sema4d antibody (murine: mAb67-2, human: VX15/2503; Vaccinex, Inc.) could restore these deficits in combination with anti-Ctla-4 or anti-Pd-1 checkpoint blockade (Clavijo et al., 2018; Evans, Jonason, et al., 2015; Evans, Paris, Smith, & Zauderer, 2015). Likewise, antibody targeting of

SEMA4C could be highly advantageous for these same reasons and others we posit here. This could allow expansion of the poor portfolio of therapies available to metastatic osteosarcoma patients and may also be applied to other cancer types in which high SEMA4C expression is clinically relevant.

SEMA4C positive tumor cells are an attractive target therapeutically. These results suggest the possibility of SEMA4C as a novel therapeutic target for the treatment of incurable metastatic osteosarcoma.

Figure 1. SEMA4C is upregulated in a subset of osteosarcoma tissue samples and cell lines

A. Relative *SEMA4C* RNA expression levels in normal human osteoblasts (n = 3) compared to two individual osteosarcoma patient sample data sets (#1: n = 12, #2: n = 184). Data shown are fold change compared to osteoblasts ± SEM; **p* < 0.05; unpaired Student's T-test. **B.** Summary of scores identified in human osteosarcoma TMA following staining with anti-SEMA4C. **C.** Representative images of SEMA4C staining with each expression intensity and number of sections with indicated staining. Representative images are shown at 20X; insets are 40X. Scale bars = 25 and 50 μm where indicated. **D.** Western blots of SEMA4C and cognate receptor PLXNB2 expression in normal human osteoblasts (NHO) and osteosarcoma cell lines. **E.** ELISA analysis of soluble SEMA4C expression in NHOs and osteosarcoma cell supernatants. Data shown as mean ± SEM (n = 2/group); **p* < 0.05, ***p* < 0.01; One-way ANOVA.

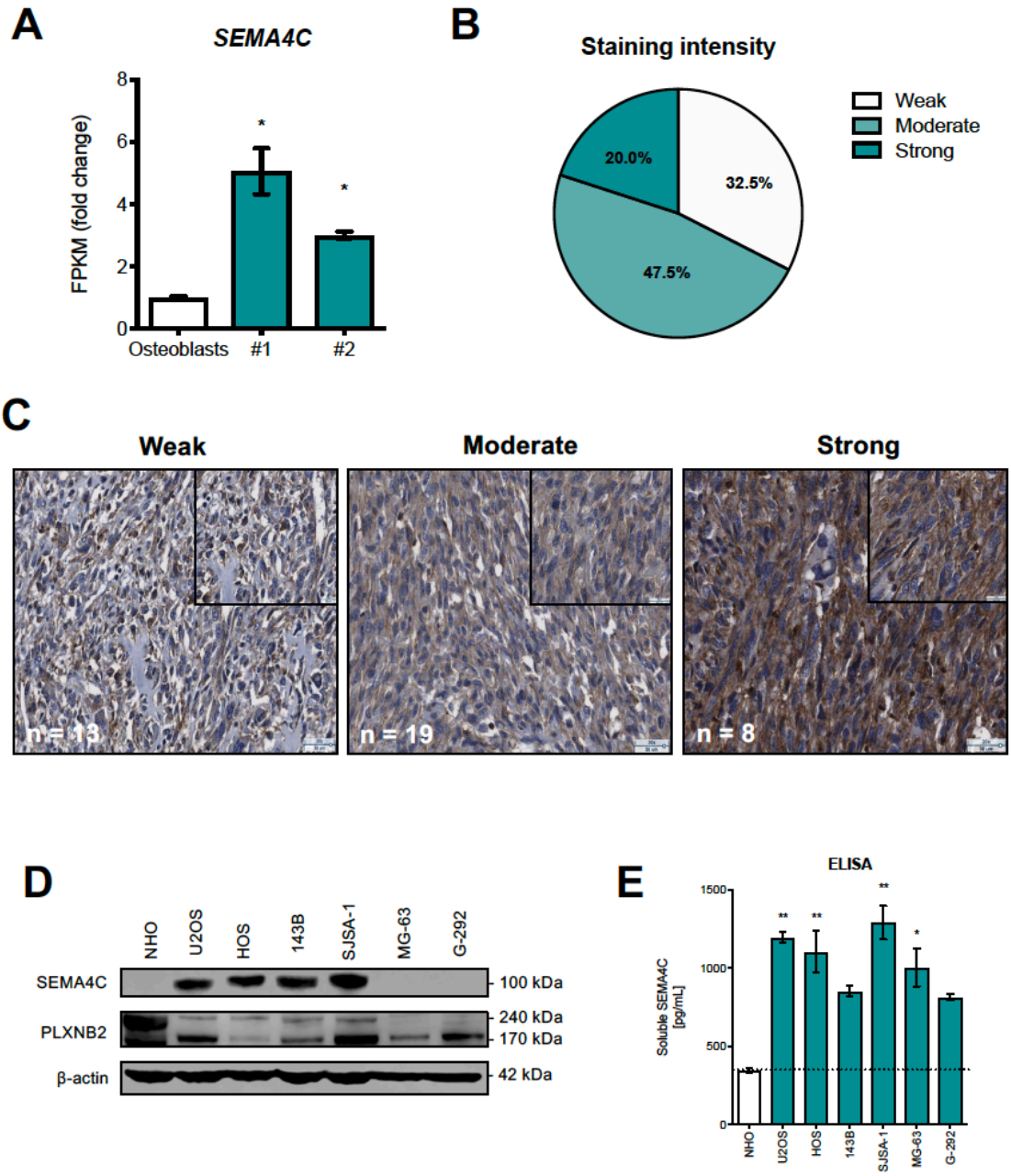
A
SEMA4C
FPKM (fold change)
8
6
4
2
0
*
*
Osteoblasts
#1
#2
B
Staining intensity
Weak
Moderate
Strong
20.0%
32.5%
47.5%
C
Weak
Moderate
Strong
n = 13
n = 19
n = 8
D
NHO
U2OS
HOS
143B
SJSA-1
MG-63
G-292
SEMA4C
PLXNB2
β-actin
100 kDa
240 kDa
170 kDa
42 kDa
E
ELISA
Soluble SEMA4C [pg/mL]
1500
1000
500
0
**
**
**
*
NHO
U2OS
HOS
143B
SJSA-1
MG-63
G-292

Figure 2. *SEMA4C* overexpression promotes increased cellular growth, colony formation, and migration in osteosarcoma cell lines

A. Western blots confirming overexpression of SEMA4C. **B.** *SEMA4C* overexpression increases the proliferation of osteosarcoma cell lines. Data shown as fold change ± SEM (n = 18/group); **p* < 0.05, *****p* < 0.0001; Two-way ANOVA. **C.** *SEMA4C* overexpression promotes anchorage-independent growth. Data as fold change ± SEM (n = 36/group); **p* < 0.05, *****p* < 0.0001; unpaired Student's T-tests. **D.** *SEMA4C* overexpression modulates migration. Data as fold change ± SEM (n = 12/group); ****p* < 0.001, *****p* < 0.0001; unpaired Student's T-tests. **E.** Representative images of cellular migration. **F.** Western blots of activated AKT signaling in *SEMA4C*-overexpressing cell lines. **G.** Relative expression of mesenchymal marker genes in cell lines ± *SEMA4C* overexpression (n = 3/group); multiple Student's T-tests.

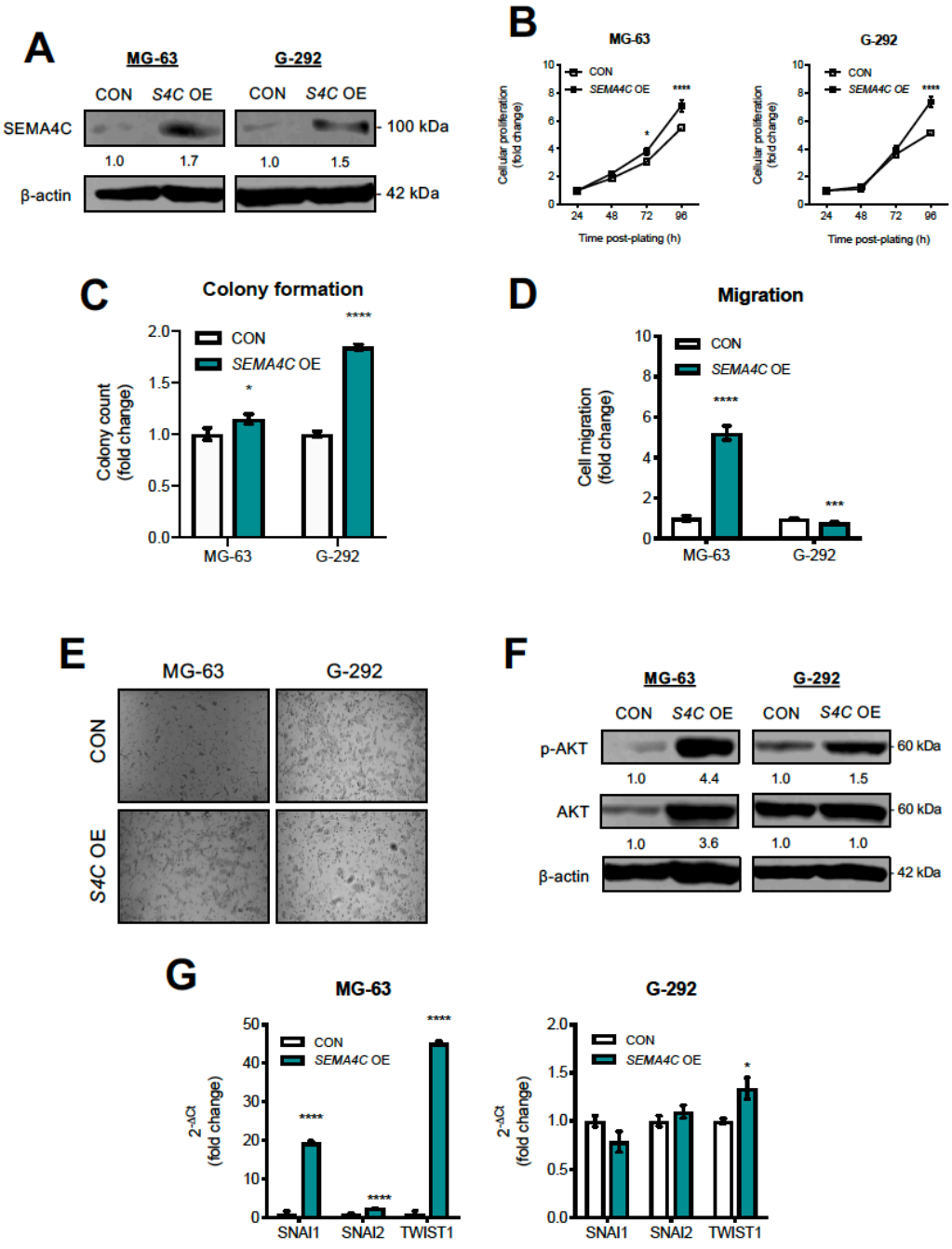
A
MG-63
G-292
CON
S4C OE
CON
S4C OE
SEMA4C
100 kDa
1.0
1.7
1.0
1.5
β-actin
42 kDa
B
MG-63
G-292
CON
SEMA4C OE
Cellular proliferation (fold change)
Time post-plating (h)
C
Colony formation
Colony count (fold change)
MG-63
G-292
D
Migration
Cell migration (fold change)
E
MG-63
G-292
CON
S4C OE
F
MG-63
G-292
p-AKT
AKT
β-actin
60 kDa
42 kDa
1.0
4.4
1.5
3.6
G
MG-63
G-292
2-ΔCt (fold change)
SNAI1
SNAI2
TWIST1

Figure 3. Knockdown of SEMA4C reduces cellular growth, colony formation, and promotes cell cycle delay

A. Confirmation of SEMA4C knockdown via qRT-PCR. Data shown as fold change ± SEM (n = 3/group); ***p* < 0.01, *****p* < 0.0001; One-way ANOVA. **B.** Western blots of SEMA4C in control shCON and shSEMA4C cell lines. **C.** Knockdown of SEMA4C reduces cellular proliferation. Data as fold change ± SEM (n = 18/group); *****p* < 0.0001; Two-way ANOVA. **D.** Colony formation in SEMA4C knockdown cell lines. Data as fold change ± SEM (n = 36/group); *****p* < 0.0001; unpaired Student's T-test. **E.** Western blots of activated AKT signaling in SEMA4C knockdown cells. **F**. Silencing of SEMA4C induces G1 cell cycle delay; Data shown as number of cells ± SEM (n = 3/group); Two-way ANOVA.

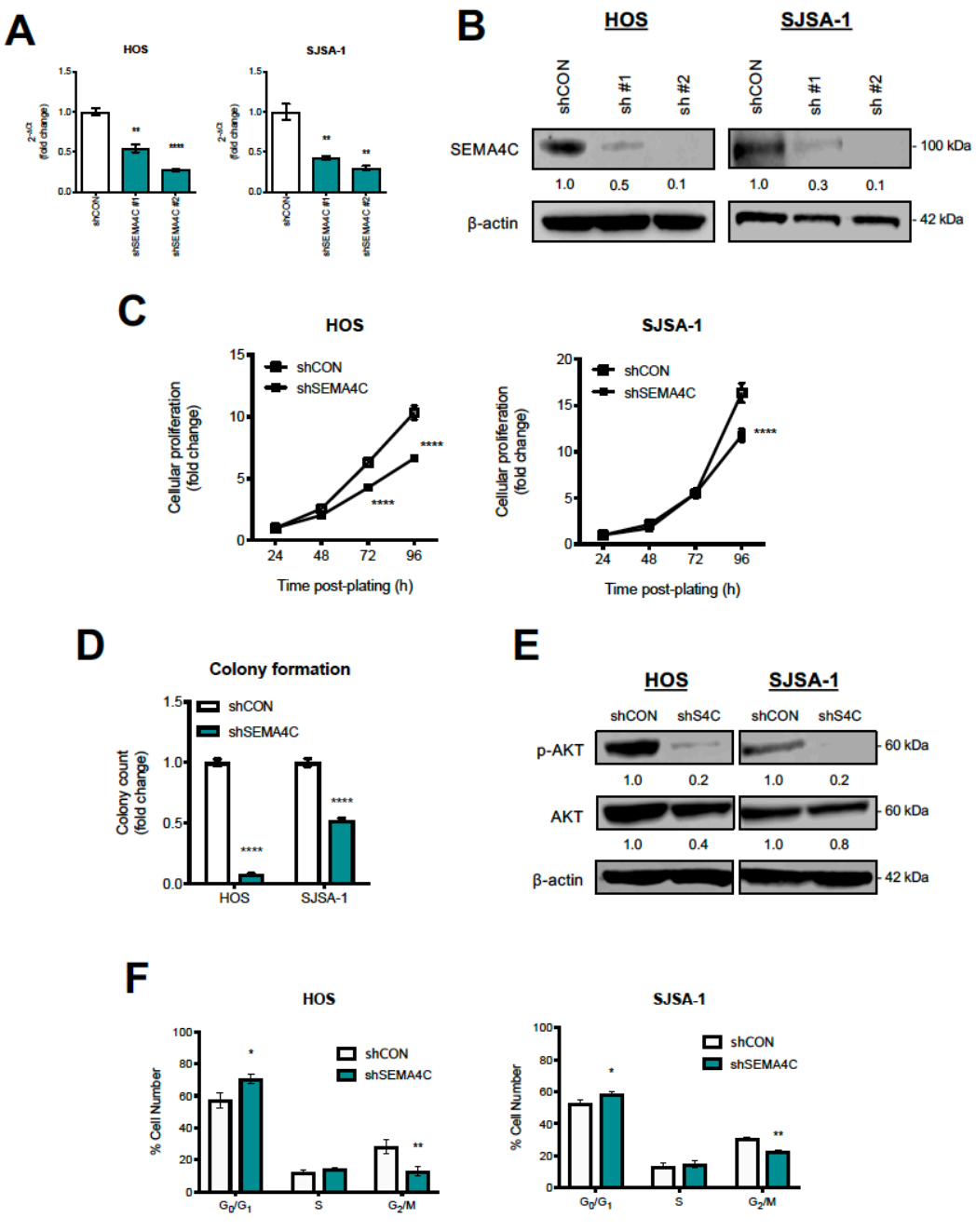
A
HOS
SJSA-1
shCON
shSEMA4C #1
shSEMA4C #2
B
HOS
SJSA-1
shCON
sh #1
sh #2
SEMA4C
100 kDa
1.0
0.5
0.1
1.0
0.3
0.1
β-actin
42 kDa
C
HOS
SJSA-1
shCON
shSEMA4C
Cellular proliferation (fold change)
Time post-plating (h)
24
48
72
96
****
D
Colony formation
shCON
shSEMA4C
Colony count (fold change)
HOS
SJSA-1
E
HOS
SJSA-1
shCON
shS4C
p-AKT
60 kDa
1.0
0.2
AKT
1.0
0.4
β-actin
42 kDa
F
HOS
SJSA-1
shCON
shSEMA4C
% Cell Number
G0/G1
S
G2/M

Figure 4. SEMA4C knockdown reduces cell motility, promotes adhesion, and downregulates mesenchymal marker expression

A. Knockdown of SEMA4C reduces cellular migration. Data as fold change ± SEM (n = 12/group); ** $p < 0.01$, **** $p < 0.0001$; unpaired Student's T-test. **B.** Representative cellular migration images in knockdown cell lines. **C.** Silencing of SEMA4C increases cellular adhesion in HOS cells (n = 5-6/group); * $p < 0.05$; unpaired Student's T-test. **D.** Representative images of cellular adhesion 24 hours post. **E.** Wound closure rate in SEMA4C-deficient cells (n = 36/group); * $p < 0.05$; unpaired Student's T-test. **F.** qRT-PCR of mesenchymal markers. Data as fold change ± SEM (n = 3/group); *** $p < 0.001$, **** $p < 0.0001$; multiple Student's T-tests.

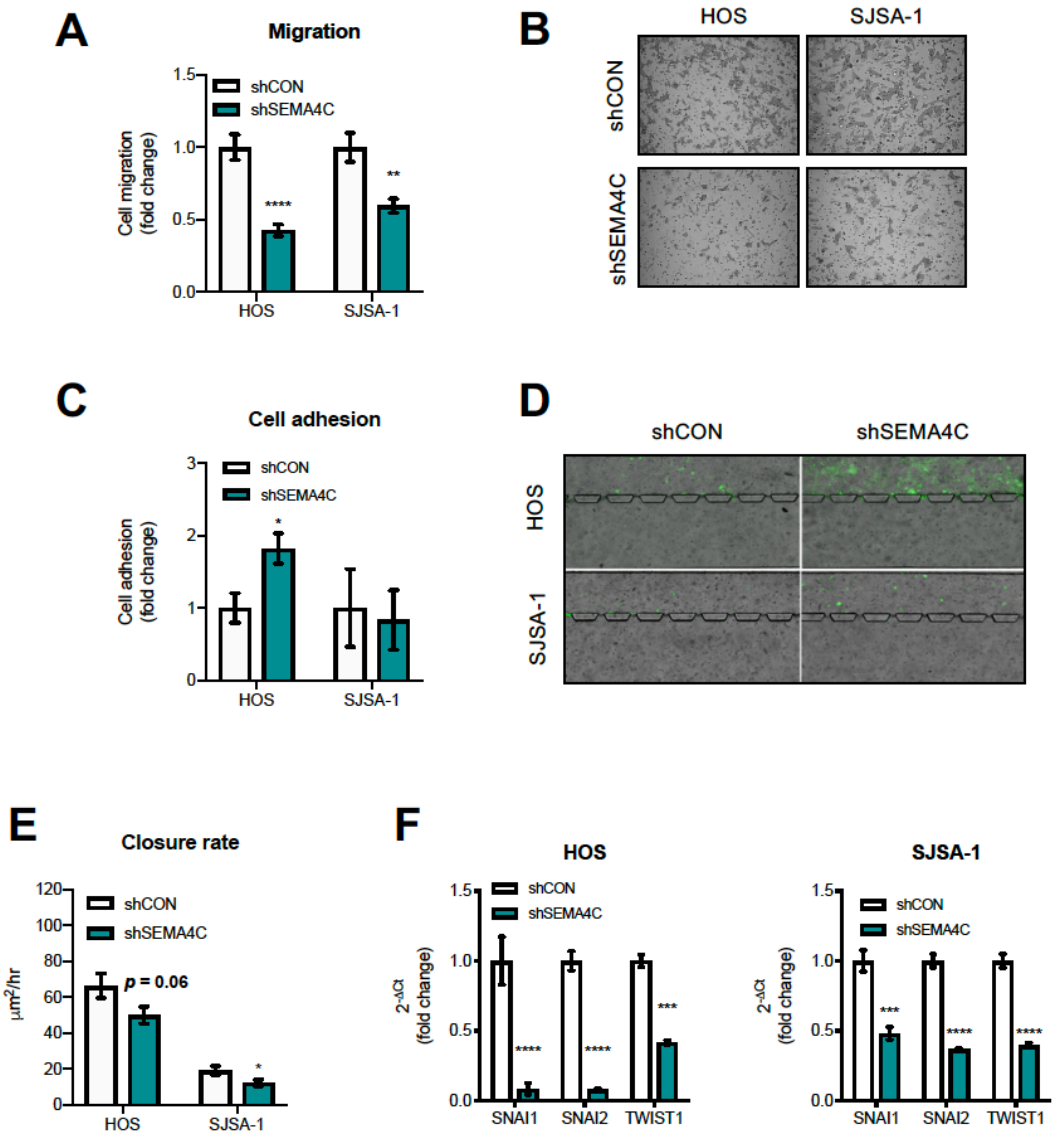
A
Migration
shCON
shSEMA4C
Cell migration (fold change)
1.5
1.0
0.5
0.0
****
**
HOS
SJSA-1
B
HOS
SJSA-1
shCON
shSEMA4C
C
Cell adhesion
shCON
shSEMA4C
Cell adhesion (fold change)
3
2
1
0
*
HOS
SJSA-1
D
shCON
shSEMA4C
HOS
SJSA-1
E
Closure rate
shCON
shSEMA4C
µm²/hr
120
100
80
60
40
20
0
p = 0.06
*
HOS
SJSA-1
F
HOS
SJSA-1
shCON
shSEMA4C
2-ΔCt (fold change)
1.5
1.0
0.5
0.0
****
***
SNAI1
SNAI2
TWIST1

Figure 5. SEMA4C knockdown decreases osteosarcoma tumor growth and lung metastasis

A. Tumor volume measurements in SEMA4C knockdown orthotopic injections. Data shown as mean volume in $mm^3 \pm$ SEM; *$p < 0.05$, ***$p < 0.001$, ****$p < 0.0001$; Two-way ANOVA. **B.** Representative gross lung images from a HOS control and SEMA4C knockdown animal. White arrows indicate macrometastatic nodules. **C.** Representative western blot images in control and SEMA4C knockdown animals from each cell line. **D.** SEMA4C knockdown and reductions in p-AKT signaling were confirmed via densitometry. **E.** Number of micrometastatic lung nodules/section. Data shown as mean number of nodules $\pm$ SEM (n = 36/group); ****$p < 0.0001$; unpaired Student's T-test. **F.** Area measurements of micrometastases in sections. Data shown as mean area $\pm$ SEM (n = 36/group); ****$p < 0.0001$; unpaired Student's T-test. **G.** Representative H & E lung images are shown at 20X; insets are 40X. Black arrows indicate micrometastases, Scale bars = 100 μm.

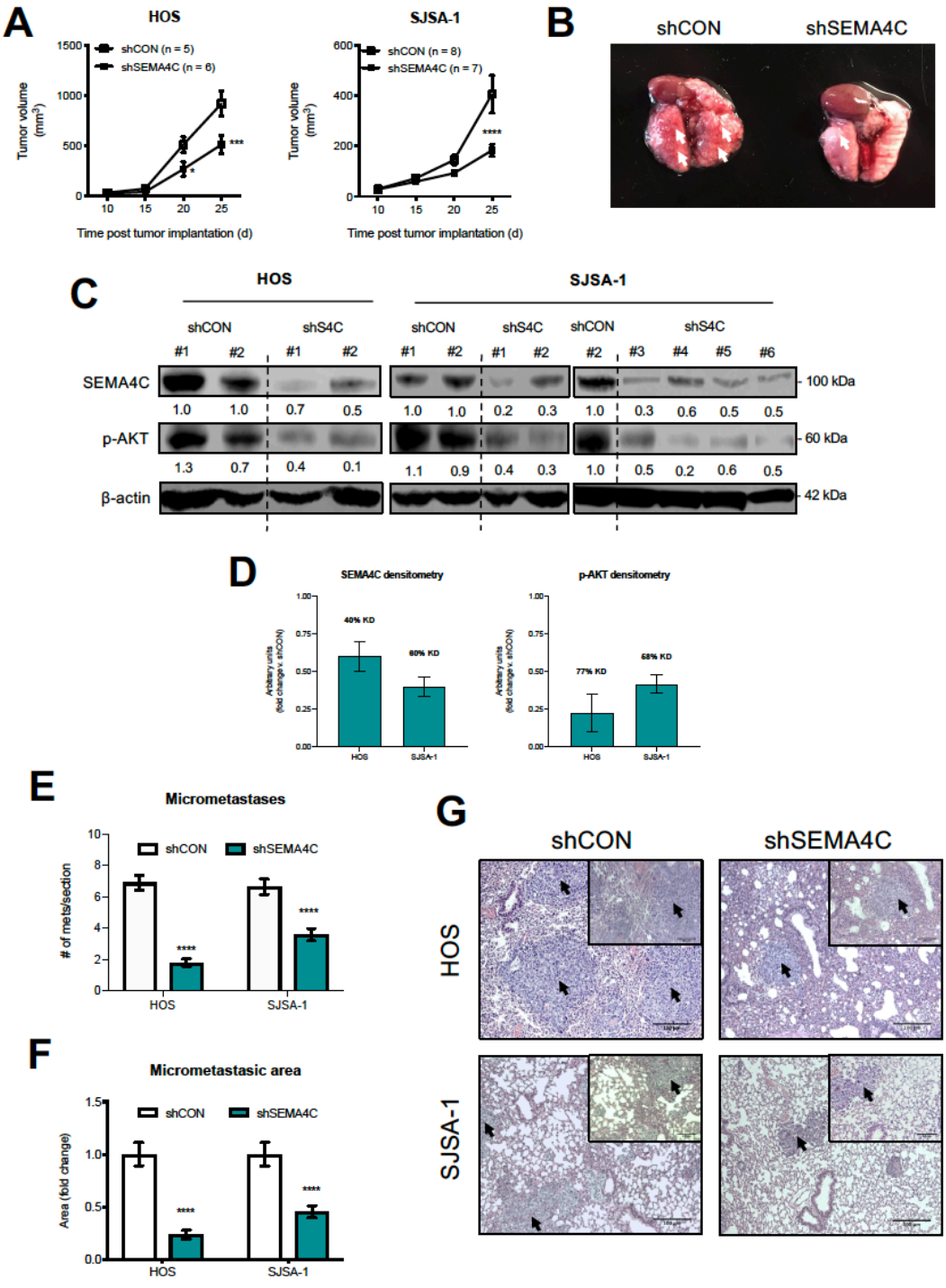
A
HOS
shCON (n = 5)
shSEMA4C (n = 6)
Tumor volume (mm3)
Time post tumor implantation (d)
SJSA-1
shCON (n = 8)
shSEMA4C (n = 7)
Tumor volume (mm3)
Time post tumor implantation (d)
B
shCON
shSEMA4C
C
HOS
SJSA-1
shCON
shS4C
SEMA4C
p-AKT
β-actin
100 kDa
60 kDa
42 kDa
D
SEMA4C densitometry
p-AKT densitometry
40% KD
60% KD
77% KD
68% KD
HOS
SJSA-1
E
Micrometastases
# of mets/section
shCON
shSEMA4C
HOS
SJSA-1
F
Micrometastasic area
Area (fold change)
G
shCON
shSEMA4C
HOS
SJSA-1

Figure 6. Anti-SEMA4C monoclonal antibody blockade is effective *in vitro*

A. SEMA4C antibody blockade reduces cellular growth following a 48-hour incubation in osteosarcoma cell lines only. Data as fold change ± SEM (n = 18); ****$p < 0.0001$; One-way ANOVA. **B.** Antibody blockade reduces cellular migration. Data shown as fold change ± SEM (n = 12); ****$p < 0.0001$; Student's T-test. **C.** Representative images of migration in isotype control IgG and anti-SEMA4C treated lines. **D.** Anti-SEMA4C treatment induces G1 cell cycle delay. Data shown as number of cells ± SEM (n = 3); *$p < 0.05$, **$p < 0.01$, ***$p < 0.001$, ****$p < 0.0001$; Two-way ANOVA. **E.** Model of SEMA4C function. SEMA4C promotes downstream activation of AKT signaling which ultimately leads to upregulation of mesenchymal genes, promotion of cellular migration, proliferation, tumor growth, and metastasis. Monoclonal antibody blockade can effectively inhibit these downstream events and induce cell cycle delay. $S4C_{TM}$ = transmembrane SEMA4C, $S4C_{sol}$ = soluble SEMA4C.

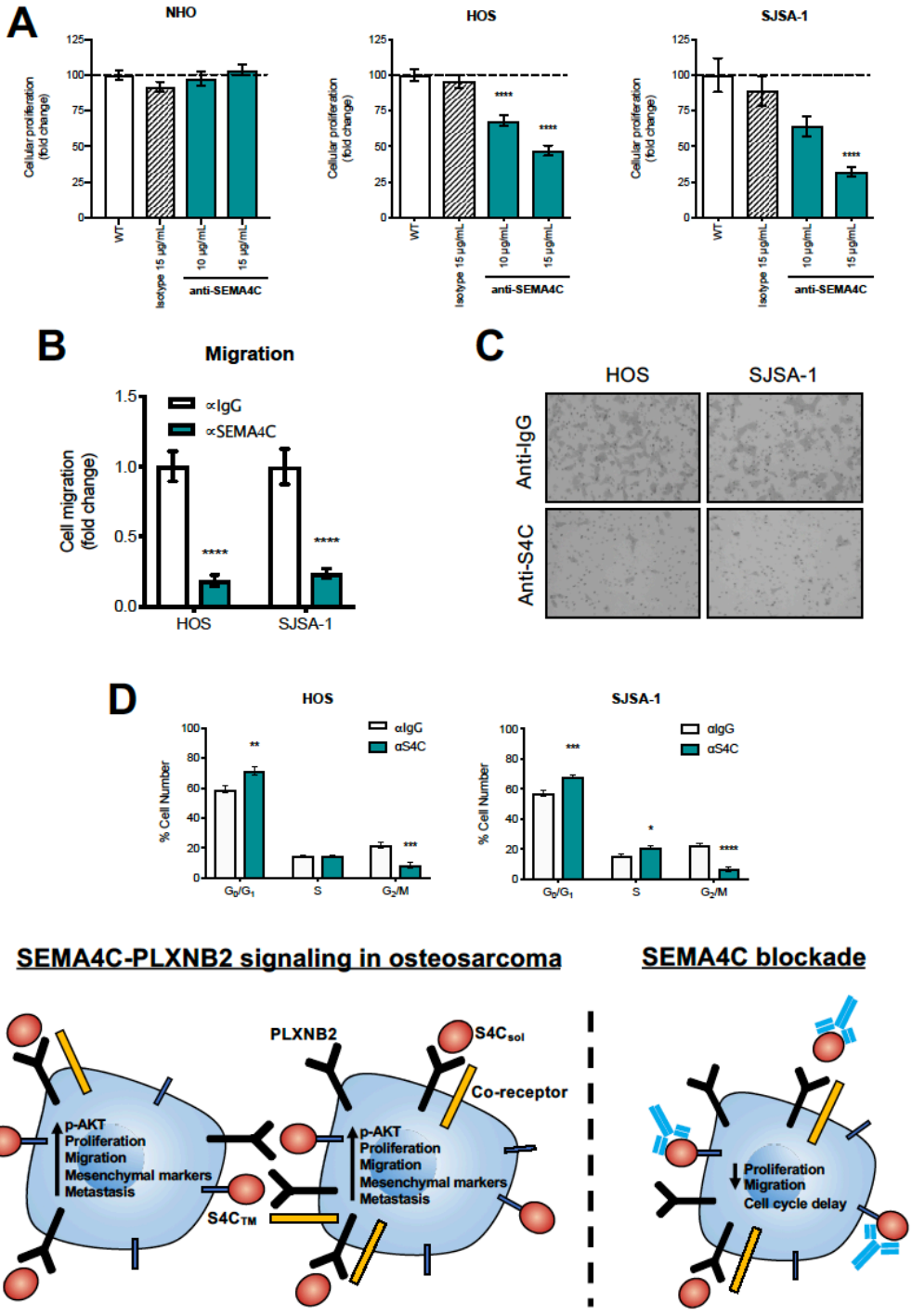
A
NHO
HOS
SJSA-1
Cellular proliferation (fold change)
WT
Isotype 15 µg/mL
10 µg/mL
15 µg/mL
anti-SEMA4C
B
Migration
∝IgG
∝SEMA4C
Cell migration (fold change)
HOS
SJSA-1
C
HOS
SJSA-1
Anti-IgG
Anti-S4C
D
HOS
SJSA-1
αIgG
αS4C
% Cell Number
G0/G1
S
G2/M
E
SEMA4C-PLXNB2 signaling in osteosarcoma
SEMA4C blockade
PLXNB2
S4Csol
Co-receptor
S4CTM
p-AKT
Proliferation
Migration
Mesenchymal markers
Metastasis
Proliferation
Migration
Cell cycle delay

Supplementary Figure 1. Increased SEMA4C expression is associated with osteosarcoma

A. Summary of the percent positive SEMA4C staining per section in a human osteosarcoma TMA. Data shown as number of samples with indicated percent staining in each of the four categories. **B.** Bar graph depicting percentage of SEMA4C staining localization (cytoplasmic/membraneous, nuclear, or both). SEMA4C staining was predominantly cytoplasmic/membraneous in sections.

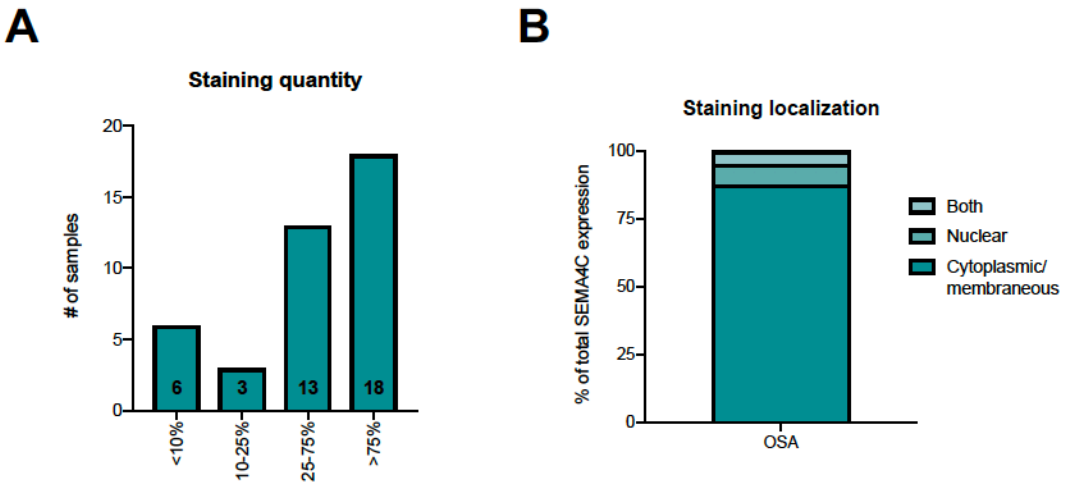
A
Staining quantity
# of samples
20
15
10
5
0
6
3
13
18
<10%
10-25%
25-75%
>75%
B
Staining localization
% of total SEMA4C expression
100
75
50
25
0
OSA
Both
Nuclear
Cytoplasmic/
membraneous

Supplementary Figure 2. Silencing of SEMA4C does not induce apoptosis

A. Representative flow cytometry plots of cleaved CASP3 positivity (cCas3+) in SEMA4C knockdown cell lines. **B.** Quantification of flow cytometry plots. Data shown as mean area ± SEM (n = 3); $p > 0.05$; unpaired Student's T-test.

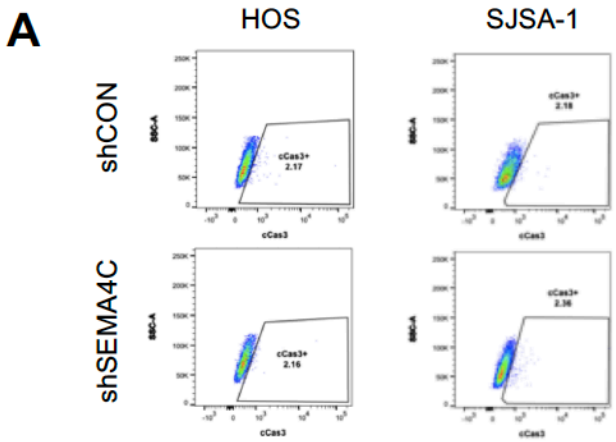
A
HOS
SJSA-1
shCON
shSEMA4C
cCas3+
2.17
cCas3+
2.18
cCas3+
2.16
cCas3+
2.36
cCas3
B
Cell death; HOS
Cell death; SJSA-1
% cCas3+
15
10
5
0
4
3
2
1
shCON
shSEMA4C

Supplementary Figure 3. Description of 3D microfluidic chambers and representative images

A. An AutoCAD schematic of the entire device. **B.** Collagen (blue) is allowed to polymerize in the lower channel, then human umbilical vein endothelial cells (HUVECs, orange) are perfused through the adjacent channel. **C.** HUVECs are allowed to become confluent. Green fluorescent protein (GFP)-expressing cancer cells are perfused through the endothelial cell channel. **D.** Modified osteosarcoma cell lines adhere to the endothelium and may transmigrate and invade into the collagen.

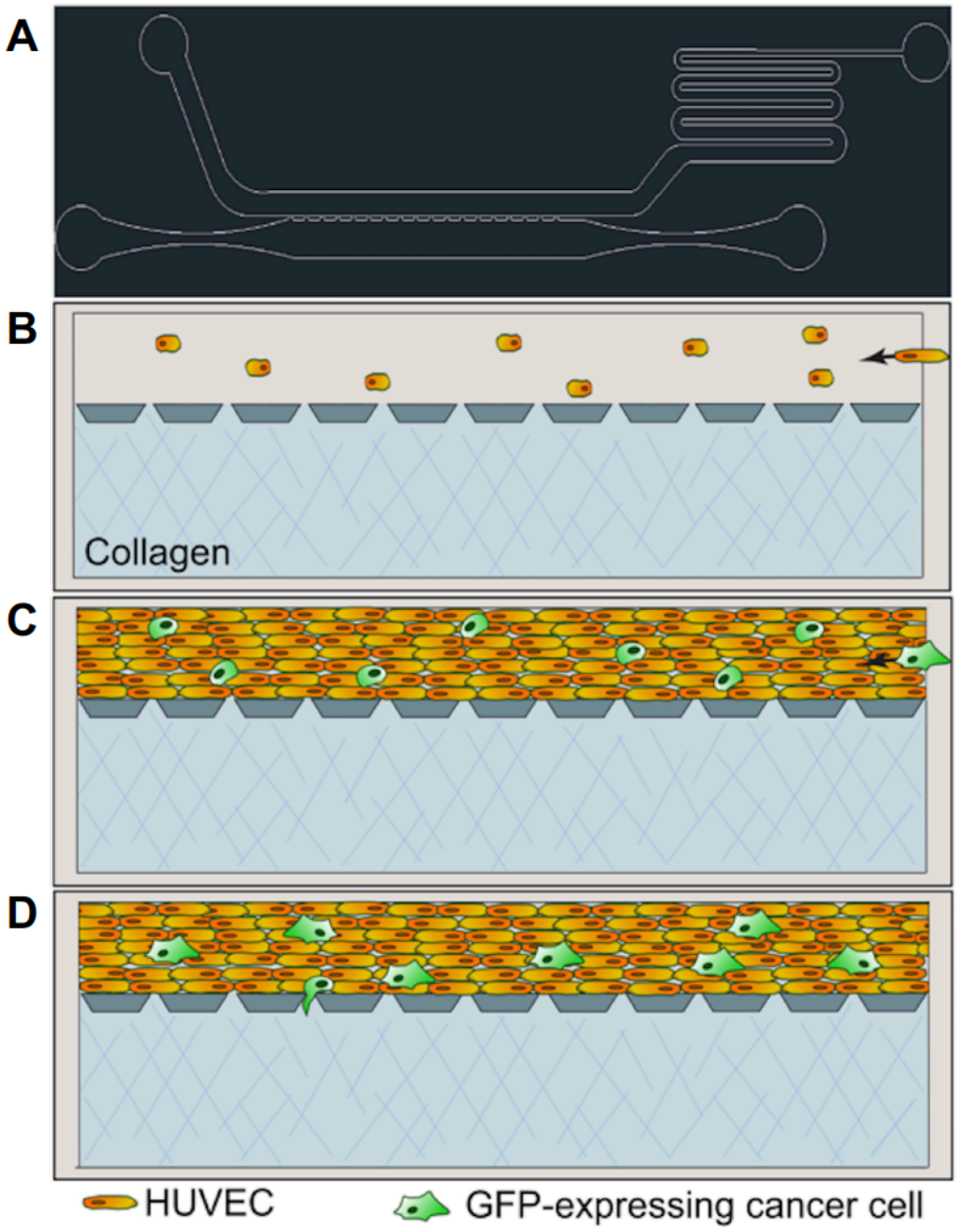
A
B
Collagen
C
D
HUVEC
GFP-expressing cancer cell

Supplementary Figure 4. Representative illustration of wound closure assay analysis

A. Representative photo montages of phase contrast images of wound closure assays in cell lines ± SEMA4C deficiency at indicated time points.

A

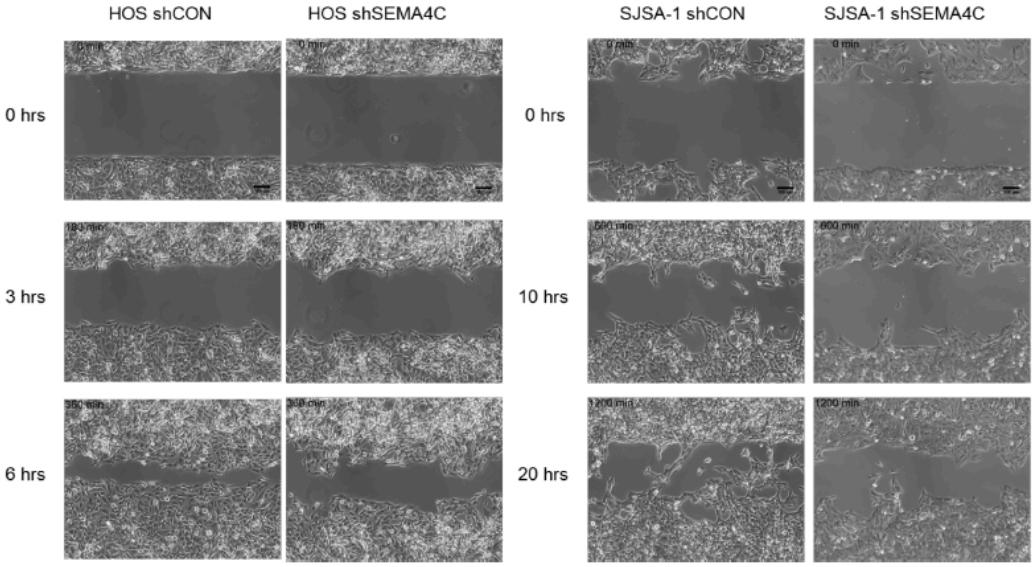
HOS shCON
HOS shSEMA4C
SJSA-1 shCON
SJSA-1 shSEMA4C
0 hrs
3 hrs
6 hrs
0 hrs
10 hrs
20 hrs

Supplementary Table 1.

Table of primer sequences used in this manuscript.

Primary antibodies				
Antigen	**Source**	**Dilution**	**Catalog**	**Company**
SEMA4C	Mouse	1:250	136445	Santa Cruz Biotechnology
PLXNB2	Sheep	1:500	AF5329	R & D Systems
p-AKT (Ser473)	Rabbit	1:1000	4060	Cell Signaling Technologies
AKT	Rabbit	1:1000	4691	Cell Signaling Technologies
B-ACTIN	Mouse	1:5000	3700	Cell Signaling Technologies

Supplementary Table 2.

Table of all antibodies used in manuscript.

qRT-PCR primers		
Target	**Sense**	**Anti-sense**
SNAI1	5'-GCAAATACTGCAACAAGG-3'	5'-GCACTGGTACTTCTTGACA-3'
SNAI2	5'-AGATGCATATTCGGACCCAC-3'	5'-CCTCATGTTTGTGCAGGAGA-3'
TWIST1	5'-GGAGTCCGCAGTCTTACGAG-3'	5'-TCTGGAGGACCTGGTAGAGG-3'
B-ACTIN	5'-CACAGGGGAGGTGATAGCAT-3'	5'-CTCAAGTTGGGGGACAAAAA-3'

CHAPTER 4

PLX3397 treatment inhibits constitutive CSF1R-induced oncogenic ERK signaling, reduces tumor growth, and metastatic burden in osteosarcoma

*Branden A. Smeester[1,3,4], *Nicholas J. Slipek[1,3,4], Emily J. Pomeroy[1,3,4], Kanut Laoharawee[1,3,4], Sara H. Osum[1,3,4], Alex T. Larsson[4], Kyle B. Williams[1,3,4], Natalie Stratton[1], Kenta Yamamoto[1,3], Joseph J. Peterson[1], Susan K. Rathe[1,4], Lauren J. Mills[1,6], Wendy A. Hudson[1,4], Margaret R. Crosby[1,4], Minjing Wang[1,3,4], Eric P. Rahrmann[5], *Branden S. Moriarity[1,3,4], *David A. Largaespada[1,2,3,4]

[1]Department of Pediatrics, University of Minnesota
[2]Department of Genetics, Cell Biology and Development, University of Minnesota
[3]Center for Genome Engineering, University of Minnesota
[4]Masonic Cancer Center, University of Minnesota
[5]Cancer Research UK Cambridge Institute, University of Cambridge
[6]Childhood Cancer Genomics Group, University of Minnesota

*Contributed equally

A published version of this chapter is available below:

Smeester BA, Slipek NJ, Pomeroy EJ, Osum SH, Larsson AT, Peterson JJ, Rathe SK, Hudson WA, Wang M, Laoharawee K, Stratton N, Rahrmann EP, Moriarity BS, Largaespada DA. PLX3397 treatment inhibits constitutive CSF1R-induced oncogenic ERK signaling, reduces tumor growth, and metastatic burden in osteosarcoma. Bone. Apr 3:115353. doi: 10.1016/j.bone.2020.115353.

Conception and design: BAS, NJS, BSM, DAL
Development and acquisition of data: BAS, NJS, EJP, KL, SHO, ATL, KBW, NS, KY, JJP, SKR, LJM, WAH, MRC, MW, EPR
Analysis and interpretation: BAS, NJS, BSM, DAL
Writing, review and revisions: BAS, NJS, EJP, KL, SHO, ATL, KBW, NS, KY, JJP, SKR, LJM, WAH, MRC, MW, EPR, BSM, DAL
Study oversight: BAS, NJS, BSM, DAL

Summary

Osteosarcoma (OSA) is a heterogeneous and aggressive solid tumor of the bone. We recently identified the colony stimulating factor 1 receptor (*Csf1r*) gene as a novel driver of osteosarcomagenesis in mice using the *Sleeping Beauty* (SB) transposon mutagenesis system. Here, we report that a CSF1R-CSF1 autocrine/paracrine signaling mechanism is constitutively activated in a subset of human OSA cases and is critical for promoting tumor growth and contributes to metastasis. We examined CSF1R and CSF1R expression in OSAs. We utilized gain-of-function and loss-of-function studies (GOF/LOF) to evaluate properties of cellular transformation, downstream signaling, and mechanisms of CSF1R-CSF1 action. Genetic perturbation of CSF1R in immortalized osteoblasts and human OSA cell lines significantly altered oncogenic properties, which were dependent on the CSF1R-CSF1 autocrine/paracrine signaling. These functional alterations were associated with changes in the known CSF1R downstream ERK effector pathway and mitotic cell cycle arrest. We evaluated the recently FDA-approved CSF1R inhibitor Pexidartinib (PLX3397) in OSA cell lines *in vitro* and *in vivo* in cell line and patient-derived xenografts. Pharmacological inhibition of CSF1R signaling recapitulated the *in vitro* genetic alterations. Moreover, in orthotopic OSA cell line and subcutaneous patient-derived xenograft (PDX)-injected mouse models, PLX3397 treatment significantly inhibited OSA tumor growth and lessened metastatic burden. In summary, CSF1R is utilized by OSA cells to promote tumorigenesis and may represent a new molecular target for therapy.

Introduction

Osteosarcoma (OSA) is a rare and aggressive cancer affecting the growing long bones of adolescents and is characterized by a high propensity to metastasize to the lungs (Misaghi, Goldin, Awad, & Kulidjian, 2018). While the current standard of care improves survival outcomes in patients with localized disease, neo-adjuvant chemotherapy fails to provide any substantial survival benefit to patients with lung metastases (Durfee, Mohammed, & Luu, 2016; Misaghi et al., 2018). A hallmark of OSA is widespread genomic instability, and a paucity of obvious activated oncogenes, making it difficult to identify specific drivers of OSA development and fatal metastatic spread (Kuijjer, Hogendoorn, & Cleton-Jansen, 2013). Also, heterogeneity between individual tumors is considered one of the major reasons for the lack of progress in leveraging any targetable drivers to date (Sayles et al., 2019). Therefore, it is imperative that we improve our understanding of commonly altered OSA-specific signaling pathways known to promote malignancy and tumor maintenance in order to develop effective molecularly targeted therapies for patients with metastatic disease (Saraf, Fenger, & Roberts, 2018). For these reasons, we performed a *Sleeping Beauty* (SB) transposon-based forward genetic screen for OSA which identified numerous (>250) previously unknown drivers of OSA development and metastasis (Moriarity et al., 2015). In particular, *Csf1r* (c-fms proto-oncogene) was identified as a candidate OSA driver oncogene in a subset of our primary OSA samples (Moriarity et al., 2015).

CSF1R is a transmembrane, tyrosine kinase receptor known to mediate cellular effects of macrophage colony stimulating factor 1 (M-CSF, also known as CSF1) and is primarily expressed by cells in the mononuclear phagocytic lineage (Stanley & Chitu, 2014). In normal growing bones, osteoblasts produce CSF1, which stimulates proliferation and differentiation of CSF1R-expressing osteoclast progenitors (Wittrant, Gorin, Mohan, Wagner, & Abboud-Werner, 2009). We hypothesized that increased CSF1R expression could potentiate CSF1-induced signaling in OSA and may represent a therapeutically exploitable pro-tumorigenic, autocrine/paracrine signaling loop. To test this hypothesis, we characterized CSF1R expression and signaling in OSA and coupled these studies with therapeutic targeting of active signaling using a small molecule inhibitor of CSF1R. Together, our studies demonstrate that CSF1R is highly expressed and constitutively active in a subset of OSA samples, CSF1R-CSF1 signaling is oncogenic in immortalized osteoblasts and OSA cell lines, and CSF1R tyrosine kinase inhibition reduces properties of cellular transformation *in vitro* and OSA tumor growth and metastatic burden *in vivo*. Further, we provide rationale for continued preclinical evaluation of PLX3397 for the treatment of OSA.

Methods and materials

RNA-sequencing data

CSF1, *IL-34*, and *CSF1R* expression levels were examined in three independent and publicly available human OSA patient RNA-sequencing data

sets and compared to normal human osteoblast data (Moriarity et al., 2015; Perry et al., 2014; Scott et al., 2018). The results published in data set #3 are in whole or part based upon data generated by the Therapeutically Applicable Research to Generate Effective Treatments (TARGET) initiative, phs000218, managed by the NCI. Information about TARGET can be found at http://ocg.cancer.gov/programs/target.

Tissue microarray (TMA) samples and scoring

OSA tissue microarrays (TMAs) containing 40 samples in duplicate were used for p-CSF1R^{Tyr723} and total CSF1R staining (#OS804c, US Biomax). Immunohistochemistry (IHC) was performed as previously described (Moriarity et al., 2015). IHC for p-CSF1R^{Tyr723} was performed using a rabbit anti-p-CSF1R^{Tyr723} primary antibody (#HPA012323, Sigma), and a rabbit c-fms oncoprotein primary antibody was used for total CSF1R (#CBL776, Millipore). Both antibodies were detected with diaminobenzidine (DAB) as the chromogen. Evaluation of the immunohistochemical staining was carried out using the CYTONUCLEAR module of the HALO imaging analysis platform (Indica labs). Each IHC stain was evaluated to determine the optimal thresholds for defining cellular staining patterns: negative and positive staining for both the membraneous/cytoplasmic and nuclear staining. (http://www.indicalab.com/halo/)

Cell culture

Immortalized osteoblast cell line hFOB1.19, 293T, and OSA cell lines SJSA-1, 143B, HOS, and U2OS were all obtained from the American Type Culture Collection (ATCC). All cell lines were maintained in accordance with ATCC's culture recommendations. Patient-derived xenograft (PDX) cells were provided under Materials Transfer Agreement by Stanford University. hFOB1.19 cells were maintained in DMEM/F12 and 0.3 mg/mL G418, SJSA-1 were maintained in RPMI-1640, 143B and HOS were maintained in DMEM, and U2OS and SaOS-2 were maintained in McCoy's 5A. All lines were fortified with 10% fetal bovine serum (FBS) and 1X penicillin/streptomycin. Cells were incubated in a water-jacketed incubator set at 5% carbon dioxide (CO_2) and at 37°C. With the exception of hFOB1.19 and SaOS-2 cells, all OSA cell lines (SJSA-1, 143B, HOS, and U2OS) were previously authenticated by the University of Arizona Genetics Core (UAGC) using short tandem repeat profiling.

Recombinant human CSF1 (rhCSF1)

Recombinant human CSF1 (#AF30025, Peprotech) was utilized at indicated concentrations and timepoints denoted throughout.

RNAi

Transient knockdown of CSF1 (#M-017514-00-0005, Dharmacon) and CSF1R (#M-003109-03-0005, Dharmacon) were accomplished with pooled siRNAs and compared to pooled non-silencing siRNAs as a control (#D-001206-14-05, Dharmacon). Cells were transfected at a final working concentration of 87

nM using RNAiMAX (#13778150, Thermo). Downstream analyses were performed at times indicated throughout.

RT-qPCR

Total RNA was extracted from cell lines using the GeneJet RNA purification kit (#K0731, Thermo). 500 ng of extracted RNA was DNase treated (#AM1906, Thermo) and reverse transcribed into cDNA using the Transcriptor First Strand Synthesis kit (#04379012001, Roche). Quantitative RT-qPCR was performed in triplicate using SYBR green mix (#4472908, Thermo) on an ABI 7500 machine (Applied Bio Systems). Primer sequences are available in Supplementary Table 1. All measurements were calculated using the ΔΔCT method(Schmittgen & Livak, 2008).

Overexpression plasmids

CSF1R overexpression (*CSF1R* OE), ligand-independent constitutively active (*CSF1RΔ*), and empty vector (EV) control plasmids were a generous gift from Dr. Martine Roussel and provided by Materials Transfer Agreement. The *CSF1R* sequence from each plasmid was cloned into a pLEX-307 lentiviral expression vector (#41392, Addgene). Lentiviral particles were produced with 293T cells co-transfected with the pLEX-307 vectors containing the CSF1R cDNA, *CSF1RΔ* cDNA, or EV, pMD2.G envelope (#12259, addgene), and psPAX2 (#12260, Addgene) packaging vectors. Virus was concentrated with

Lenti-X (#631232, Clontech) and stable lines were established via puromycin selection at 1 μg/mL following viral transduction.

Flow cytometry

For detection of surface CSF1R, cells were washed with 1X PBS containing 0.2% BSA and 2 mM EDTA, and stained with anti-human CSF1R or isotype control. For detection of intracellular p-CSF1R^{Tyr723}, cells were first fixed and permeabilized using BD Cytofix/Cytoperm (BD Biosciences) according to manufacturer's instructions. Cell cycle analysis was performed as previously described (Branden A. Smeester et al., 2019). Briefly, cells were fixed and permeabilized prior to staining with PI/RNase Staining Buffer (#550825, BD Pharmingen). For apoptosis analysis, cells were resuspended in Annexin-V binding buffer and stained with Annexin-V and 7-AAD according to manufacturer's instructions (#BDB556547, BD Pharmingen). Cells were analyzed on an LSR II or Fortessa digital flow cytometer (BD Biosciences) at the University of Minnesota Flow Cytometry Resource. Analysis was performed using FlowJo software (FlowJo, LLC). A complete list of antibodies and other reagents utilized is available in supplementary table 2.

ELISA

Wild-type and RNAi-modified lines were plated in 6-well dishes at 1.5 x 10^5 cells/well. Quantification of levels of both soluble CSF1 (sCSF1) and/or IL-34 secreted in the conditioned media were assessed 48-hours post-plating via

manufacturer's instructions were indicated respectively (CSF1: #DMC00B; IL-34: #D3400, R & D Systems).

Drug treatment

In vitro experiments: Pexidartinib (PLX3397, #S7818, Selleckchem) was dissolved and prepared in DMSO according to manufacturer's instructions. Tumor cell viability and western blot studies following *in vitro* PLX3397 treatment were performed in base media containing 2% FBS. *In vivo* experiments: PLX3397 drug was provided under Materials Transfer Agreement by Plexxikon Inc., formulated into 290 ppm PLX3397 or control chow, and was administered to mice *ad libitum* beginning when tumors reached palpable and measurable sizes of ~50-75 mm^3.

Western blotting

Total protein lysate was extracted from cultured cells in RIPA buffer (#R0278, Sigma) containing protease (#11873580001, Sigma) and phosphate inhibitors 2/3 (#P5726 and #P0044, Sigma). Lysates were quantified via BCA (#23225, Thermo Fisher) using pre-diluted albumin standards (#23208, Thermo Fisher), loaded into/run on Bis-Tris gels (Thermo Fisher), and transferred to 0.2 μM PVDF membranes (#1620177, Bio-Rad). Membranes were blocked in either 5% non-fat dry milk (#31FZ84, RPI) or 5% bovine serum albumin (BSA, #A2153, Sigma) diluted in PBS-T for 1 hour and incubated gently shaking overnight at 4°C in 1° antibody/PBS-T. Following washing, conjugated 2° antibody incubation for 1

hour at room temperature and subsequent washing, membranes were developed using the WesternBright Quantum detection kit (#K-12042-D20, Advansta) and the LICOR Odyssey (LICOR). A complete list of antibodies and other reagents utilized is available in Supplementary table 2.

Immunohistochemical and H&E staining

Immunohistochemistry (IHC) and H&E staining procedures were performed as previously reported (Moriarity et al., 2015). Formalin-fixed and paraffin embedded tissue sectioned at 4 μM. A complete list of antibodies and other reagents utilized is available in Supplementary table 2.

MTS cellular proliferation assay

Cell growth assays were performed as previously described (Moriarity et al., 2015; Branden A. Smeester et al., 2019). Briefly, modified cells (1.2×10^3) were seeded in 96-well plates. Absorbance was measured at 490 nm and 650 nm using a SynergyMx (BioTek) fluorescence plate reader at 24, 48, 72, and 96 hours post-plating.

Soft agar colony formation assay

Soft agar assays were performed at previously described (Moriarity et al., 2015; Branden A. Smeester et al., 2019). Both modified and drug-treated cells (1×10^4) were seeded into a 0.35% agar solution placed on top of a 0.5% agar in six-well plates and allowed to incubate for 1-4 weeks. The resultant colonies

were fixed, divided into four quadrants, and imaged using microscopy. Colonies were quantified via ImageJ v1.52a software using a standard colony quantification macro.

Tumor cell viability almarBlue assay

OSA cells (2 x 10^3) were seeded in 96-well plates and cultured overnight. Cells were then treated with increasing concentrations of PLX3397 or DMSO control and incubated for 48 hours. almarBlue cell viability reagent (#DAL1100, Thermo Fisher) was added to each well (1:10) and plates were incubated at 37°C for 1-3 hours. Luminescence was measured at 560 nm and 590 nm using a fluorescence plate reader (SynergyMx BioTek).

***In vivo* mouse models**

All animal procedures were performed in accordance with protocols approved at the University of Minnesota in conjunction with the Institutional Animal Care and Use Committee (#1808-36277A, IACUC). Human OSA cell lines or patient-derived xenograft (PDX) cells (2.5 x 10^5 and 1.0 x 10^6 respectively) were injected into the calcaneus or subcutaneous respectively of male and female 6-8-week-old immunocompromised mice (NOD Rag Gamma, Jackson Labs, (B. A. Smeester, Al-Gizawiy, & Beitz, 2012; B. A. Smeester et al., 2013)). Tumor volume was calculated via caliper measurements using the formula V = (W*W*L)/2 where V equals tumor volume, W equals tumor width and L equals tumor length (Faustino-Rocha et al., 2013).

Statistical analysis

All statistical analyses were performed using Prism v8 software (GraphPad). All data are presented as mean +/- standard error of the mean (SEM). Two groups were compared using a two-tailed unpaired Student's T-test. Three or more groups were compared using a One-way ANOVA or Two-way ANOVA analyses with Bonferroni's post hoc. All statistical analyses are individually indicated throughout in all figure legends. In all cases, $p < 0.05$ was considered statistically significant.

Results

CSF1R and CSF1 are expressed in human and mouse OSA

We previously identified *Csf1r* as a significantly, recurrently mutated oncogene in a subset of *SB*-accelerated OSA (Moriarity et al., 2015; Temiz et al., 2016). RNA-sequencing analysis confirmed that the presence of an *SB* transposon-*Csf1r* fusion transcript (R-CIS) (Moriarity et al., 2015; Temiz et al., 2016) was associated with greatly increased expression of *Csf1r* (Fig. 1a, blue dots). These RNA-sequencing findings were further confirmed at the protein level in cell lines generated from *SB*-fusion positive/negative tumors when stained for CSF1R expression (Fig. 1b). Together, our data suggest that ectopic, high-level CSF1R expression can promote OSA formation in mice, and that ectopic, active CSF1R expression, as well as its ligand CSF-1, is a feature of a significant

subset of human OSA cases. Therefore, autocrine and paracrine CSF1R signaling may be an oncogenic driver of human OSA.

Next, we used three independent and published data sets to examine the expression of *CSF1R* and its ligands *CSF1*/*IL-34* in OSA samples and compared them to normal human osteoblasts (NHOs). When compared to NHOs, *CSF1R* was highly expressed in all data sets (Fig. 1c), while *CSF1* RNA levels were not significantly different (Fig. 1d) and *IL-34* RNA levels were significantly lower (Fig. 1e). Interestingly, high IL-34 expression has been previously shown to promote OSA tumor progression and metastasis (Segaliny et al., 2015).

Analysis of 40 human tissue microarray (TMA) samples in duplicate using the Halo quantitative pathology software platform demonstrated positive membranous/cytoplasmic and nuclear CSF1R staining in 54.4% and 67.4% of cases, respectively (Fig. 1f). To assess for constitutive activation, we stained a second TMA for p-CSF1R^{Tyr723}. Similar to CSF1R expression, p-CSF1R^{Tyr723} was found to be positively expressed in the membrane/cytoplasm and nucleus in 73.5% and 60.8% of cases respectively (Fig. 1g). Representative images of CSF1R and p-CSF1R^{Tyr723} expression and localization are shown in Figure 1h. Overall, these findings demonstrate that CSF1R and CSF1 are expressed in OSA and that active CSF1R signaling may occur via autocrine and/or paracrine signaling mechanisms.

Overexpression of *CSF1R* increases colony formation and activation of growth signaling in immortalized osteoblasts

Next, we aimed to investigate whether ectopic *CSF1R* expression and activation is sufficient to drive properties of cellular transformation in an immortalized osteoblast cell line hFOB1.19 (Harris, Enger, Riggs, & Spelsberg, 1995). While reports of endogenous CSF1R expression in osteoblasts are variable (Wittrant et al., 2009), soluble CSF1 production characterizes osteoblasts (Yao, Sun, Weir, & Insogna, 2002), which we positively confirmed via ELISA in hFOB1.19 cells (157.2 +/- 13.4 pg/mL). To evaluate the potential oncogenic properties induced by high-level CSF1R, we established both *CSF1R*-overexpressing cells and a ligand-independent, constitutively active *CSF1R*-overexpressing mutant (Cioce et al., 2014) (*CSF1RΔ*). Overexpression was confirmed via RT-qPCR as compared to empty vector control (EV) (Fig. 2a) and via western blot (Fig. 2b). Both *CSF1R* and *CSF1RΔ*-expression promoted anchorage-independent colony formation compared to control cells; however, *CSF1RΔ* had a more pronounced effect (Fig. 2c). Increases in colony formation were associated with modest increases in ERK activity (Fig. 2d). Thus, these data suggest a link between elevated CSF1R expression/constitutive activity in osteoblasts, increased colony formation, and activation of oncogenic ERK signaling; together triggering early cellular transformation events that could potentially promote OSA formation, growth, and progression.

Human OSA cell lines have a functional CSF1R-CSF1 autocrine/paracrine signaling loop

To understand the function of CSF1R in OSA cells, we first probed four human OSA cell lines for p-CSF1R^{Tyr723} and CSF1R surface expression. Flow cytometry analysis revealed a small subpopulation of cell surface p-CSF1R$^{Tyr723+}$ cells (2.2% - 4.7%, white bars) and CSF1R^{+} cells (2.6% - 15.5%, light blue bars). Representative flow plots of staining are shown to the right and in Supplementary Figures 1a-b. P-CSF1R^{Tyr723} and CSF1R were also detected in cell lysates via western blot (Fig. 3b). Likewise, soluble CSF1 (sCSF1) was detected by ELISA (Fig. 3c). IL-34, another cytokine that binds CSF1R (Chihara et al., 2010) was below the threshold for detection via ELISA in all cell lines. Given that all cell lines had a subset of cells expressing both CSF1R and sCSF1, we hypothesized that a potential autocrine/paracrine signaling pathway may be active in OSA.

It has previously been reported that CSF1R^{+} breast and glioma tumor cells are responsive to sCSF1 stimulation (Coniglio et al., 2012; Morandi, Barbetti, Riverso, Dello Sbarba, & Rovida, 2011). To determine whether CSF1R^{+} OSA cells were responsive to exogenous sCSF1, we stimulated previously serum-starved SJSA-1 and U2OS cells with sCSF1 or PBS control for five minutes. sCSF1-induced CSF1R hyperactivation was observed in both cell lines (Fig. 3d) and activated ERK signaling in a concentration-dependent manner (Supp. Fig. 2a). sCSF1 knockdown was associated with reduced cell proliferation and ERK activity (Fig. 3e, Supp. Figs. 2b-c). Knockdown of CSF1R (Fig. 3f) in both SJSA-1 and U2OS cells also reduced proliferation (Figs. 3g) colony formation (Fig. 3h). Pooled siRNA knockdown of CSF1R was also associated with downregulation of ERK signaling activity (Fig. 3i) and G_0/G_1 mitotic cell arrest (Fig. 3j). These

findings were further supported by gain-of-function (GOF) *CSF1R* overexpression studies (Supp. Figs. 3a-c). Together, our results argue that targeting sCSF1-induced CSF1R signaling may be a clinically relevant strategy in OSA using small molecule tyrosine kinase inhibition of CSF1R.

Pharmacological manipulation of CSF1R signaling significantly alters OSA oncogenic properties *in vitro*

Through complementary loss- and gain-of-function studies (LOF/GOF), we established expression of an autocrine/paracrine signaling potential through active CSF1R signaling in OSA. Given this, we chose to further validate these studies therapeutically with the recently FDA-approved selective CSF1R kinase inhibitor PLX3397 (Giustini, Bernthal, Bukata, & Singh, 2018). To confirm active CSF1R kinase blockade following PLX3397 treatment and downregulation of ERK signaling (as observed in our genetic studies), we treated constitutively expressing $CSF1R^{Tyr723+}$ cell lines for 48-hours and confirmed decreased phosphorylation levels via western blot (Fig. 4a). Reduced receptor activation and ERK modulation were accompanied by concentration-dependent reductions in tumor cell viability (Fig. 4b) and colony formation (Fig. 4c). To understand the underlying mechanism(s) of these PLX3397-induced phenotypic effects, we further investigated its effects on the cell cycle and apoptosis. Consistent with our genetic studies (Fig. 3j), PLX3397 treatment induced mitotic G_0/G_1 cell cycle arrest (Fig. 4d, Supp. Fig. 4a) and modest apoptosis in U2OS, but not SJSA-1 OSA cells (Figs. 4e-f). These findings argue that a subset of OSA cells require

active CSF1R signaling for growth mediated in part through initiating/maintaining enhanced cell cycling and/or anti-apoptotic signaling.

PLX3397 reduces OSA tumor growth and metastasis

With the early success of PLX3397 for the treatment of tenosynovial giant cell tumor (TGCT) (Giustini et al., 2018), we next examined the effects of this treatment on human OSA cell line xenograft and PDX models *in vivo*. We found that PLX3397-containing chow treatment reduced OSA tumor growth in SJSA-1 and U2OS cell line xenografts as compared to control chow in an orthotopic mouse model (Fig. 5a). Representative tissue sections confirming decreased p-CSF1R^{Tyr723} and p-ERK in PLX3397-treated SJSA-1 animals are shown in Figure 5b. While no discernable differences in the number of microscopic lung metastases between control and treated animals were found, PLX3397-treated SJSA-1-bearing animals had reduced nodule area burden by 24.7% (Fig. 4c). These effects are demonstrated in representative H & E lung sections in Figure 5d. These tumor-reducing effects were mirrored in CSF1^{+}/CSF1R^{+} OSA PDX cells (Fig. 5e) in a subcutaneous mouse model (Fig. 5f). Representative tissue sections confirming decreased p-CSF1R^{Tyr723} in PLX3397-treated PDX animals are shown in Figure 5g. No lung metastases were detected in any PDX-bearing animals macroscopically or microscopically via H&E staining (Fig. 5g, rightmost). Together, these data indicate that active CSF1R inhibition can effectively reduce OSA tumor growth and metastatic burden (Fig. 6).

Discussion

In our previously published *Sleeping Beauty* (SB) transposon-based screen (Moriarity et al., 2015), the *Csf1r* gene was identified as a common insertion site (CIS) locus in a subset of accelerated OSA samples. Evaluation of RNA-sequencing data from this set of OSA samples (Temiz et al., 2016) revealed high expression levels of *Csf1r* mRNA in the same tumor samples that had been identified to carry putative *Csf1r* driving *SB* transposon insertion mutations. It is well-established that human OSAs are remarkably heterogeneous from a genetic standpoint (Wang et al., 2019). Given the known potential of receptor tyrosine kinases in driving oncogenesis (Lemmon & Schlessinger, 2010), it is not surprising that we have found strong evidence they can drive OSA and here we provide evidence for the existence of $CSF1R^{+}$ cells in human OSA patient samples and cell lines. But, in contrast to the heterogeneity for many features of OSA, we found that the majority of OSA cases examined had positive CSF1R staining, which was found in both the membrane/cytoplasm and nuclear compartments. Most OSA samples were also positive for p-$CSF1R^{Tyr723}$ found similarly in the membrane/cytoplasm and nuclear compartments. Recent reports in breast cancer and primary human monocytes provide new evidence for cytoplasmic and nuclear localization of CSF1R, as does our new data reported here, suggesting dynamic non-canonical functions for CSF1R that are previously unappreciated (Barbetti et al., 2013; Bencheikh et al., 2019). Furthermore, chromatin-bound CSF1R in mesothelioma has been shown to induce a functional transcriptional program directly promoting chemo-resistance, pluripotency, and

epithelial-to-mesenchymal transition (EMT) (Cioce et al., 2014). The specific roles of CSF1R in the plasma membrane, cytoplasmic, and nuclear compartments must be addressed in OSA through future research. Our results confirm the presence of constitutively activated CSF1R^{Tyr723} expression in malignant primary patient tissues which suggests an active autocrine/paracrine signaling loop that is therapeutically targetable.

The oncogenic potential of CSF1R has long been recognized since its early report by Roussel and colleagues more than thirty years ago (Roussel et al., 1987). CSF1R has since been shown to promote tumorigenesis in other cancers including lung (Hung et al., 2014), epithelial (Wrobel et al., 2004), in a chondrosarcoma cell line (Wen, Li, Zhang, Ling, & Lin, 2017), and recently in peripheral T cell lymphomas (PTCLs) (Murga-Zamalloa et al., 2019). Ectopic expression of wild-type CSF1R or a constitutively active mutant in normal immortalized osteoblasts allows dependent, and independent, mitogenic response to endogenous CSF1 respectively and fosters properties of cellular transformation. These data demonstrate a role for CSF1R expressing cells in promoting osteosarcomagenesis, as found in our *SB* studies (Moriarity et al., 2015; Temiz et al., 2016) and recently in inducing high levels of telomerase reverse transcriptase (hTERT) promoting immortalization of epithelial cells (Li et al., 2009). Our data demonstrate that CSF1R promotes and sustains cellular proliferation, 3D colony formation, and ERK activation in OSA cell lines. Our studies with exogenous CSF1 stimulation and RNAi-mediated knockdown of CSF1 further confirm these findings. We also found that RNAi disruption of

CSF1R signaling induces early G_0/G_1 cell cycle arrest, as previously described in epithelial cancer and others (Azzam, Wang, Bell, & Murphy, 2013; Roussel, 1994).

The findings of this work may be clinically important as well. Tyrosine kinase inhibitor (TKI) treatment *in vitro* and *in vivo* with the small molecule CSF1R inhibitor PLX3397 exerted cytostatic and cytotoxic effects that led to reduced tumor cell viability, colony formation, ERK signaling, and tumor growth in an orthotopic mouse model with OSA cell lines and in a subcutaneous PDX xenograft model. It is highly encouraging that PLX3397 specifically has been used clinically to treat tenosynovial giant cell tumor (TGCT) with success (Giustini et al., 2018) considering other CSF1R inhibitors such as JNJ-40346527 have been tried for Hodgkin's lymphoma (HL) with limited anti-tumor results despite being well-tolerated (von Tresckow et al., 2015). Further, preclinical evidence in PTCLs (Murga-Zamalloa et al., 2019) and lung cancer suggests that CSF1R can potentiate oncogenic signaling through phospho-proteomic alterations and drive bone metastases respectively (Hung et al., 2014) and that TKI treatment can reduce tumor growth and sensitize tumors to clinically relevant levels of chemotherapy agents (Pass et al., 2016). While PLX3397 treatment did not alter the number of metastatic nodules present, it did reduce the size of those nodules, which was encouraging. Many previous studies involving small molecule CSF1R blockade attributed reduced cell invasion and metastasis in part through inhibition of CSF1R-expressing tumor-associated macrophages (TAMs), which are known to foster tumor development and metastasis in other solid

cancers (Sharma et al., 2014; Wesolowski et al., 2019; Wesolowski et al., 2016). Our studies here solely focused on the tumor cell-autonomous properties of CSF1R-CSF1 signaling and did not seek to examine CSF1R signaling or blockade in the context of an intact immune system. Yet, while it is well-established that aggressive chemotherapy followed by surgical resection is beneficial to patients with low metastatic burden, this strategy is not effective for patients with higher burdens at clinical presentation (Bacci et al., 2000). This suggests a strong clinical rationale for PLX3397 treatment in patients with positive active CSF1R expression, which may overcome these current limitations

In summary, our genetic and pharmacological studies illuminate the tumor autonomous effects of CSF1R-CSF1 autocrine/paracrine signaling and provide rationale for continued study of CSF1R signaling in OSA and the potential for small molecule CSF1R TKI for the treatment of OSA.

Figure 1. CSF1R is upregulated in OSA

(a) Associated $\log_{10}$ transformed FPKMs from *SB*-mutagenized tumors driving *Csf1r* expression (blue dots). (b) Western blot confirming CSF1R positivity in cell line made from *SB*-fusion^{+} mouse tumor. Violin plots of RNA-seq $\log_{10}$ transformed FPKM values of (c) *CSF1R*, (d) CSF1, and (e) *IL-34* in 3 independent OSA patient data sets compared to normal human osteoblasts (NHOs); NHOst (n = 3), #1 (n = 20) , #2 (n = 35), #3 (n = 117). Quantification of positive and negative (f) CSF1R and (g) p-CSF1R^{Tyr723} staining in human TMAs. (h) Representative images of positive staining localization. Data shown as mean +/- SEM. Magnification and scale bars are indicated in lower right area of images (20X, 50 μM). Panels (a,b) Student's T-test. *p< 0.05, ****p < 0.0001.

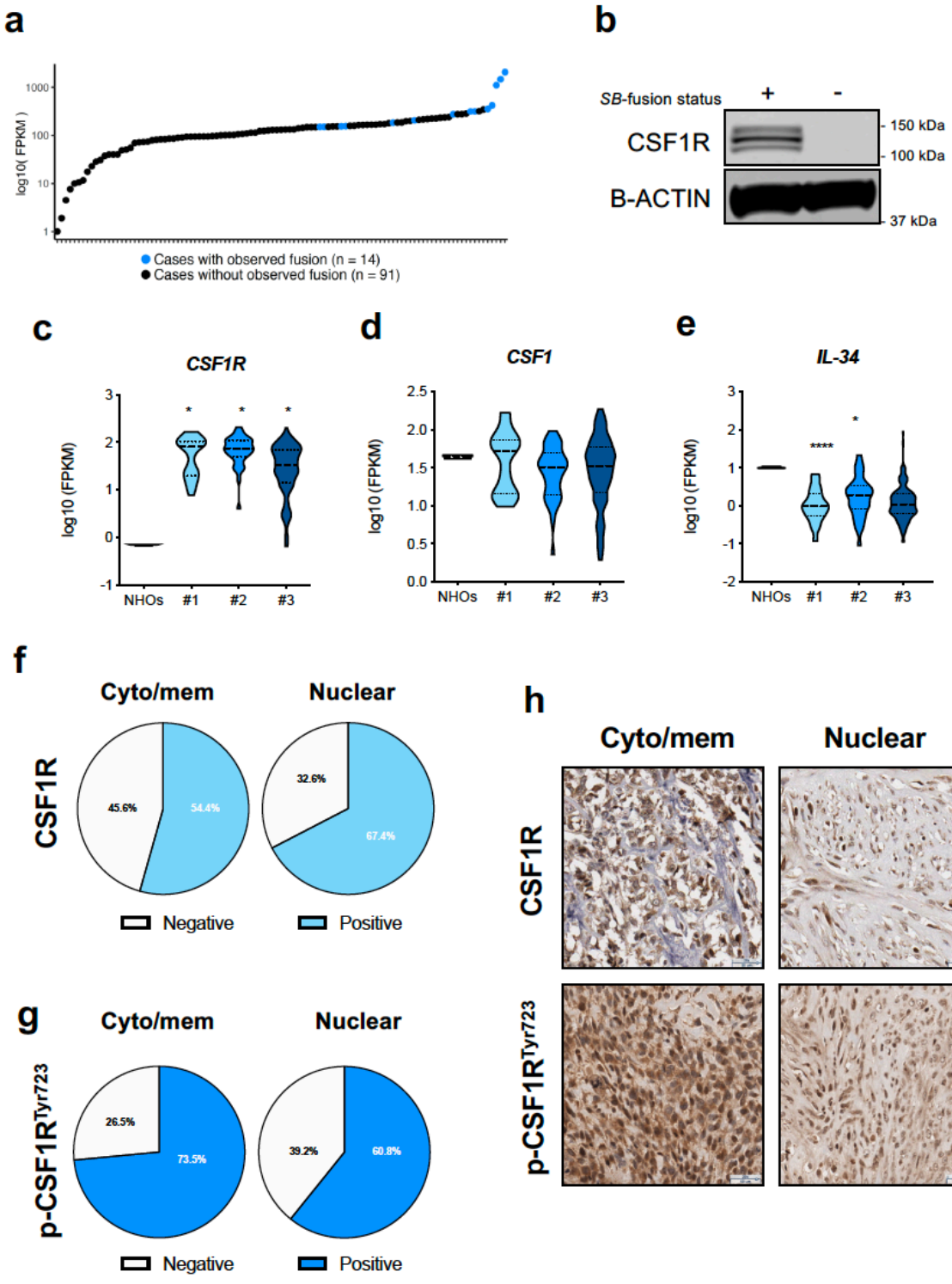
a
log10(FPKM)
1000
100
10
1
Cases with observed fusion (n = 14)
Cases without observed fusion (n = 91)
b
SB-fusion status
+
-
CSF1R
B-ACTIN
150 kDa
100 kDa
37 kDa
c
CSF1R
log10 (FPKM)
NHOs
#1
#2
#3
d
CSF1
log10 (FPKM)
NHOs
#1
#2
#3
e
IL-34
log10 (FPKM)
NHOs
#1
#2
#3
f
Cyto/mem
Nuclear
CSF1R
45.6%
54.4%
32.6%
67.4%
Negative
Positive
g
Cyto/mem
Nuclear
p-CSF1R Tyr723
26.5%
73.5%
39.2%
60.8%
Negative
Positive
h
Cyto/mem
Nuclear
CSF1R
p-CSF1R Tyr723

Figure 2. Overexpression of *CSF1R* induces properties of cellular transformation in immortalized osteoblasts

Overexpression of *CSF1R* or constitutively active, ligand-independent *CSF1R* (*CSF1RΔ*) were confirmed via (a) RT-qPCR and (b) western blotting. *CSF1R* OE and *CSF1RΔ* increases the (c) colony formation potential of immortalized osteoblasts. Representative images of colonies shown to right of graph (n = 36). (d) *CSF1R* OE/*CSF1RΔ* overexpressing osteoblasts have a modest increase in active ERK signaling. All data shown as mean +/- SEM. Panels (a,c) Student's T-test. $^{**}p < 0.01$, $^{****}p < 0.0001$.

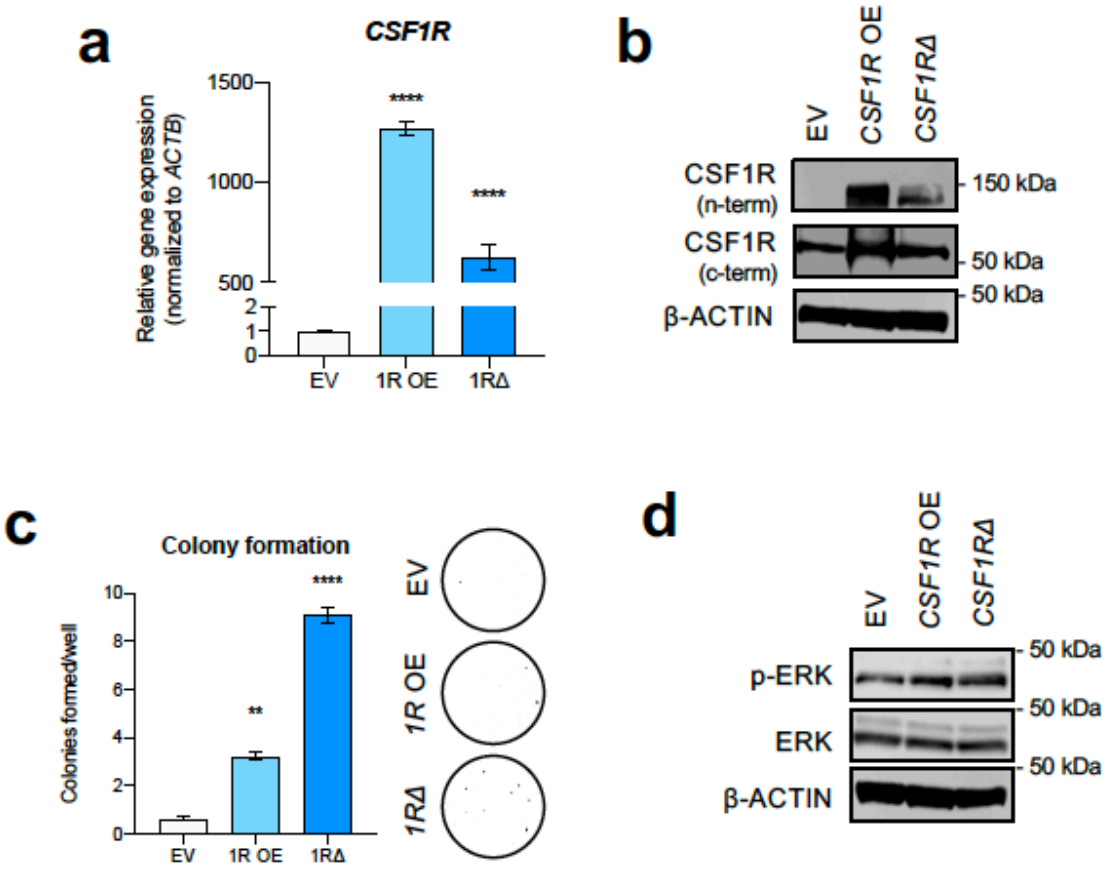
a
CSF1R
Relative gene expression (normalized to ACTB)
1500
1000
500
2
1
0
****
****
EV
1R OE
1RΔ
b
EV
CSF1R OE
CSF1RΔ
CSF1R (n-term)
150 kDa
CSF1R (c-term)
50 kDa
β-ACTIN
50 kDa
c
Colony formation
Colonies formed/well
10
8
6
4
2
0
**
****
EV
1R OE
1RΔ
EV
1R OE
1RΔ
d
EV
CSF1R OE
CSF1RΔ
p-ERK
50 kDa
ERK
50 kDa
β-ACTIN
50 kDa

Figure 3. Oncogenic CSF1R-CSF1 autocrine/paracrine signaling in OSA cell lines

Flow analyses of positive (a) p-CSF1R^{Tyr723} and CSF1R surface expression in human OSA cell lines gated on live, single cells (n = 3). Representative flow plots of SJSA-1 cells are shown to the right. (b) Total cell lysates were subjected to western blotting using p-CSF1R^{Tyr723}-specific and c-terminal CSF1R-specific antibodies. (c) Soluble CSF1 was detectable via ELISA in cell culture supernatants (n = 2). (d) Cells were stimulated with 25 ng/mL CSF1. Stimulation induced CSF1R hyperactivation 5 minutes post stimulation. (e) CSF1 knockdown reduced cellular proliferation (n = 18). (f) Conformation of CSF1R knockdown. CSF1R silencing reduced (g) cell proliferation (n = 18) and (h) colony formation (n = 24-36). (i) Silencing of CSF1R was associated with reduced ERK activity. All data shown as mean +/- SEM. Panel (e) Two-way ANOVA; Panels (e,h) Student's T-test; Panels (g,j) Two-way ANOVA. *$p < 0.05$, **$p < 0.01$, ***$p < 0.001$, ****$p < 0.0001$.

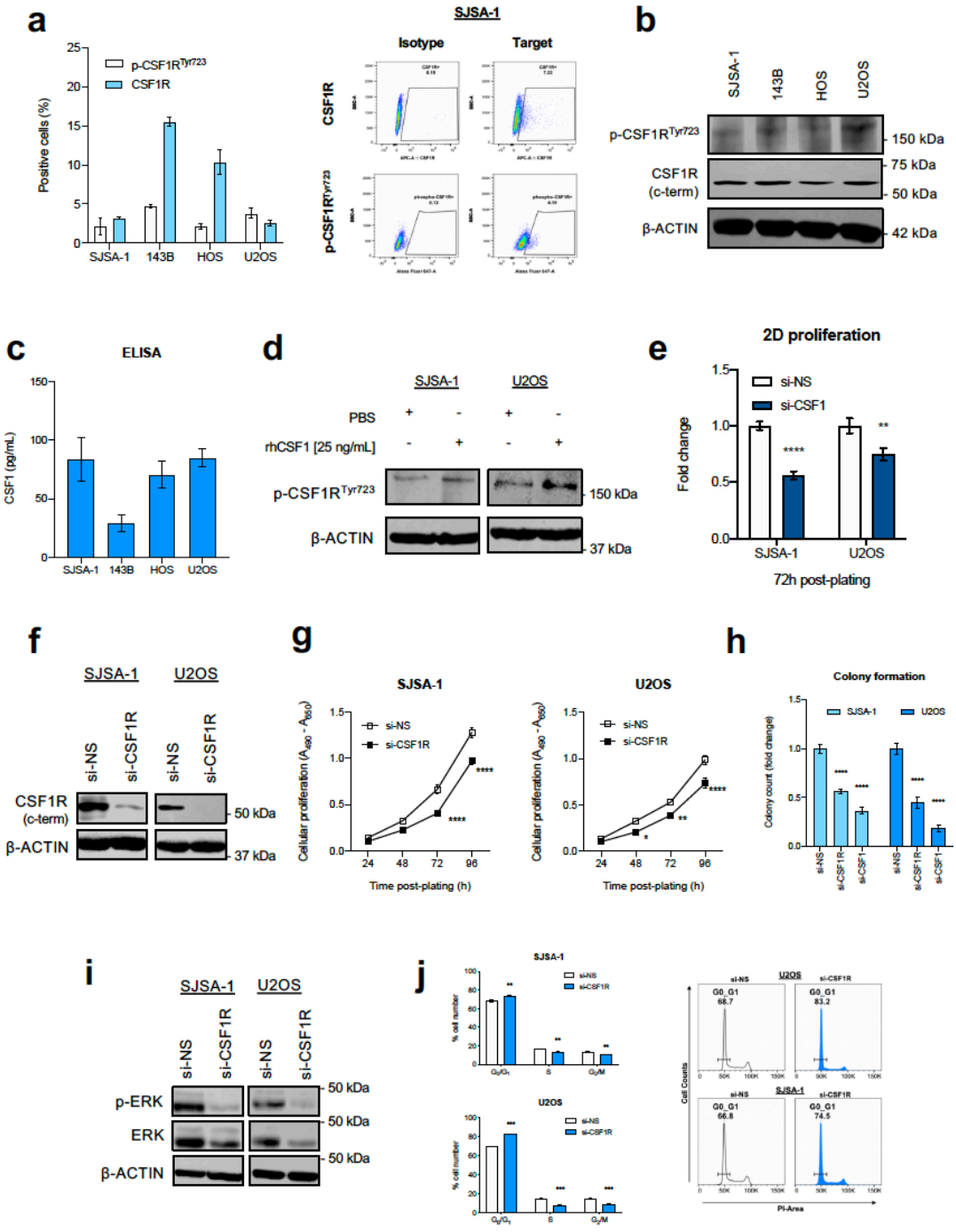
a
SJSA-1
Isotype
Target
CSF1R
p-CSF1R Tyr723
Positive cells (%)
p-CSF1R Tyr723
CSF1R
SJSA-1
143B
HOS
U2OS
b
SJSA-1
143B
HOS
U2OS
p-CSF1R Tyr723
CSF1R (c-term)
β-ACTIN
150 kDa
75 kDa
50 kDa
42 kDa
c
ELISA
CSF1 (pg/mL)
SJSA-1
143B
HOS
U2OS
d
SJSA-1
U2OS
PBS
rhCSF1 [25 ng/mL]
p-CSF1R Tyr723
β-ACTIN
150 kDa
37 kDa
e
2D proliferation
si-NS
si-CSF1
Fold change
SJSA-1
U2OS
72h post-plating
f
SJSA-1
U2OS
si-NS
si-CSF1R
CSF1R (c-term)
β-ACTIN
50 kDa
37 kDa
g
SJSA-1
U2OS
si-NS
si-CSF1R
Cellular proliferation
Time post-plating (h)
h
Colony formation
SJSA-1
U2OS
Colony count (fold change)
i
SJSA-1
U2OS
si-NS
si-CSF1R
p-ERK
ERK
β-ACTIN
50 kDa
50 kDa
50 kDa
j
SJSA-1
U2OS
si-NS
si-CSF1R
% cell number
Cell Counts
PI-Area

Figure 4. Pharmacological blockade of CSF1R signaling with PLX3397 is cytostatic and cytotoxic *in vitro*

(a) A 48-hour PLX3397 treatment inhibits constitutive CSF1R signaling and reduces ERK activity. (b) PLX3397 reduces tumor cell viability (n = 18) and (c) colony formation (n = 24-36) in a concentration-dependent manner. Representative colony formation images shown to the right. PLX3397 treatment (3μM) promoted (d) cell cycle arrest (n = 3) and (e-f) apoptosis (n = 3). All data shown as mean +/- SEM. Panels (b,c) One-way ANOVA; Panel (d) Two-way ANOVA; Panel (e) Student's T-test. *$p < 0.05$, **$p < 0.01$, ***$p < 0.001$, ****$p < 0.0001$.

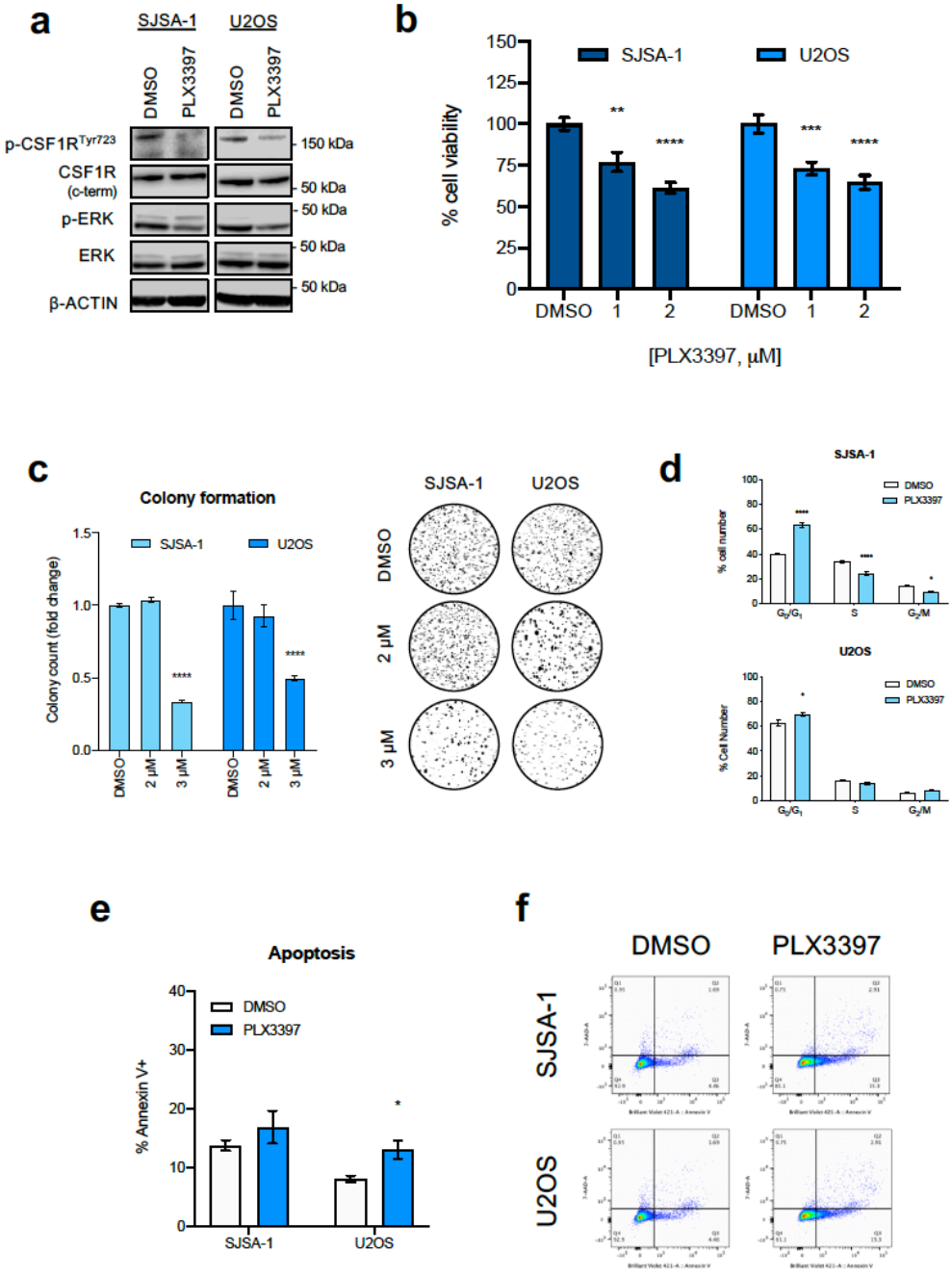
a
SJSA-1
U2OS
DMSO
PLX3397
DMSO
PLX3397
p-CSF1R Tyr723
CSF1R (c-term)
p-ERK
ERK
β-ACTIN
150 kDa
50 kDa
50 kDa
50 kDa
50 kDa
b
SJSA-1
U2OS
% cell viability
150
125
100
75
50
25
0
**
****
***
****
DMSO
1
2
DMSO
1
2
[PLX3397, μM]
c
Colony formation
SJSA-1
U2OS
Colony count (fold change)
1.5
1.0
0.5
0.0
****
****
DMSO
2 μM
3 μM
DMSO
2 μM
3 μM
SJSA-1
U2OS
DMSO
2 μM
3 μM
d
SJSA-1
DMSO
PLX3397
% cell number
100
80
60
40
20
0
****
****
*
G0/G1
S
G2/M
U2OS
DMSO
PLX3397
% Cell Number
100
80
60
40
20
0
*
G0/G1
S
G2/M
e
Apoptosis
DMSO
PLX3397
% Annexin V+
40
30
20
10
0
*
SJSA-1
U2OS
f
DMSO
PLX3397
SJSA-1
U2OS

Figure 5. PLX3397 has potent anti-tumor effects *in vivo*

(a) PLX3397 chow-treated OSA cell lines displayed reduced tumor growth compared to control chow-treated animals. (b) Representative IHC staining of p-CSF1R^{Tyr723} and p-ERK in SJSA-1 treated and control animals. (c) Micro-metastatic lung nodule counts and area per section (n = 3/group). (d) Representative H&E staining in lung sections. (e) RT-qPCR of *CSF1*/*CSF1R* expression and western blot of CSF1R using n- and c-terminal specific antibodies in a human patient-derived xenograft line (PDX). (f) PDX-bearing mice with access to PLX3397 chow had reduced tumor growth as compared to control chow-treated mice. (g) Representative IHC images of p-CSF1R^{Tyr723} (leftmost) and H&E images of lung sections (rightmost) in treated and control PDX-bearing animals. All data shown as mean +/- SEM. Magnification and scale bars are indicated in lower right area of images (IHC: 20X, 50 μM; H&E: 10X, 200 μM). Black arrows indicate micro-metastatic nodules. Panels (a, f) Two-way ANOVA; Panel (c) Student's T-test; *$p < 0.05$, ***$p < 0.001$, ****$p < 0.0001$.

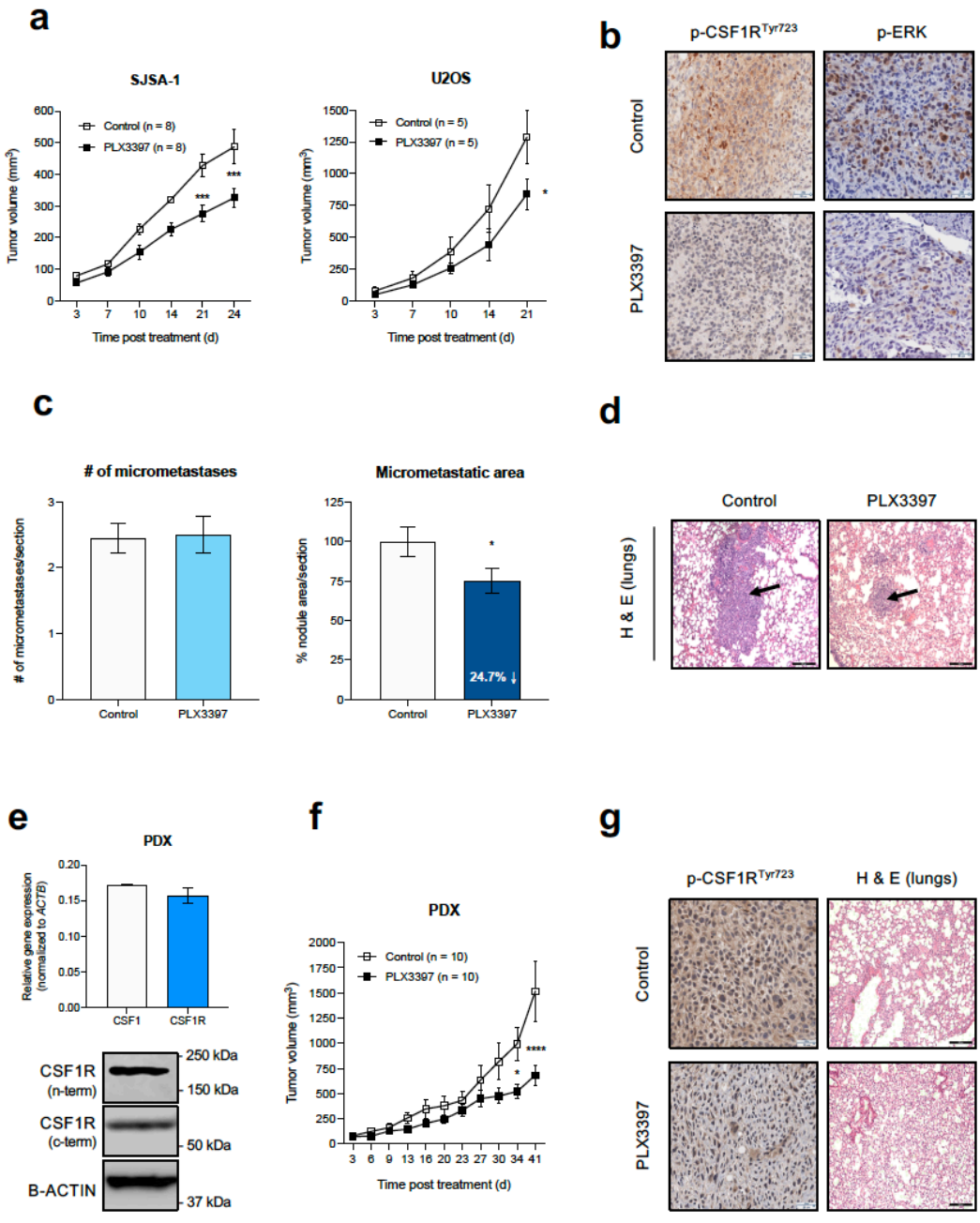
a
SJSA-1
Control (n = 8)
PLX3397 (n = 8)
Tumor volume (mm3)
Time post treatment (d)
U2OS
Control (n = 5)
PLX3397 (n = 5)
Tumor volume (mm3)
Time post treatment (d)
b
p-CSF1R Tyr723
p-ERK
Control
PLX3397
c
# of micrometastases
# of micrometastases/section
Control
PLX3397
Micrometastatic area
% nodule area/section
24.7% ↓
Control
PLX3397
d
Control
PLX3397
H & E (lungs)
e
PDX
Relative gene expression (normalized to ACTB)
CSF1
CSF1R
CSF1R (n-term)
CSF1R (c-term)
B-ACTIN
250 kDa
150 kDa
50 kDa
37 kDa
f
PDX
Control (n = 10)
PLX3397 (n = 10)
Tumor volume (mm3)
Time post treatment (d)
g
p-CSF1R Tyr723
H & E (lungs)
Control
PLX3397

Figure 6. CSF1R/CSF1 autocrine signaling axis in OSA

Proposed mechanism of CSF1R-CSF1 autocrine signaling in OSA cells to promote transformation and cell cycle entry. Active CSF1R signaling blockade with PLX3397 treatment inhibits cellular transformation, promotes cell cycle arrest, apoptosis, reduces tumor growth and micro-metastatic nodule area.

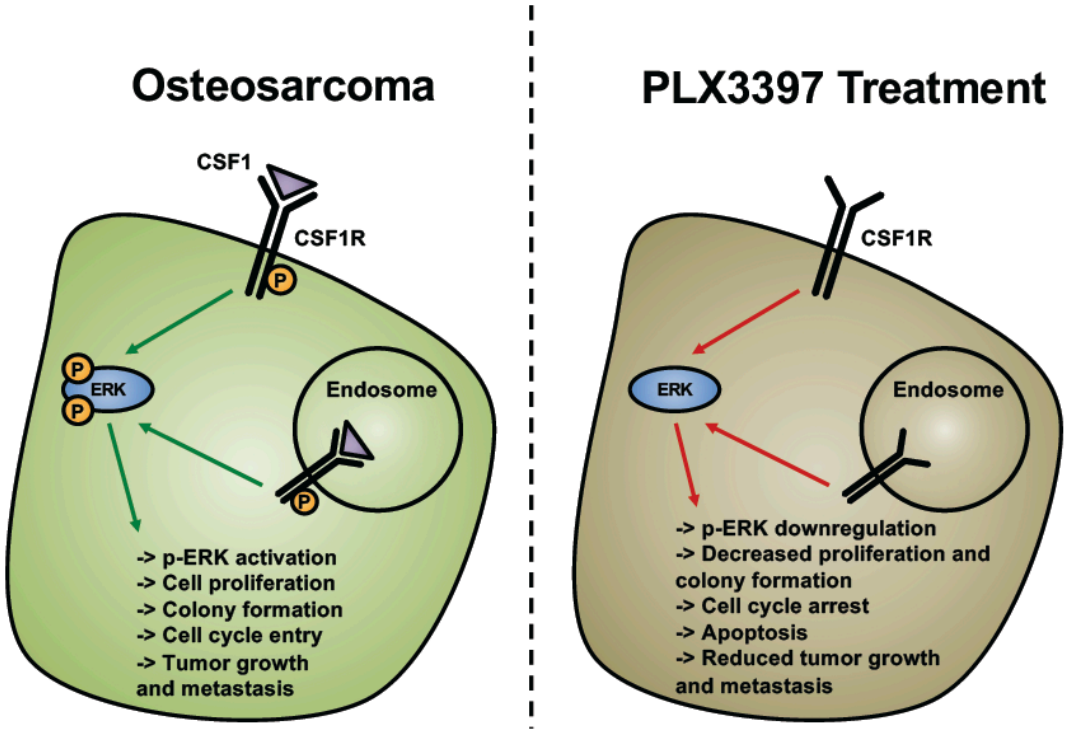
Osteosarcoma
CSF1
CSF1R
P
P
ERK
P
Endosome
P
-> p-ERK activation
-> Cell proliferation
-> Colony formation
-> Cell cycle entry
-> Tumor growth
and metastasis
PLX3397 Treatment
CSF1R
ERK
Endosome
-> p-ERK downregulation
-> Decreased proliferation and
colony formation
-> Cell cycle arrest
-> Apoptosis
-> Reduced tumor growth
and metastasis

Supplementary Figure 1. Flow plots of positive CSF1R staining in OSA cell lines

Representative flow plots of (a) $CSF1R^{+}$ surface and (b) p-$CSF1R^{Tyr723}$ staining in HOS, 143B, and U2OS OSA cell lines.

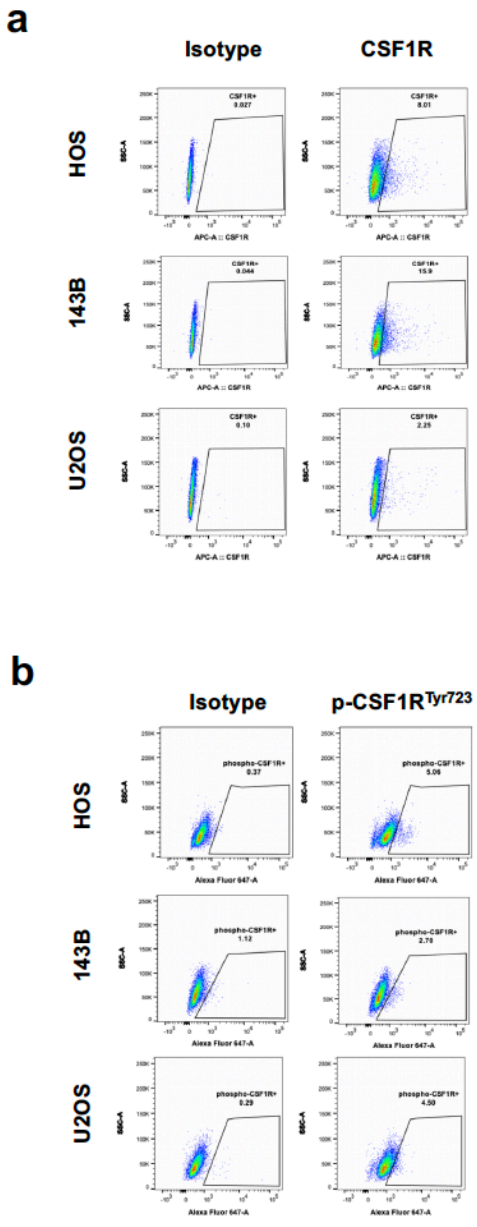
a
Isotype
CSF1R
HOS
143B
U2OS
b
Isotype
p-CSF1R Tyr723
HOS
143B
U2OS

Supplementary Figure 2. Soluble CSF1 (sCSF1) signaling

(a) A 5-minute rhCSF1 stimulation induces ERK activity in a concentration dependent manner in SJSA-1 and U2OS cells. (b) RNA-mediated knockdown of sCSF1 signaling was confirmed via ELISA (n = 2). (c) sCSF1 knockdown reduces active ERK signaling. Data shown as mean +/- SEM. LD indicates below limit of detection.

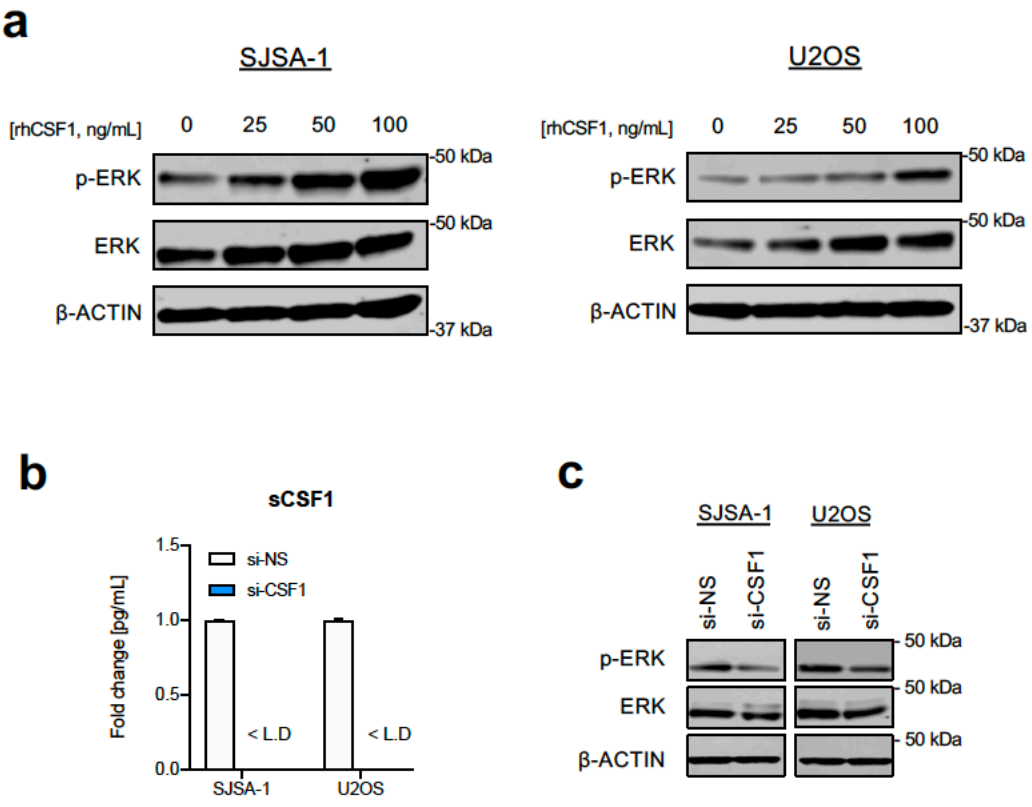
a
SJSA-1
U2OS
[rhCSF1, ng/mL]
0
25
50
100
p-ERK
ERK
β-ACTIN
50 kDa
50 kDa
37 kDa
b
sCSF1
si-NS
si-CSF1
Fold change [pg/mL]
1.5
1.0
0.5
0.0
< L.D
< L.D
SJSA-1
U2OS
c
SJSA-1
U2OS
si-NS
si-CSF1
si-NS
si-CSF1
p-ERK
ERK
β-ACTIN
50 kDa
50 kDa
50 kDa

Supplementary Figure 3. Overexpression of *CSF1R* in SJSA-1 OSA cells

(a) Overexpression of *CSF1R* and activation of ERK signaling in SJSA-1 OSA cells was confirmed via western blot. Overexpression modestly increases (b) cellular proliferation (n = 18) and (c) colony formation (n = 36). Data shown as mean +/- SEM. Panel (b) Two-way ANOVA; Panel (c) Student's T-Test. *p < 0.05, ****p < 0.0001.

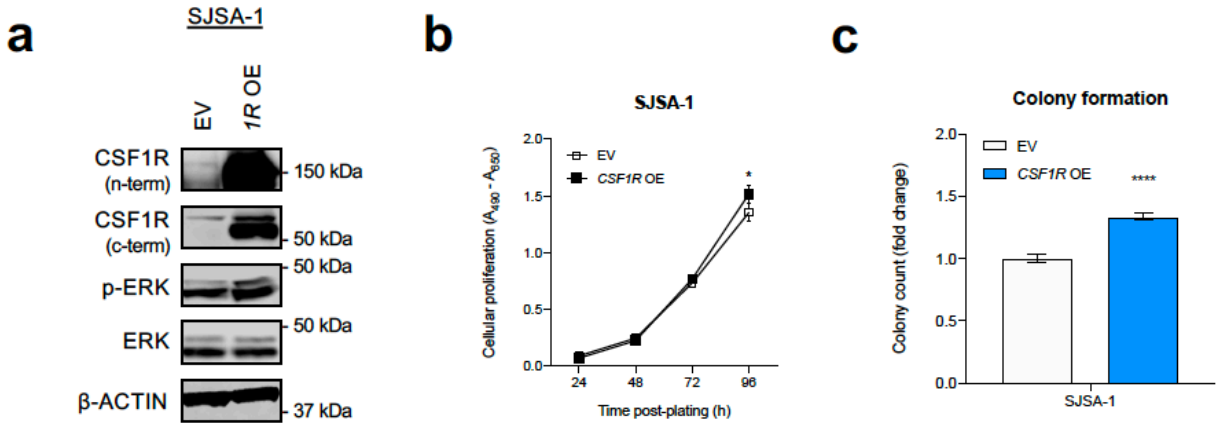
a
SJSA-1
EV
1R OE
CSF1R (n-term)
150 kDa
CSF1R (c-term)
50 kDa
p-ERK
50 kDa
ERK
50 kDa
β-ACTIN
37 kDa
b
SJSA-1
EV
CSF1R OE
*
Cellular proliferation (A490 - A650)
2.0
1.5
1.0
0.5
0.0
24
48
72
96
Time post-plating (h)
c
Colony formation
EV
CSF1R OE
****
Colony count (fold change)
2.0
1.5
1.0
0.5
0.0
SJSA-1

Supplementary Figure 4. Cell cycle flow plots in PLX3397-treated cell lines

PLX3397 treatment induces G_0/G_1 mitotic cell cycle arrest in SJSA-1 and U2OS OSA cell lines. (a) Representative flow plots of cell cycle staining.

a

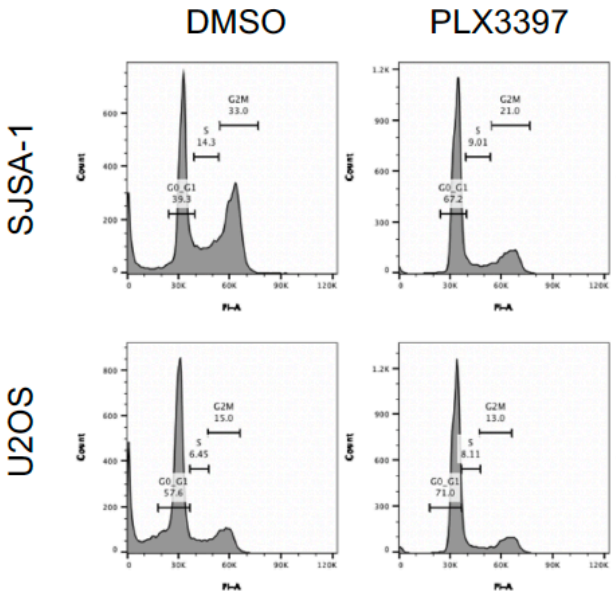
DMSO
PLX3397
SJSA-1
U2OS
G2M
33.0
S
14.3
G0_G1
39.3
G2M
21.0
S
9.01
G0_G1
67.2
G2M
15.0
S
6.45
G0_G1
57.6
G2M
13.0
S
8.11
G0_G1
71.0
Count
PI-A

Supplementary Table 1.

RT-qPCR primer sequences utilized.

RT-qPCR primers

Target	Sense	Anti-sense
CSF1	5'-CGCTTCAGAGATAACACCCC-3'	5'-TCATAGAAAGTTCGGACGCAG-3'
CSF1R	5'-GTAAGACCCTCGGAGCTGGA-3'	5'-CTCCATGGGTACAGGCTC-3'
ACTB	5'-CACAGGGGAGGTGATAGCAT-3'	5'-CTCAAGTTGGGGGCACAAAA-3'

Supplementary Table 2.

Antibodies and other reagents utilized.

Primary antibodies

Antigen	Application	Source	Congugate	Catalog	Company
CSF1R	FACS	Rat	APC	347306	Biolegend
Isotype	FACS	Rat	APC	400412	Biolegend
p-CSF1RTyr723	FACS/WB	Rabbit	N/A	3155	Cell Signaling Technologies
Isotype	FACS	Rabbit	N/A	3900	Cell Signaling Technologies
CSF1R (n-term)	WB	Rabbit	N/A	67455	Cell Signaling Technologies
CSF1R (c-term)	WB	Rabbit	N/A	3152	Cell Signaling Technologies
p-ERK1,2	WB	Rabbit	N/A	4370	Cell Signaling Technologies
ERK1,2	WB	Rabbit	N/A	4695	Cell Signaling Technologies
B-ACTIN	WB	Mouse	N/A	3700	Cell Signaling Technologies
CSF1R	IHC	Rabbit	N/A	CBL776	Millipore
p-CSF1RTyr723	IHC	Rabbit	N/A	HPA012323	Sigma

Secondary antibodies

Epitope	Application	Congugate	Catalog	Company
Anti-rabbit IgG	FACS	Alexa 647	4414	Cell Signaling Technologies
Anti-rabbit IgG	WB	HRP	1706515	Bio-Rad
Anti-mouse IgG	WB	800CW	925-32212	LiCOR

CHAPTER 5

Targeted suppression of ZNF217-induced AKT signaling inhibits tumor growth and metastasis in osteosarcoma

*Branden A. Smeester, *Garrett M. Draper, Nicholas J. Slipek, Alex T. Larsson, Natalie Stratton, Emily J. Pomeroy, Kelsie L. Becklin, Kenta Yamamoto, Kyle B. Williams, Kanut Laoharawee, Joseph J. Peterson, Juan E. Abrahante, Susan K. Rathe, Lauren J. Mills, Margaret R. Crosby, Wendy A. Hudson, Eric P. Rahrmann, David A. Largaespada, Branden S. Moriarity

[1]Department of Pediatrics, University of Minnesota
[2]Department of Genetics, Cell Biology and Development, University of Minnesota
[3]Center for Genome Engineering, University of Minnesota
[4]Masonic Cancer Center, University of Minnesota
[5]Cancer Research UK Cambridge Institute, University of Cambridge
[6]Childhood Cancer Genomics Group, University of Minnesota

A version of this chapter has been submitted for review at the time of this writing.

Conception and design: BAS, GMD, BSM
Development and acquisition of data: BAS, GMD, NJS, ATL, NS, EJP, KLB, KY, KBW, KL, JJP, JEA, LJM, SKR, MRC, WAH, EPR, DAL, BSM
Analysis and interpretation: BAS, GMD, BSM
Writing, review and revisions: BAS, GMD, NJS, ATL, NS, EJP, KLB, KY, KBW, KL, JJP, JEA, LJM, SKR, MRC, WAH, EPR, DAL, BSM
Study oversight: BAS, GMD, BSM

Summary

We previously identified *ZNF217* as an oncogenic driver of a subset of osteosarcomas (OSAs) using the *Sleeping* Beauty (SB) transposon system. Here, we followed up investigating the role of candidate osteosarcoma cancer gene *ZNF217* and combined these studies with an orthotopic preclinical animal model and culture experiments targeting ZNF217-induced AKT signaling with a small molecule inhibitor as a novel approach to treating ZNF217^{+} OSAs. Here, we demonstrate that ZNF217 is involved in numerous facets of cellular transformation including proliferation, cell motility, colony formation, and ultimately promoting OSA growth, progression, and metastasis in part through AKT survival pathway modulation. Preclinical blockade of AKT signaling with nucleoside analogue triciribine (TCN) in ZNF217^{+} orthotopically-injected OSA cell lines reduced tumor growth, metastasis, and was well-tolerated. TCN treatment was also found to synergize with common broad-spectrum chemotherapeutic doxorubicin. Our data demonstrate that TCN treatment may be a relevant and efficacious therapeutic strategy for OSA patients with ZNF217^{+} and p-AKT^{Ser473}-rich tumors. With the recent revitalization of triciribine for clinical studies in other solid cancers (PTX-200, Prescient Therapeutics), our study provides rationale for further evaluation preclinically with the purpose of clinical evaluation in patients with incurable OSA.

Introduction

Osteosarcoma (OSA) is a heterogeneous, rare malignancy of the bone most often arising in children and adolescents (Kansara, Teng, Smyth, & Thomas, 2014). Surgical resection and combinatorial chemotherapy are beneficial to ~70% of localized cases, however, patients with advanced metastatic and/or relapsed disease continue to have poor survival outcomes (Kansara et al., 2014; Misaghi, Goldin, Awad, & Kulidjian, 2018). Despite remarkable progress in advancing our knowledge of OSA, disease recurrence (Leary et al., 2013) and chemotherapeutic resistance (Yang et al., 2019; Y. Zhang et al., 2018) continue to be major roadblocks to curative successes. This significantly underlines the need for new genetic targets and therapeutics. For these reasons, we performed a *Sleeping Beauty* (*SB*) transposon-based forward genetic screen for OSA which identified >250 previously known and unknown drivers of OSA development and metastasis (Moriarity et al., 2015). In particular, zinc finger protein transcription factor (TF) *ZNF217* (murine *Zfp217*) was identified as a candidate OSA driver oncogene in a subset of our primary murine OSA samples (Moriarity et al., 2015).

ZNF217 is a member of the Kruppel-like transcription factor family that was originally described with repressive transcriptional function (Quinlan, Verger, Yaswen, & Crossley, 2007). Recent reports have demonstrated that ZNF217 interacts with and can influence endogenous signaling networks governing hallmarks of cancer (Hanahan & Weinberg, 2000, 2011) including sustained proliferation, invasion/metastasis, and resistance to chemotherapy-induced cell

death (Huang et al., 2005; J. Li, Song, Qiu, Yin, & Zhong, 2014; Thollet et al., 2010; Vendrell et al., 2012). Emerging evidence suggests TFs could represent novel candidates for therapy in OSA (Morrow & Khanna, 2015). However, many of these TFs are not currently directly targetable demonstrating the necessity of identifying upstream mediators regulating their biological function or downstream effectors of their activity.

In this report, we describe a distinct oncogenic role for ZNF217 in driving OSA growth, progression, and metastasis. This occurs in part through transcriptional changes that lead to hyperactivation of PI3K-AKT signaling. Importantly, we show that blockade of AKT signaling with a clinically relevant small molecule inhibitor (triciribine, TCN) is effective at reducing tumor progression and metastasis in ZNF217^{+} tumors, and synergizes with doxorubicin treatment. Together, our results suggest continued preclinical evaluation of TCN as a neoadjuvant therapy for patients with incurable OSA.

Materials and methods

ZNF217 expression in OSA data sets

RNA-sequencing data was analyzed from data sets previously published (Moriarity et al., 2015; Branden A. Smeester et al., 2019) and compared to normal human osteoblasts (NHOs). The results published in Figure 1a, data set #3, are in whole or part based upon data generated by the Therapeutically Applicable Research to Generate Effective Treatments (TARGET) initiative,

phs000218, managed by the NCI. Information about TARGET can be found at http://ocg.cancer.gov/programs/target.

Tissue microarray staining (TMA) and analysis

TMA staining and quantification was performed with methods previously described (Branden A. Smeester et al., 2019). Briefly, two individual OSA TMAs containing 40 samples in duplicate were stained for ZNF217 and p-AKT^{Ser473} respectively and evaluated using the HALO imaging analysis platform (Indica labs). Antibodies and other reagents used are available in Supplementary Table 1.

Cell lines and culturing

All OSA cell lines, immortalized osteoblasts (hFOB1.19), and HEK 293Ts were obtained and maintained in accordance with American Type Culture Collection's (ATCC) recommendations. All cell lines were cultured as previously described (Branden A. Smeester et al., 2019). Normal human osteoblasts (NHOs) were obtained from Lonza and cultured in osteoblast growth medium (#CC-3207, Lonza). With the exception of hFOB1.19, NHOs, and SaOS-2 cells, cell lines were authenticated by the University of Arizona Genetics Core (UAGC) using short tandem repeat profiling.

RNAi and overexpression

ZNF217 (#M-004987-00-0005, Dharmacon) and/or control non-silencing (#D-001206-14-05, Dharmacon) pooled siRNAs were used for all transient knockdown studies. OSA cells were transfected at a final working concentration of 17 nM using RNAiMAX (#13778150, Thermo) and all analyses were performed 48 hours post-transfection. Stable knockdown and overexpression of *ZNF217* were achieved with methods previously described (Branden A. Smeester et al., 2019). Briefly, stable knockdown of ZNF217 was accomplished with pGIPZ lentiviral vectors expressing an shRNA against ZNF217 in conjunction with GFP and a puromycin selection marker (shZNF217: #V2LHS_196547, Open Biosystems). Control pGIPZ vector (shCON) with non-targeting shRNA was used as a control (#RHS4346, Open Biosystems). Stable overexpression (OE) was achieved via a lentiviral *ZNF217* vector (#98384, addgene) or empty vector (EV) control (#41392, addgene). Lentiviral particles were produced with HEK 293T cells co-transfected with shRNA- or OE-containing vectors, pMD2.G envelope (#12259, addgene), and psPAX2 (#12260, addgene) packaging vectors. Viruses were concentrated with Lenti-X (#631232, Clontech) and stable lines were established via puromycin selection at 1 μg/mL following viral transduction.

RT-qPCR

RT-qPCR was performed as previously described (Branden A. Smeester et al., 2019). Following RNA extraction, 1 μg of total RNA was reverse transcribed into cDNA (#04379012001, Roche) and RT-qPCR was performed in

triplicate using SYBR green mix (#4472908, Thermo) on a CFX96 Touch System (Bio-Rad). All measurements were calculated using the ΔΔCT method (Schmittgen & Livak, 2008).

ZNF217 Forward: 5'-GATGTTACTCCTCCTCCGGATG-3'

ZNF217 Reverse: 5'-CACACTTGGCCTGTATCTGCA-3'

ACTB Forward: 5'-CACAGGGGAGGTGATAGCAT-3'

ACTB Reverse: 5'-CTCAAGTTGGGGGCACAAAA-3'

Western blotting

Western blotting was performed as previously described (Branden A. Smeester et al., 2019). Briefly, total lysates were transferred to PDVF membranes, incubated with 1° and 2° antibodies, developed, and imaged using a LICOR Odyessy. A complete list of antibodies and other reagents utilized is available in Supplementary Table 1.

Immunohistochemistry (IHC)

IHC and H&E staining procedures were performed as previously reported (Moriarity et al., 2015). Formalin-fixed and paraffin embedded tissue was sectioned at 4 μM. A complete list of antibodies and other reagents utilized is available in Supplementary Table 1.

Immunofluorescence (IF)

OSA cells (HOS and SJSA-1) were plated onto sterile glass coverslips and incubated overnight at 37°C in normal media. Cells were washed with PBS and fixed with 10% neutral buffered formalin (NBF) for 10 minutes at room temperature. Following 3X washing with PBS, cells were permeabilized in 0.1% Triton X-100/PBS (#T8787, Sigma Aldrich) for 10 minutes. After 3X washes in PBS, cells were blocked for 1 hour at room temperature in 4% FBS/PBS followed by incubation in 1° antibody/blocking buffer overnight at 4°C. Post-1° incubation, cells were washed 3X in PBS and then incubated in conjugated 2° antibody/blocking buffer for 2 hours at room temperature. Following a gentle PBS wash, antifade mountant containing DAPI (#P36931, Thermo Fisher) was added, coverslips were mounted on glass slides, and imaged using the Cytation 5 cell imaging reader (BioTek). Cytation 5 software was utilized to acquire and merge IF and DAPI channels. Incubation with 2° only controls yielded no significant IF staining.

Cell fractionation

Cell fractionation was performed according to manufacturer's instructions using the subcellular protein fractionation kit for cultured cells (#78840, Thermo Fisher).

Compounds

Both triciribine (TCN, #S1117, Selleckchem) and LY294002 (#S1105, Selleckchem) were prepared according to manufacturer's instructions. Both

compounds were dissolved in DMSO for all *in vitro* experiments. TCN was prepared in a 1% DMSO/30% polyethylene glycol/1% Tween-80 solution for all *in vivo* studies. Animals received 40 mg/kg TCN or control three times weekly (3X) intraperitoneally (IP).

MTS proliferation assay

Cell growth assays were performed as previously described (Moriarity et al., 2015; Branden A. Smeester et al., 2019). Briefly, modified cells (1.2×10^3) were seeded in 96-well plates. Absorbance was measured at 490 nm and 650 nm using a SynergyMx (BioTek) plate reader at 24, 48, 72, and 96 hours post-plating.

Transwell migration assay

RNAi-modified or drug-treated cells (2.5×10^4) were seeded in 500 μL of serum free media in the upper chamber of 8 μm inserts (#353097, Corning). The lower chamber was filled with 750 μL media fortified with 10% fetal bovine serum (FBS) as a chemo attractant. After 24 hours, non-migrating cells where removed with a cotton swab. Migrated cells located on the lower side of the chamber were fixed with crystal violet, air-dried, and photographed to quantify migration of cells.

Soft agar colony formation assay

RNAi-modified or TCN-treated cells (1×10^4) were seeded into a 0.35%

agar solution placed on top of a 0.5% agar in six-well plates and allowed to incubate for 1-4 weeks. The resultant colonies were fixed, divided into four quadrants, and imaged using microscopy. Colonies were quantified via ImageJ v1.52a software using a standard colony quantification macro (Moriarity et al., 2015).

Flow cytometry

Apoptosis assays were performed as previously described (Branden A. Smeester et al., 2019). Briefly, cells were resuspended in Annexin-V binding buffer and stained with Annexin-V and 7-AAD according to manufacturer's instructions (#BDB556547, BD Pharmingen). Cells were analyzed on an LSR II or Fortessa digital flow cytometer (BD Biosciences) at the University of Minnesota Flow Cytometry Resource. Analysis was performed using FlowJo software (FlowJo, LLC).

Fluorescence *in situ* hybridization (FISH)

Suspension cultures from fresh mouse spleen cells were initiated: after 48-hr incubation with Concanavalin A, cells were harvested using standard cytogenetic methods (colcemid arrest, followed by treatment with 0.75 M KCl hypotonic solution, and fixation with 3:1 methanol:acetic acid). Harvested cells were spread onto glass slides. ZNF217 DNA probes were labeled by nick translation reaction (Nick Translation Kit - Abbott Molecular) using Orange 552 dUTP (Enzo Life Science). Sizes of the nick translated fragments are checked by

electrophoresis on a 1% TBE gel. The labeled DNA is precipitated in COT-1 DNA, salmon sperm DNA, sodium acetate and 95% ethanol, then dried and resuspended in 50% formamide hybridization buffer. The probe/hybridization buffer mix and slide were denatured, probe was applied to the slide, and slide was hybridized for 48 hours at 37° in a humidified chamber. After hybridization, the FISH slides were washed in a 2xSSC solution at 72° for 15 seconds, and counterstained with DAPI stain. Fluorescent signals were visualized on an Olympus BX61 microscope workstation (Applied Spectral Imaging, Vista, CA) with DAPI and Texas Red filter sets. FISH images were captured using an interferometer-based CCD cooled camera (ASI) and FISHView ASI software.

Genotyping

Control animals (*Trp53*^{R270H} and *Sp7-cre*) utilized have been described previously (Moriarity et al., 2015). With the use of many transgenes, all animals had mixed genetic backgrounds. Animals were aged until tumor development or until moribund. Small tail biopsies from weaned animals were collected and genomic DNA (gDNA) was extracted using phenol:chloroform:isoamyl alcohol extraction following overnight digestion in SDS extraction buffer(Moriarity et al., 2015). PCR was performed using GoTaq green master mix (#M7121, Promega). Amplicons were resolved on 1% agarose gels and analyzed for the presence of transgenes.

ZNF217 Forward: 5'-TCCAGCTCGACGTTAGAAGG-3'

ZNF217 Reverse: 5'-AGGAACTGCTTCCTTCACGA-3'

Trp53^{R270H} Forward: 5'-TTACACATCCAGCCTCTGTGG-3'

Trp53^{R270H} Reverse: 5'-CTTGGAGACATAGCCACACTG-3'

Trp53^{R270H} LSL: 5'-AGCTAGCCACCATGGCTTGAGTAAGTCTGCA-3'

Sp7-cre Forward: 5'-CTCTTCATGAGGAGGACCCT-3'

Sp7-cre Reverse: 5'-GCCAGGCAGGTGCCTGGACAT-3'

Bioluminescent imaging

Animals were injected intraperitoneally (IP) with luciferin (#XR- 1001, Xenogen) in sterile PBS at 10 µl/g body weight 10-15 minutes prior to imaging. Following administration, animals were gently anesthetized using a mixture of isoflurane and oxygen and imaged using the IVIS 50 *in vivo* bioluminescent system (BLI).

ZNF217 knockdown RNA sequencing and analysis

Raw fastq sequencing data (2x75bp PE, ~20M reads per sample) was trimmed for low quality and adapter specific sequences. Quality sequence was aligned to GRCh38 using HISTAT2 and gene level count data was produced by subread featurecounts using an GTF file containing protein coding Ensembl genes. DESeq2 was used for differential expression analysis. TPMs were calculated using a custom R script and the lengths and counts from the featurecount output. PCA was done using the R function prcomp and heatmaps were generated using the R library pheatmap. STRINGDB was used for pathway enrichment analysis using the top 150 DEGs based on adjusted p-value.

In vitro drug inhibition analysis

OSA cells were seeded into 384-well plates at 2 x 10^3 cells/well using a Biomek 2000 24 hours prior to experiments. Drug compounds (TCN/doxorubicin and associated controls) were added in quadruplicate wells per dose in a 12-point two-fold dose-response manner using the acoustic Echo 550 liquid dispenser (Labcyte). Drug combinations were plated in a constant ratio as indicated in each legend. 48 hours post drug treatment, cells were incubated with alamarBlue reagent (#Thermo Fisher) and fluorescence was read on a CLARIOstar microplate reader (BMG LABTECH). Cell viability was calculated by fluorescence of experimental wells in percent of unexposed control wells with blank values subtracted. Dose-response curves were generated using nonlinear regression log(inhibitor) vs. response-variable slope model. Drug interactions were determined using the median-effect principle of Chou-Talalay (Chou, 2006, 2010). CI values were calculated using CalcuSyn software (Biosoft) as previously described (Matthews, Deakin, Rajab, Idris-Usman, & Nirmalan, 2017). CI<1, =1, and >1 indicate synergism, additive effect, and antagonism, respectively.

Orthotopic mouse model

All animal procedures were performed in accordance with protocols approved at the University of Minnesota (#1905-37099A) in conjunction with the Institutional Animal Care and Use Committee (IACUC). OSA cells (2.5 x 10^5) were injected into the calcaneus of 6-8-week-old male and female

immunocompromised mice (NOD Rag Gamma, Jackson Labs, (B. A. Smeester, Al-Gizawiy, & Beitz, 2012; B. A. Smeester et al., 2013)). Tumor volume was calculated via caliper measurements using the formula V = (W*W*L)/2 where V equals tumor volume, W equals tumor width and L equals tumor length (Faustino-Rocha et al., 2013).

TCN treatment *in vivo*

Once orthotopic OSA tumors were established (PID 10), animals were randomized and enrolled onto study. Previous clinical research indicated that adult cancer patients received doses of TCN between 20-48 $mg^2/m^2/d$, however; cumulative toxicity was noted in adult patients receiving 30 $mg^2/m^2/d$ (~10 mg/kg/d in mice(Nair et al., 2016)) despite no toxicities with a 45 mg/m^2 single administration (Garrett et al., 2011). Given the majority of OSA cases are in adolescence (Kansara et al., 2014) and that higher dosages can be required for efficacy in pediatric patients (Ivanovska et al., 2016; O'Hara et al., 2016), we rationalized that a less frequent, higher-dose regimen of TCN may overcome these clinical limitations to date in adults and better serve future pediatric patients. As such, animals received 40 mg/kg TCN or control treatment three times weekly (3X) IP beginning PID 10. TCN was prepared in a 1% DMSO/30% polyethylene glycol/1% Tween-80 solution for all *in vivo* studies.

Statistical analyses

All statistical analyses were performed using Prism v8 software (GraphPad). Two groups were compared using a two-tailed unpaired Student's T-test. Three or more groups were compared using a One-way ANOVA or Two-way ANOVA analyses with Bonferroni's post hoc. All statistical analyses are individually indicated throughout. In all cases, $p < 0.05$ was considered statistically significant.

Results

ZNF217 is expressed in primary OSA tumors and cell lines

First, we explored the expression of *ZNF217* in available human OSA data sets and compared them to normal human osteoblasts (NHOs). RNA-seq analysis of three independent data sets found no significant expression differences when OSA samples from each data set were compared to NHOs (Fig. 1a), though there were many outlier samples with high ZNF217 expression. Next, using TMA sections, we evaluated ZNF217 expression across a series of patient samples in duplicate using immunohistochemical (IHC) staining. Positive ZNF217 staining was detectable in 51.2% of samples (41/80) (Figs. 1b-c). As expected, ZNF217 was found in the nucleus of positive cells, but interestingly, was also detected in the cytoplasm (Figs. 1d-e). Consistent with these findings, ZNF217 was aberrantly expressed in OSA cell lines as compared to NHOs and an immortalized osteoblast cell line (hFOB1.19) (Fig. 1f). Likewise, ZNF217 was also found localized in both the nucleus and the cytoplasm of cell lines (Supp. Figs. 1a-b). Overall, this data supports the existence of $ZNF217^{+}$ OSA cells in

human samples and OSA cells localized in both the nuclear and cytoplasmic compartments.

ZNF217 accelerates OSA tumor development and contributes to metastasis

Having established positive ZNF217 expression in human samples and cell lines, we adopted a loss-of-function (LOF) strategy using pooled siRNAs to understand the potential oncogenic role of ZNF217 in OSA. Transient knockdown of ZNF217 (Supp. Figs. 2a-b) reduced cellular proliferation (Fig. 2a), colony formation in soft agar (Fig. 2b), and cellular migration (Fig. 2c). As further evidenced in our gain-of-function (GOF) studies, overexpression of *ZNF217* in immortalized osteoblasts and in SJSA-1 OSA cells increased proliferation (Supp. Figs. 3a-b). These phenotypes were further investigated *in vivo* following establishment of a stable shZNF217 SJSA-1 cell line (Supp. Fig. 2c). Similar to our *in vitro* experiments, shRNA knockdown of *ZNF217* led to reduced OSA tumor growth (Fig. 2d) and metastasis (Fig. 2e). Together, these data indicate a potential driver role for ZNF217 in OSA progression, and metastasis.

Development of a conditional, tissue specific *ZNF217* overexpression model

Given the strong phenotypic and cellular signaling responses observed in ZNF217 knockdown cell lines and the fact that a subset of *SB*-mutagenized tumors were driven by *ZNF217* insertions in our previous work (Moriarity et al., 2015), we hypothesized that *ZNF217* may be a driver gene in

osteosarcomagenesis. To study this hypothesis, we generated a novel model relevant to human OSA disease in the context of conditional, tissue-specific *ZNF217* expression by combining *ZNF217* and *Trp53*^{R270H} alleles with *Sp7-cre* mice (Fig. 3a, *Sp7-cre*;*Trp53*^{R270H};*ZNF217* mice). *ZNF217* transgene cassette integration was confirmed via fluorescence *in situ* hybridization (FISH) (Fig. 3b) and polymerase chain reaction (PCR, Fig. 3c) in generated animals. Functional *ZNF217* expression was validated *in vivo* using bioluminescent imaging (Fig. 3d). *ZNF217* overexpression accelerated tumor development compared to control animals (*Sp7-cre*;*Trp53*^{R270H}) (Fig. 3e). No OSAs were observed in *Sp7-cre* or *Trp53*^{R270H} alone animals (data not shown). Accelerated tumors were confirmed histologically to be consistent with OSA (Moriarity et al., 2015) (Fig. 3f, H & E) and contained positive ZNF217 expression via western blot (Fig. 3g). In sum, these data indicate a potential driver role for ZNF217 in accelerating OSA.

Global transcriptome analysis reveals ZNF217 is associated with regulation of PI3K-AKT signaling, cytoskeletal rearrangement, and apoptosis

In order to characterize the OSA transcriptome influenced by *ZNF217* expression, we subjected SJSA-1 OSA cells to RNA-sequencing following *ZNF217* knockdown and analyzed mRNA libraries generated. Scaled gene expression from differentially expressed genes (DEGs) were clustered from two biological replicates, demonstrating that *ZNF217* knockdown cells (si-ZNF217) formed distinct clusters when compared to non-silencing controls (si-NS) (Supp. Fig. 4a, heatmap). We obtained a total of 240 DEGs in our dataset. This included

145 upregulated DEGs and 31 downregulated DEGs (p_{adj} < 0.05, FC +/- 1.5). The top 25 DEGs are shown in Supplementary Table 2.

To identify biological attributes and functional categories of the DEGs identified, Gene Ontology (Biological process GO) and Kyoto Encyclopedia of Genes and Genomes (KEGG) pathway analyses were performed on the top 150 out of 240 DEGs (p_{adj} < 0.05, FC +/- 1.5) altered using Stringdb (https://string-db.org). Among the most significantly enriched GO terms were DEGs involved in cell migration/adhesion, proliferation, surface receptor signaling, localization, signaling transduction, and apoptosis (Fig. 4a). Significant KEGG pathways enriched included TNF signaling, PI3K-AKT signaling, focal adhesion, ECM-matrix regulation, and apoptosis among others (Fig. 4b).

An increasing body of literature suggests PI3K-AKT signaling is highly important in OSA biology and contributes to numerous facets of transformation including epithelial-to-mesenchymal transition (EMT), tumor progression, and metastasis (Cohen, Donini, Nguyen, Lincet, & Vendrell, 2015; Krig et al., 2010; Littlepage et al., 2012; Vendrell et al., 2012; Moriarity et al, 2015). Since our transcriptome analysis implicated the PI3K-AKT pathway and we previously established a significant role for ZNF217 in osteosarcomagenesis/metastasis, we validated and examined the role of PI3K-AKT signaling in the context of ZNF217 further. Similar to our RNA and IHC analyses on ZNF217, we explored the expression of *AKT1*, *AKT2*, and *AKT3* in available human OSA data sets and compared them to normal human osteoblasts (NHOs). RNA analysis of three independent data sets found significantly increased expression of *AKT1* and

AKT2 when OSA samples from each data set were compared to NHOs (Supp. Fig. 5a). When TMA sections were evaluated, positive p-AKT^{Ser473} staining was detectable in 96.3% of samples (77/80) (Supp. Figs. 5b-c) and was localized to both the nucleus and cytoplasm (Supp. Fig. 5d). In further agreement with our transcriptomics data, knockdown of ZNF217 was also associated with reduced p-AKT^{Ser473} signaling (Fig. 4c) and increased apoptosis (Fig. 4d). Together, these alterations in the gene expression signature suggest that *ZNF217* promotes a highly invasive and proliferative signaling program that enhances OSA malignancy and metastasis in part through regulation of PI3K-AKT signaling.

AKT blockade is cytotoxic in OSA cells *in vitro*

Recent studies have sought to identify candidate small molecules and miRNA-based therapeutics for combating ZNF217-induced oncogenic signaling, particularly in breast cancer (Cohen et al., 2015). To date, one such compound, triciribine (TCN), has been identified and shown to effectively reduce tumor growth and metastases in ZNF217^{+} breast tumor cells (Littlepage et al., 2012). We hypothesized that TCN treatment would be an effective therapy for treatment of ZNF217-expressing OSAs. When evaluated *in vitro*, TCN treatment effectively reduced soft agar colony formation (Fig. 4a), cellular migration (Fig. 4b), and cell viability (Fig. 4c). Similar to our genetic findings, TCN treatment reduced p-AKT^{Ser473} signaling (Fig. 4d), ZNF217 protein expression (Fig. 4e), and induced apoptosis (Fig. 4f). Treatment with PI3K inhibitor LY294002 also inhibited cell viability (Supp. Fig. 6a), ZNF217 protein expression (Supp. Fig. 6b), and

produced a modest induction of apoptosis (Supp. Fig. 6c). This data suggests that targeting the PI3K-AKT signaling pathway has robust cytotoxic effects on ZNF217-expressing OSA cell lines treated *in vitro* and that ZNF217 is part of a feedforward loop involving PI3K-AKT signaling.

Triciribine effectively reduces growth and metastasis in OSA tumors

Lastly, the therapeutic potential of TCN was evaluated in an orthotopic mouse model of OSA using two different OSA cell lines. Tumor-bearing animals were treated three times weekly (3X) with TCN or control and tumors were measured until endpoint (post-implantation day 31, PID31). Both tumor volume (Fig. 5a) and tumor weights at endpoint (Fig. 5b) were significantly reduced in animals receiving TCN. No appreciable toxicity was observed as evidenced by animals' body weights during treatment (Fig. 5c). IHC analysis of tumor tissue confirmed that ZNF217 was significantly reduced in TCN-treated animals (Fig. 5d). TCN treatment was also associated with reduced micro-metastatic nodule formation (Fig. 5e). In sum, AKT signaling blockade with TCN effectively reduces $ZNF217^{+}$ OSA tumor growth and metastasis (Supp. Fig. 7).

Combination chemotherapy and AKT blockade is synergistic

Recent evidence suggests that tumor cells expressing *ZNF217* are chemo-resistant (Frietze et al., 2014; Littlepage et al., 2012; Thollet et al., 2010). We examined the *in vitro* efficacy of combination therapy targeting the AKT signaling axis and traditional standard of care chemotherapy on human OSA cell

lines. This was done with the AKT inhibitor TCN and the broad-spectrum chemotherapeutic doxorubicin. In all cases, significant synergy was observed with the combination treatment, particularly at an effective dose 90 (ED_{90}) (Fig. 6a-b). Cell lines SJSA-1 and SaOS-2 show extremely strong susceptibility to the combination therapy with combination index (CI) values at ED_{90} of ~0.1 or lower (Fig. 6b). Together, these results suggest that combination therapy is highly effective *in vitro*.

Discussion

It is undeniable that novel treatment options are urgently needed for OSA patients. Here we find that ZNF217 is responsible for the regulation of a malignant gene network involved in OSA development, progression, and metastasis. We recently identified *ZNF217* (murine *Zfp217*) as an important driver of a subset of *SB*-induced OSAs (Moriarity et al., 2015), which suggests ZNF217 may be important in osteosarcomagenesis during osteoblastic development. Encouragingly, other ZNF family members have been implicated in osteoblastic differentiation (Twine, Harkness, Kassem, & Wilkins, 2016), facilitating commitment to the osteoblast lineage (Qi et al., 2003) and were also found to be putative drivers in some of our *SB*-induced OSAs (Moriarity et al., 2015) (*ZNF592*). This is further supported by complementary reports of oncogenic ZNF217 signaling in colon (Rooney et al., 2004), prostate (Sehrawat et al., 2018), breast (Littlepage et al., 2012), and ovarian (J. Li et al., 2014) solid tumors. Here, we provide new information on the oncogenic roles ZNF217 plays

in OSA. While *ZNF217* RNA levels were relatively similar to NHOs, ZNF217 protein was abundantly detectable (>50% of samples probed) in OSA tumors in a subset of human samples and cell lines. Both human samples and cell lines had detectable nuclear and cytoplasmic localization. Interestingly, aberrant cytoplasmic ZNF217 expression has recently been reported in solid tumors of the breast and colon (Z. Li et al., 2015; Messana, Yang, & Littlepage, 2014) and has been functionally linked to estrogen receptor alpha trafficking in MCF-7 breast cancer cells (Nguyen et al., 2014). In combination with our findings, further investigation into the mechanisms of ZNF217 localization are needed. This could be approached through the use of structure-function studies where site-directed mutagenesis is utilized systematically to determine the functional importance of key molecular domains within *ZNF217* and how cytoplasmic and nuclear ZNF217 may be playing distinct or redundant roles as they relate to OSA tumor development, progression, and metastasis.

Given the diverse roles ZNF217 can play, it is not surprising that genetic knockdown of *ZNF217* significantly inhibited hallmarks of cellular transformation, ultimately culminating in reduced OSA tumor progression and metastasis in our orthotopic mouse model. Moreover, ZNF217 also protected cells from death, as knockdown readily induced apoptosis. In combination with our transcriptomics data, our studies suggest ZNF217 promotes tumorigenesis and metastasis in part through regulation of PI3K-AKT signaling. Our group and others have demonstrated dysregulated PI3K-AKT signaling can drive a subset of murine (Moriarity et al., 2015), canine (Levine, Forest, & Smith, 2002; Russell, Jaworski,

& Kisseberth, 2018), and human OSAs (Xi & Chen, 2017; Xi, Qi, Ma, & Chen, 2020; J. Zhou, Xiao, Wang, & Luo, 2019). Moreover, this dysregulation is present in a majority of localized OSA cases and in all advanced-stage cases (J. Zhang, Yu, Yan, Wang, & Wang, 2015; W. Zhou et al., 2014). Mirroring these previous studies, we found upregulation of *AKT1* and *AKT2* transcripts when compared to NHOs across available OSA data sets; isoforms known to be involved in the proliferation and metastasis of OSAs (J. Zhu et al., 2017; Y. Zhu, Zhou, Ji, & Yu, 2014). Additionally, significant presence of active AKT staining (p-AKT^{Ser473}) in our OSA TMA was apparent. Given our identification of PI3K-AKT signaling as a therapeutically targetable axis in ZNF217-expressing OSA cells, these data provided an attractive rationale for investigating small molecule AKT inhibitors preclinically for the treatment of OSA.

Transcription factors account for approximately 20% of all oncogenes identified to date and historically have been difficult to drug directly (Lambert, Jambon, Depauw, & David-Cordonnier, 2018). Despite this, recent work has identified a candidate small molecule for combating ZNF217-induced oncogenic AKT signaling. Triciribine (TCN) is a nucleoside analog with strong selectivity for AKT (Yang et al., 2004). TCN is thought to mechanistically inhibit the activation of the AKT signaling pathway directly as TCN was not found to act as an ATP/substrate inhibitor of the enzyme directly (Yang et al., 2004). In support of our genetic findings, cytotoxic TCN treatment significantly reduced phenotypes of cellular transformation *in vitro*, ZNF217 expression, and tumor growth/metastasis *in vivo*. We also found that treatment of OSA cells with PI3K inhibitor LY294002

also inhibited cell viability, ZNF217 protein expression, and produced a modest induction of apoptosis. This suggests a positive feedforward mechanism for ZNF217-induced AKT signaling which agrees with our overexpression studies that demonstrate hyperactivation of AKT (p-AKT^{Ser473}) in *ZNF217*-overexpressing immortalized osteoblasts and SJSA-1 OSA cells.

Both Phase I and II clinical trials of TCN have been conducted in advanced malignancies previously (Feun, Blessing, Barrett, & Hanjani, 1993; Feun et al., 1984; Garrett et al., 2011; Hoffman et al., 1996; Schilcher, Haas, Samson, Young, & Baker, 1986). While treatment was associated with some side effects, including hepatotoxicity and hyperglycemia, modest benefits in stabilizing disease were observed in at least 1 breast cancer patient undergoing treatment (Hoffman et al., 1996). More recent work suggests that TCN bioavailability may explain the poor clinical results to date (Berndt et al., 2010). A new activated form of TCN (TCN-P) has been developed (PTX-200, Prescient Therapeutics) and is currently recruiting patients with refractory or relapsed acute leukemia (NCT02930109) and has active status for Phase I treatment of ovarian (NCT01690468) and Phase I/II treatment of stages II-IV breast cancer (NCT01697293) in combination with chemotherapy.

Although TCN was well-tolerated in our animal studies as evidenced by statistically insignificant differences in weekly body weight measurements, we sought to build upon our TCN monotherapy experiments through combinatorial studies with doxorubicin. Excitingly, strong synergy was observed in all OSA lines treated in combination. Interestingly, the HOS cell line and its KRAS-

activated derivative 143B (Ottaviano et al., 2010) had CI values that were slightly higher than SJSA-1 and SaOS-2 cell lines (CI at ED_{90} ~0.6). Previous work from She and colleagues has demonstrated that concurrent activation of RAS-MAPK and PI3K-AKT signaling induced resistance to AKT blockade (She et al., 2010). This was also observed in breast cancer cell lines with mutations in RAS-MAPK and PI3K-AKT pathways (Littlepage et al., 2012).

In summary, our diverse biological data demonstrate a role for ZNF217 in promoting osteosarcomacogenesis and metastasis through modulation of an oncogenic gene network regulated in part through active PI3K-AKT signaling. Importantly, our work has uncovered the therapeutic potential of targeting the PI3K-AKT signaling axis in OSA through the use of the small molecule AKT inhibitor TCN and the excellent synergism observed when combined with the broad-spectrum chemotherapy agent doxorubicin. Together, this supports the use of TCN as a neoadjuvant therapy in OSA patients with $ZNF217^{+}$ and active AKT tumors.

Figure 1 ZNF217 is expressed in OSAs

(a) Violin plots of RNA-seq $\log_{10}$ transformed FPKM values of *ZNF217* in 3 independent OSA patient data sets compared to normal human osteoblasts (NHOs); NHOs (n = 3), #1 (n = 20) , #2 (n = 35), #3 (n = 117). (b) Quantification of positive and negative ZNF217 staining in a human OSA TMA. (c) Representative images of positive and negative staining for ZNF217; mag 20X, insets 40X, scale bars 50 μm and 25 μm respectively. (d) Table indicating the number of positive cells at the indicated percentages that express ZNF217 and localization. (e) Representative images of ZNF217 localization; mag 40X, scale bars 26 μm. Black arrows indicate positive staining. (f) Total cell lysates were subjected to western blotting using ZNF217-specific antibody.

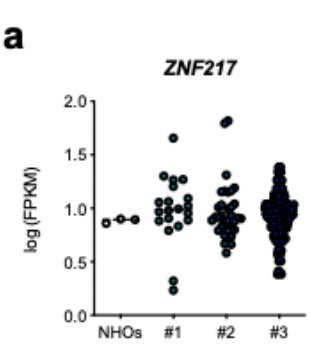

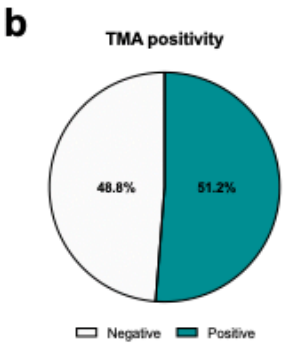

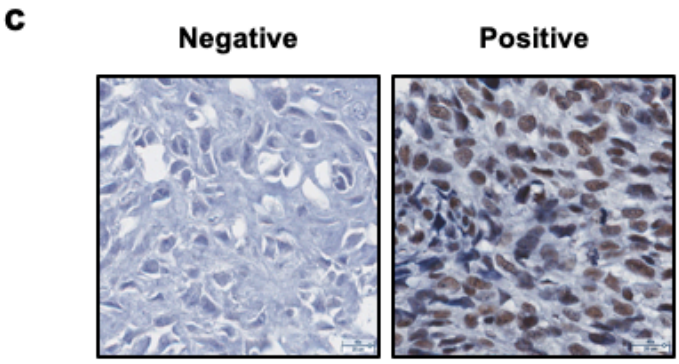

d

ZNF217					
		% of positive cells Number of samples			
Localization	# of cases	<1%	1-24%	25-50%	>50%
Nuclear	41	0	10	13	18
Cytoplasmic	41	10	28	3	0

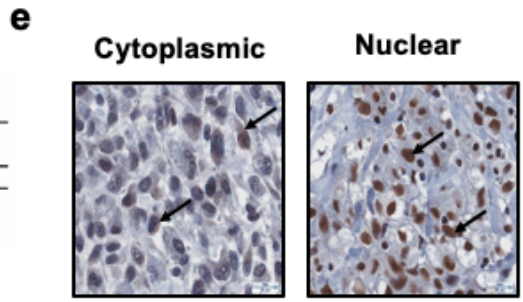

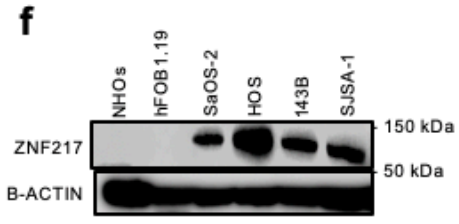

Figure 2 ZNF217 is associated with OSA tumor progression and contributes to metastasis

(a) Transient knockdown of ZNF217 reduces cellular proliferation (n = 18/group), (b) colony formation (n = 36/group), and (c) migration (n = 12/group). Stable ZNF217 knockdown reduces (d-e) tumor growth and (f) metastasis. Representative images of ZNF217 in tumors and H & E images of lung sections shown to the right respectively; mag 4X, scale bars 1000 μm, black arrows indicate micro-metastatic nodules. Data shown as mean ± SEM. Panels (a,d) Two-way ANOVA; Panels (b,c,f) Student's T-test. *$p < 0.05$, **$p < 0.01$, ****$p < 0.0001$.

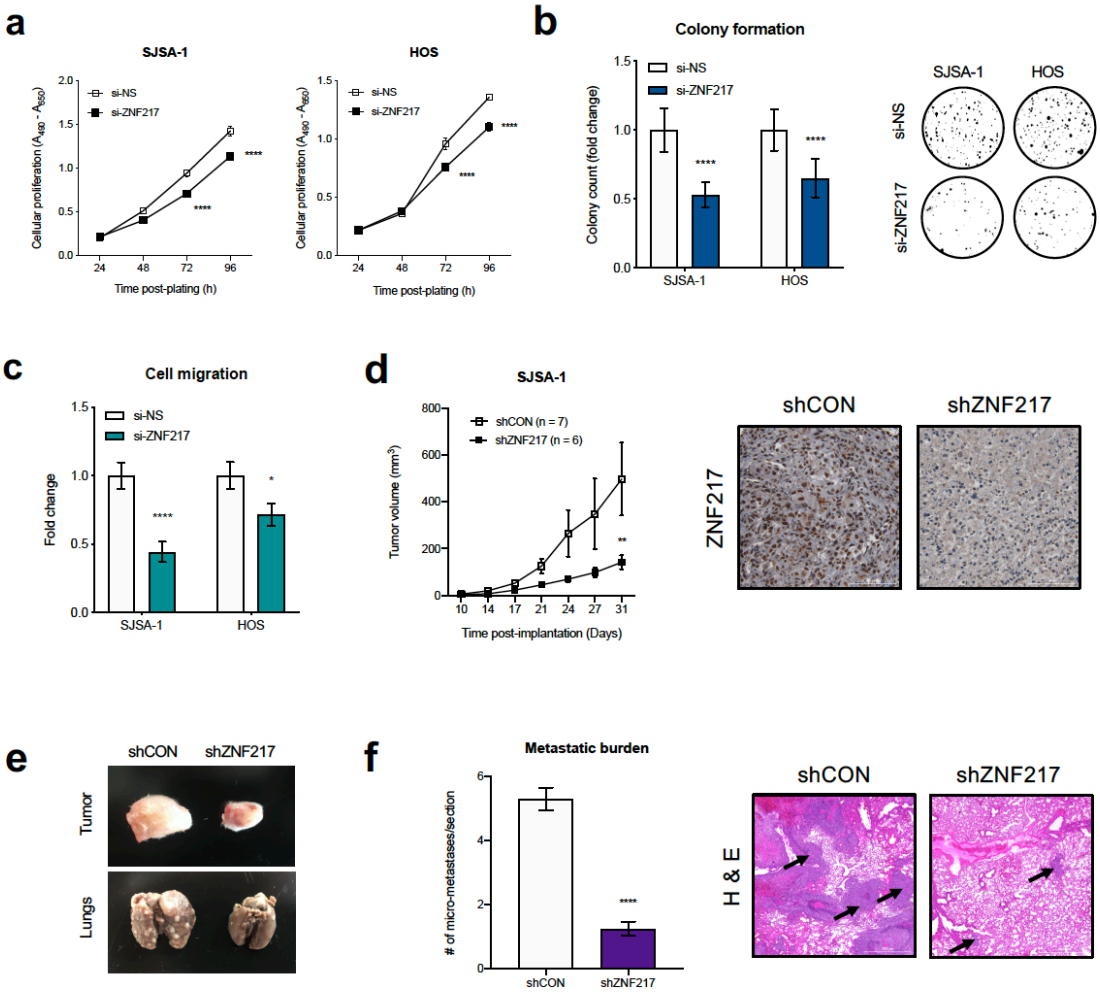
a
SJSA-1
HOS
si-NS
si-ZNF217
Cellular proliferation (A_{490} - A_{650})
Time post-plating (h)
b
Colony formation
Colony count (fold change)
SJSA-1
HOS
si-NS
si-ZNF217
c
Cell migration
Fold change
d
SJSA-1
shCON (n = 7)
shZNF217 (n = 6)
Tumor volume (mm^3)
Time post-implantation (Days)
shCON
shZNF217
ZNF217
e
Tumor
Lungs
f
Metastatic burden
# of micro-metastases/section
H & E

Figure 3 Generation and validation of *ZNF217* genetically engineered mouse model (GEMM)

(a) Breeding schematic used for generating transgenic animals. (b) Confirmation of *ZNF217*-IRES-*Luciferase* transgene cassette integration via FISH. (c) Example PCR genotyping confirmation of *ZNF217*;*Trp53*^{R270H};*Sp7*-cre^{+} animals. (d) Functional validation of positive transgene expression via bioluminescence in *ZNF217*;*Trp53*^{R270H};*Sp7*-cre^{+} animals. Red arrows indicate positivity in all images. (e) Overexpression of *ZNF217* in mouse osteoblasts accelerates tumorigenesis (n = 9/group). (f) H & E image confirming OSA-like appearance in *ZNF217*-overexpressing tumor; mag 20X, scale bars 200 μm. (g) Total cell lysates from representative tumors were subjected to western blotting using ZNF217-specific antibody (n = 2 lysates/group). Panel (e) Log rank test. *p < 0.05.

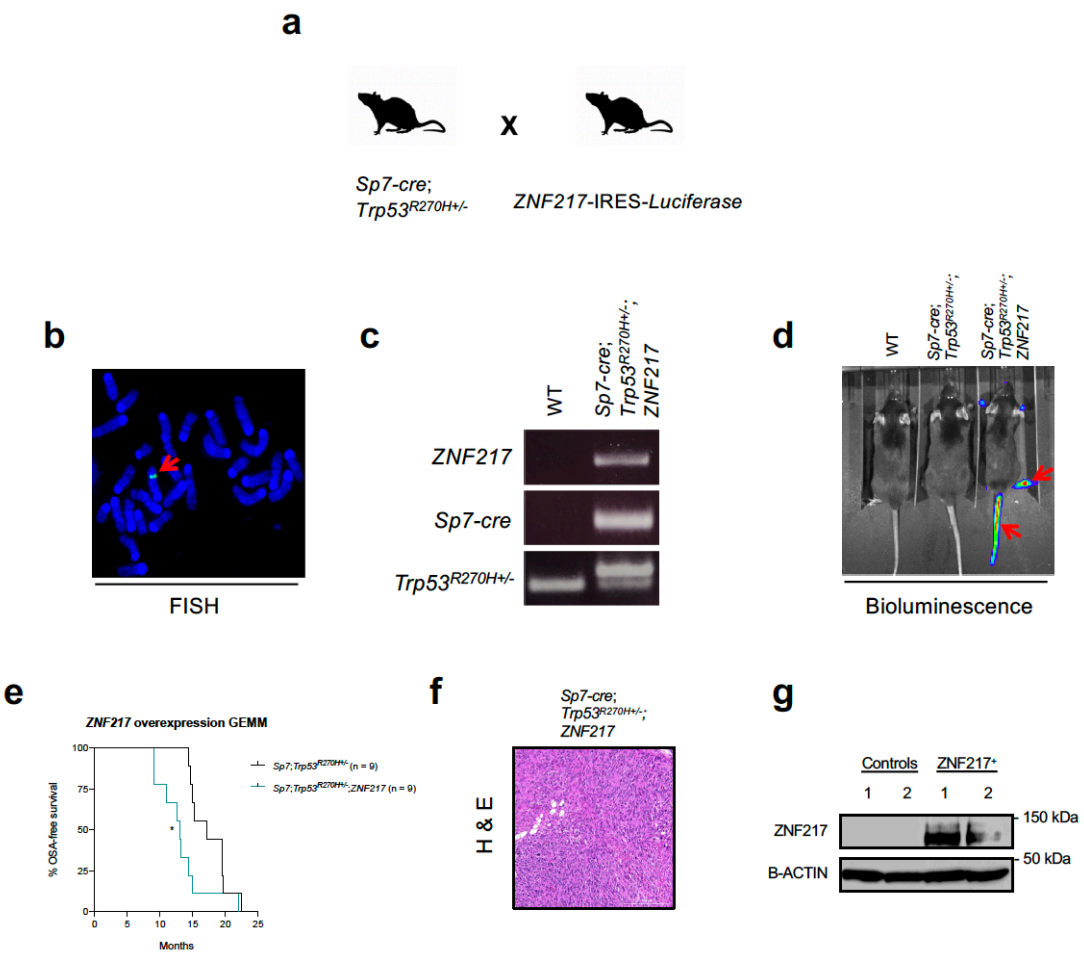
a
x
Sp7-cre;
Trp53R270H+/-
ZNF217-IRES-Luciferase
b
FISH
c
WT
Sp7-cre; Trp53R270H+/-; ZNF217
ZNF217
Sp7-cre
Trp53R270H+/-
d
WT
Sp7-cre; Trp53R270H+/-;
Sp7-cre; Trp53R270H+/-; ZNF217
Bioluminescence
e
ZNF217 overexpression GEMM
% OSA-free survival
Months
Sp7;Trp53R270H+/- (n = 9)
Sp7;Trp53R270H+/-;ZNF217 (n = 9)
f
Sp7-cre; Trp53R270H+/-; ZNF217
H & E
g
Controls
ZNF217+
1 2 1 2
ZNF217
B-ACTIN
150 kDa
50 kDa

Figure 4 Global transcriptome analysis reveals ZNF217 is associated with regulation of PI3K-AKT signaling, cytoskeletal rearrangement, and apoptosis

(a) Functional GO analysis and (b) KEGG pathway enrichment of highly significant biological processes following ZNF217 knockdown. (c) Phosphorylation of AKT (p-AKT^{Ser473}) was evaluated after ZNF217 knockdown. (d) ZNF217 knockdown induces apoptosis (n = 3/group). Representative Annexin-V^{+} flow plots are shown to the right.

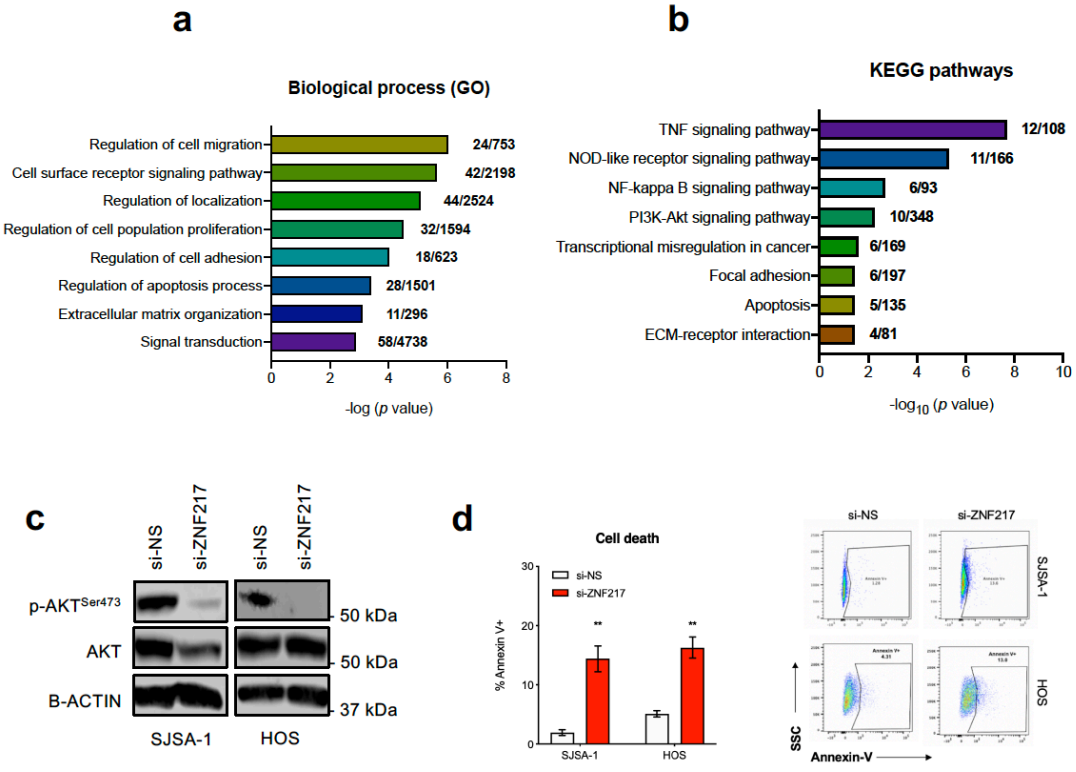
a
Biological process (GO)
Regulation of cell migration
24/753
Cell surface receptor signaling pathway
42/2198
Regulation of localization
44/2524
Regulation of cell population proliferation
32/1594
Regulation of cell adhesion
18/623
Regulation of apoptosis process
28/1501
Extracellular matrix organization
11/296
Signal transduction
58/4738
0 2 4 6 8
-log (p value)
b
KEGG pathways
TNF signaling pathway
12/108
NOD-like receptor signaling pathway
11/166
NF-kappa B signaling pathway
6/93
PI3K-Akt signaling pathway
10/348
Transcriptional misregulation in cancer
6/169
Focal adhesion
6/197
Apoptosis
5/135
ECM-receptor interaction
4/81
0 2 4 6 8 10
-log10 (p value)
c
si-NS
si-ZNF217
si-NS
si-ZNF217
p-AKTSer473
AKT
B-ACTIN
50 kDa
50 kDa
37 kDa
SJSA-1
HOS
d
Cell death
si-NS
si-ZNF217
% Annexin V+
30
20
10
0
**
**
SJSA-1
HOS
si-NS
si-ZNF217
SJSA-1
HOS
SSC
Annexin-V

Figure 5 AKT blockade is cytotoxic in OSA cells *in vitro*

A 48-hour treatment with triciribine (TCN) reduces (a) colony formation (n = 20-24/group), (b) cellular migration (n = 12/group) and (c) cell viability (n = 18/group). (d) Phosphorylation of AKT (p-AKT^{Ser473}) and (e) expression of ZNF217 was evaluated after TCN treatment. (f) TCN treatment induces apoptosis (n = 3/group). Representative Annexin-V^{+} flow plots are shown to the right. All data shown as mean ± SEM. Panels (a,b) One-way ANOVA. *p < 0.05, **p < 0.01, ***p < 0.001, ****p < 0.0001.

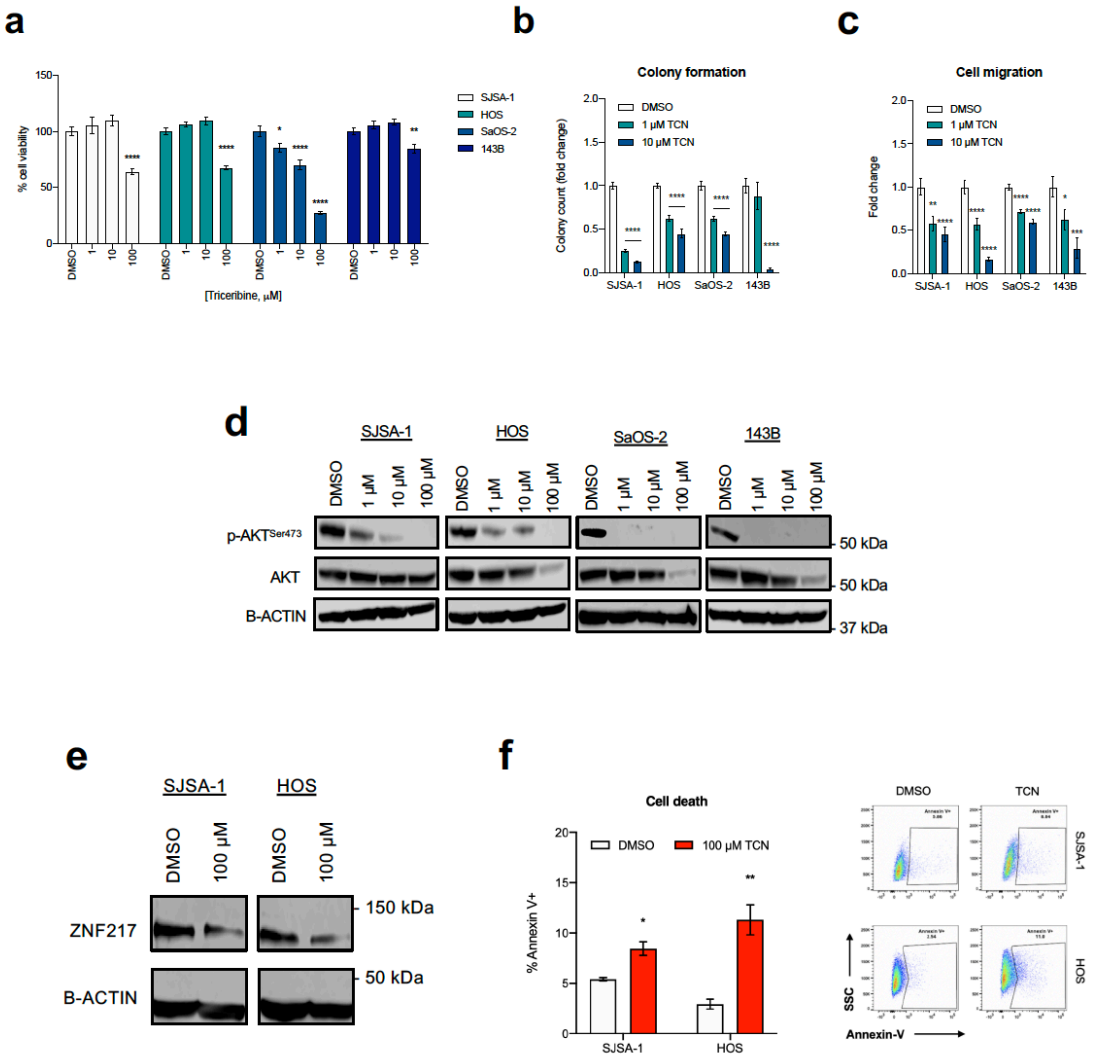
a
% cell viability
[Triceribine, μM]
SJSA-1
HOS
SaOS-2
143B
b
Colony formation
Colony count (fold change)
DMSO
1 μM TCN
10 μM TCN
c
Cell migration
Fold change
d
SJSA-1
HOS
SaOS-2
143B
p-AKTSer473
AKT
B-ACTIN
50 kDa
37 kDa
e
ZNF217
150 kDa
f
Cell death
% Annexin V+
100 μM TCN
DMSO
TCN
SSC
Annexin-V

Figure 6 Triciribine effectively reduces growth and metastasis in OSA tumors

(a) Triciribine (TCN)-treated OSA cell lines displayed reduced tumor growth compared to control-treated animals (n = 6-8/group). (b) TCN treatment reduced tumor weight at endpoint. (c) Weekly body weights of animals undergoing treatment. (d) Representative IHC staining of ZNF217 in TCN- or control-treated animals; mag 40X, scale bars 100 μm. (e) Micro-metastatic burden analysis (n = 3/group). Representative H&E staining in lung sections shown to the right; mag 4X, scale bars 1000 μm, black arrows indicate micro-metastatic nodules. All data shown as mean +/- SEM. Panel (a) Two-way ANOVA; Panel (b) Student's T-test. $^{**}p < 0.01$, $^{***}p < 0.001$, $^{****}p < 0.0001$.

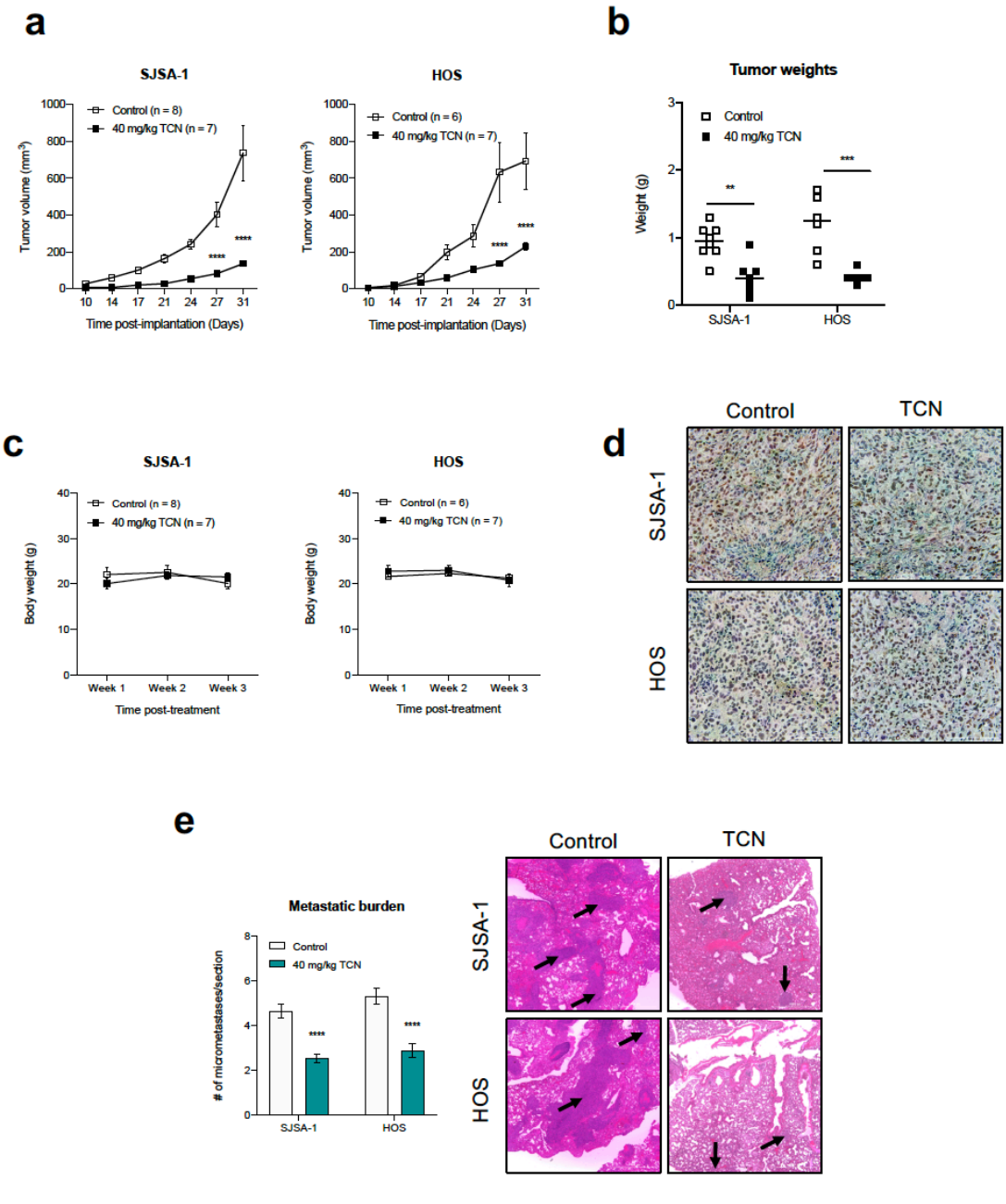
a
SJSA-1
HOS
Control (n = 8)
40 mg/kg TCN (n = 7)
Control (n = 6)
40 mg/kg TCN (n = 7)
Tumor volume (mm3)
Time post-implantation (Days)
b
Tumor weights
Control
40 mg/kg TCN
Weight (g)
SJSA-1
HOS
c
SJSA-1
HOS
Body weight (g)
Week 1
Week 2
Week 3
Time post-treatment
d
Control
TCN
SJSA-1
HOS
e
Metastatic burden
# of micrometastases/section
Control
40 mg/kg TCN
SJSA-1
HOS
Control
TCN

Figure 7 Combination chemotherapy and AKT blockade is synergistic *in vitro*

(a) Representative cell viability plots in cells treated with triciribine alone (TCN), doxorubicin alone, or in combination (green line). (b) Triciribine (TCN) in combination (400:1, 2000 – 50 μM TCN/doxorubicin) with doxorubicin exhibits synergism at each effective dose (ED_{50}, ED_{75} and ED_{90}). The r value indicates the correlation coefficient of the data to the mass-action law.

a

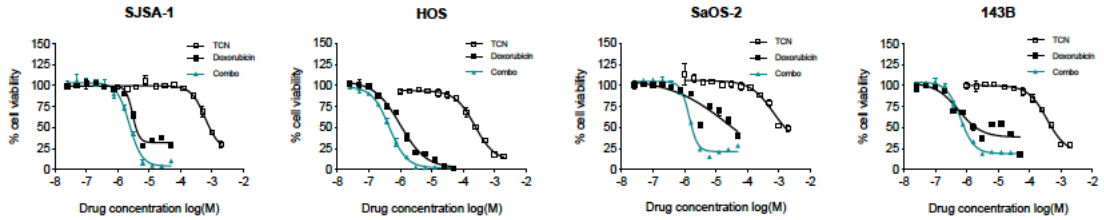

b

Drug Combo	Conc./Ratio	Cell Line	CI at ED_{50}	CI at ED_{75}	CI at ED_{90}	r
Triciribine (TCN) + Doxorubicin	2000μM:50μM (400:1)	SJSA-1	0.274	0.192	0.136	0.94
		HOS	0.716	0.698	0.697	0.95
		SaOS-2	0.172	0.104	0.063	0.87
		143B	0.679	0.634	0.605	0.91

CI Value	Indication
<0.3	Strongly Synergistic
<0.8	Synergistic
0.8-1.2	Additive
>1.2	Antagonistic

Supplementary Figure 1. Localization of ZNF217 in OSA cells

(a) Western blot staining of cytoplasmic extract (CYTO) and chromatin-bound nuclear extract (CBE) using a ZNF217-specific antibody. (b) Determination of ZNF217 localization by immunofluorescence (IF) staining; mag 40X, scale bars 100 μm, white arrows indicate positive staining.

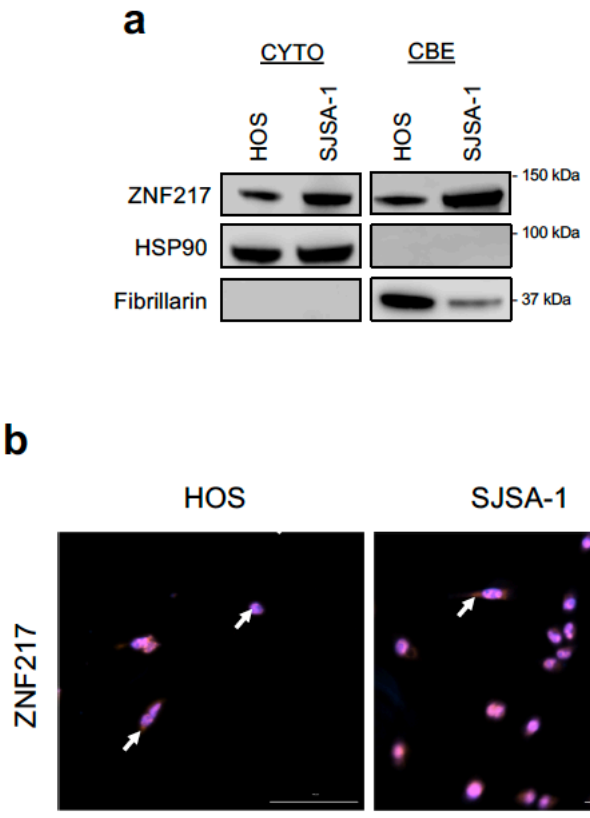
a
CYTO
CBE
HOS
SJSA-1
HOS
SJSA-1
ZNF217
HSP90
Fibrillarin
150 kDa
100 kDa
37 kDa
b
HOS
SJSA-1
ZNF217

Supplementary Figure 2. Confirmation of ZNF217 knockdown in OSA cells

(a) RT-qPCR for ZNF217 in transient control (si-NS) and knockdown cell lines (si-ZNF217) (n = 3/group). (b) Western blot confirming ZNF217 transient knockdown in SJSA-1 and HOS OSA cell lines. (c) Confirmation of stable ZNF217 knockdown in SJSA-1 cells.

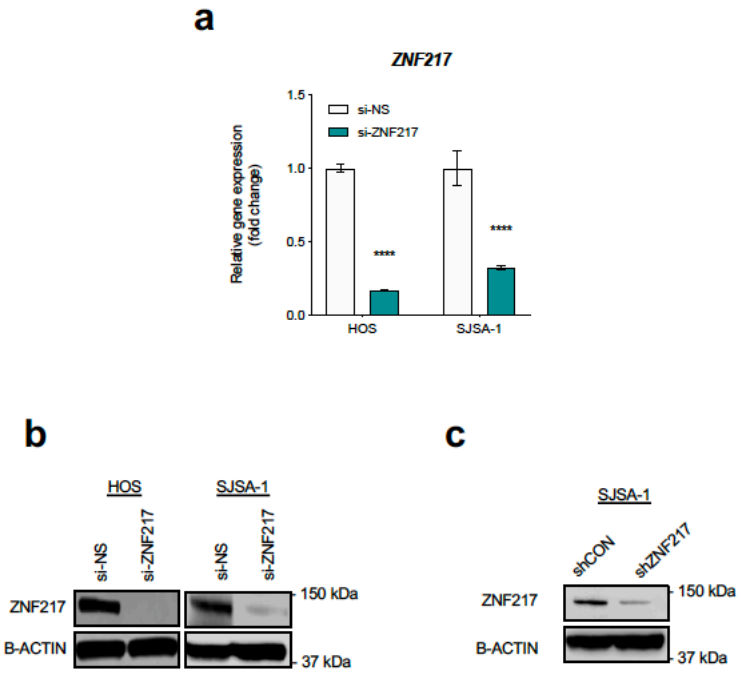
a
ZNF217
si-NS
si-ZNF217
Relative gene expression (fold change)
1.5
1.0
0.5
0.0
****
****
HOS
SJSA-1
b
HOS
SJSA-1
si-NS
si-ZNF217
si-NS
si-ZNF217
ZNF217
B-ACTIN
150 kDa
37 kDa
c
SJSA-1
shCON
shZNF217
ZNF217
B-ACTIN
150 kDa
37 kDa

Supplementary Figure 3. Activation of p-AKT^{Ser473} and increased cellular proliferation in *ZNF217*-overexpression cell lines

(a) Overexpression of *ZNF217* hyperactivates p-AKT^{Ser473} in immortalized osteoblasts (hFOB1.19) and SJSA-1 OSA cells. (b) Overexpression of *ZNF217* increases cell proliferation 48 hours post plating (n = 18). All data shown as mean +/- SEM. Panel (b) Student's t-test. ****$p < 0.0001$.

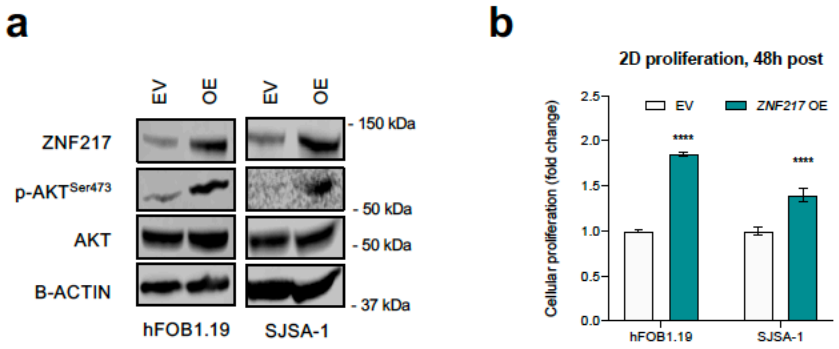
a
EV
OE
EV
OE
ZNF217
p-AKTSer473
AKT
B-ACTIN
- 150 kDa
- 50 kDa
- 50 kDa
- 37 kDa
hFOB1.19
SJSA-1
b
2D proliferation, 48h post
EV
ZNF217 OE
Cellular proliferation (fold change)
2.5
2.0
1.5
1.0
0.5
0.0
****
****
hFOB1.19
SJSA-1

Supplementary Figure 4 Heatmap of scaled gene expression

(a) Heatmap of scaled gene expression clustering in ZNF217 knockdown (si-ZNF217) and control (si-NS) replicates.

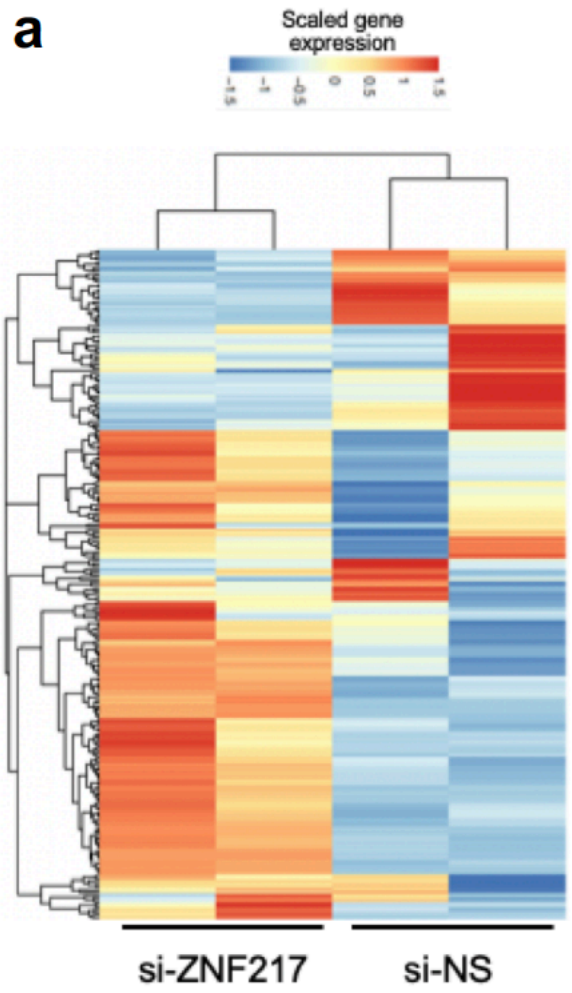
a
Scaled gene expression
si-ZNF217
si-NS

Supplementary Figure 5. Characterization of AKT signaling in human OSA samples

(a) Violin plots of RNA-seq log_{10} transformed FPKM values of *AKT1*, *AKT2*, and *AKT3* in 3 independent OSA patient data sets compared to normal human osteoblasts (NHOs); NHOs (n = 3), #1 (n = 20) , #2 (n = 35), #3 (n = 117). (b) Quantification of positive and negative p-AKT^{Ser473} staining in a human OSA TMA. (c) Representative images of positive and negative staining for p-AKT^{Ser473}; mag 20X, scale bars 50 μm. (d) Table indicating the number of positive cells at the indicated percentages that express p-AKT^{Ser473} and localization.

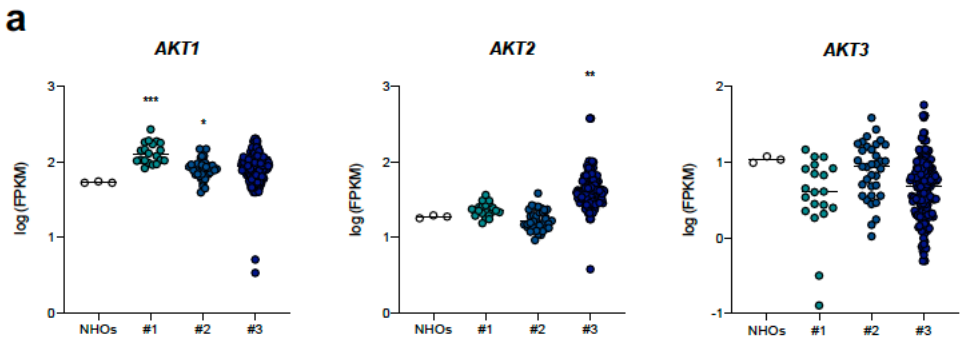

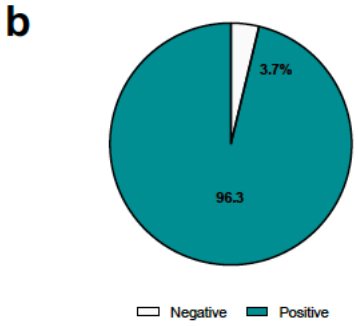

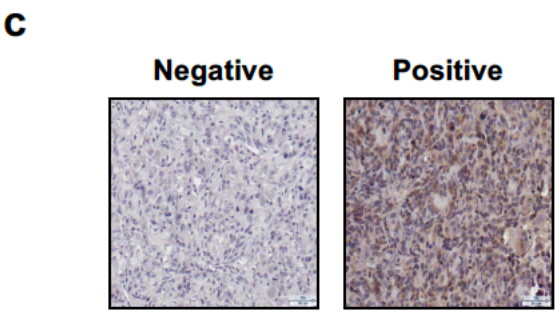

d

p-AKTSer473					
		% of positive cells Number of samples			
Localization	# of cases	<1%	1-24%	25-50%	>50%
Nuclear	77	0	17	29	31
Cytoplasmic	77	0	6	9	62

Supplementary Figure 6. PI3K blockade in OSA cells

(a) PI3K inhibition with LY294002 reduces cell viability 48 hours post-treatment (n = 18/group), (b) ZNF217 expression, and (c) induces modest apoptosis (n = 3/group). Representative Annexin-V^+ flow plots are shown to the right. All data shown as mean ± SEM. Panels (a,c) Student's t-test. *$p < 0.05$, **$p < 0.01$, ***$p < 0.001$, ****$p < 0.0001$.

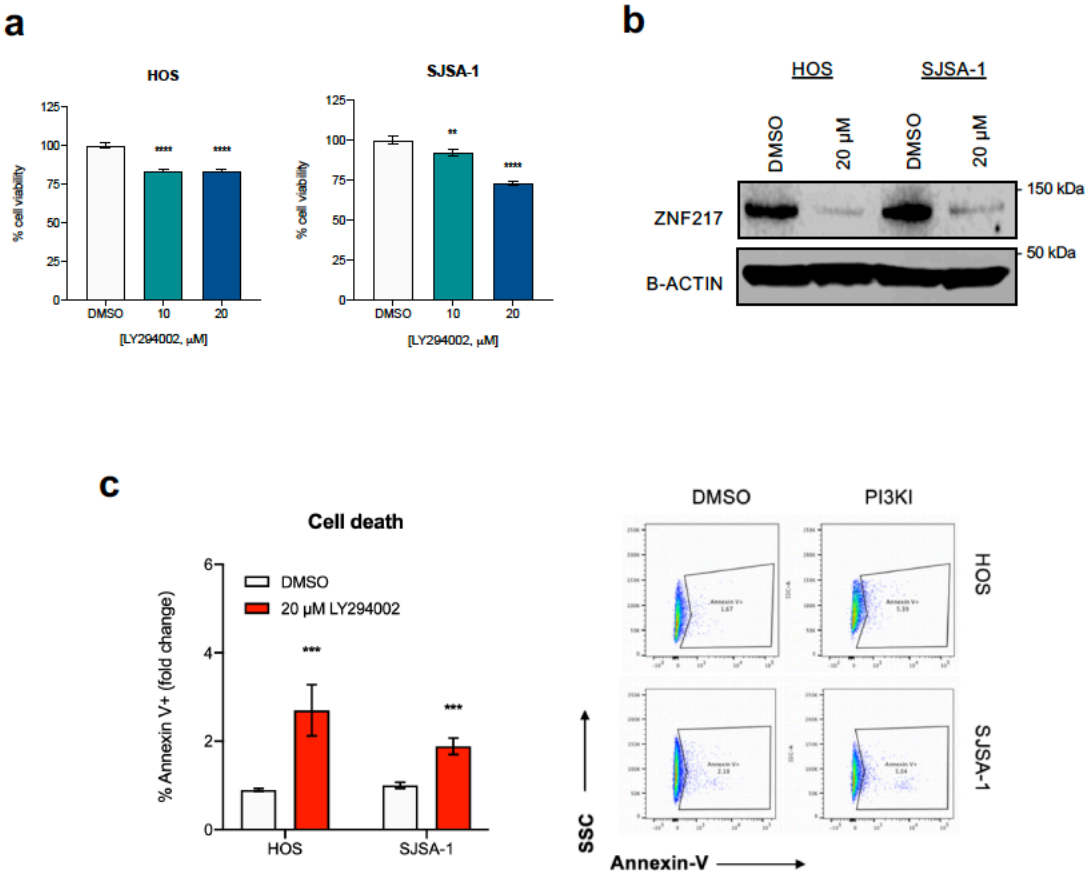
a
HOS
SJSA-1
% cell viability
125
100
75
50
25
0
****
**
DMSO
10
20
[LY294002, μM]
b
HOS
SJSA-1
DMSO
20 μM
ZNF217
B-ACTIN
150 kDa
50 kDa
c
Cell death
DMSO
20 μM LY294002
% Annexin V+ (fold change)
6
4
2
0
***
HOS
SJSA-1
DMSO
PI3KI
SSC
Annexin-V

Supplementary Figure 7. **Proposed model for oncogenic ZNF217-driven signaling in OSA**

Illustration of the model.

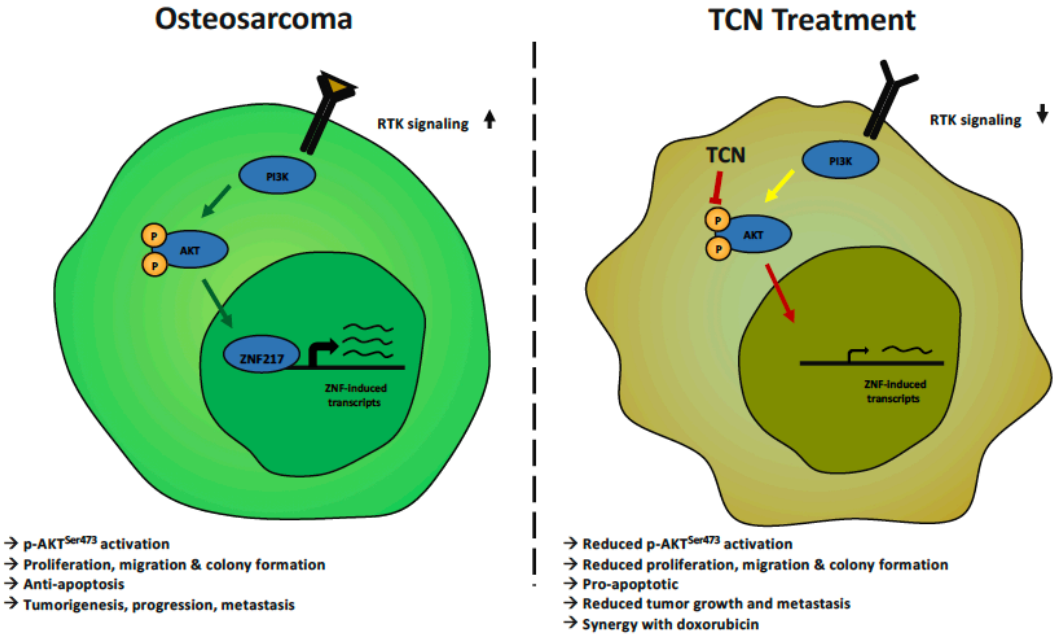
Osteosarcoma
RTK signaling
PI3K
P
P
AKT
ZNF217
ZNF-induced transcripts
→ p-AKT^{Ser473} activation
→ Proliferation, migration & colony formation
→ Anti-apoptosis
→ Tumorigenesis, progression, metastasis
TCN Treatment
RTK signaling
TCN
PI3K
P
P
AKT
ZNF-induced transcripts
→ Reduced p-AKT^{Ser473} activation
→ Reduced proliferation, migration & colony formation
→ Pro-apoptotic
→ Reduced tumor growth and metastasis
→ Synergy with doxorubicin

Supplementary Table 1.

Antibodies and other reagents utilized.

Primary antibodies

Antigen	Application	Source	Congugate	Catalog
ZNF217	IHC, WB, IF	Rabbit	N/A	HPA051857
p-AKTSer473	IHC, WB	Rabbit	N/A	4060
AKT	WB	Rabbit	N/A	4685
HSP90	WB	Rabbit	N/A	4877
Fibrillarin	WB	Rabbit	N/A	2639
B-ACTIN	WB	Mouse	N/A	3700

Secondary antibodies

Epitope	Application	Source	Congugate	Catalog
Anti-rabbit IgG	WB	Goat	HRP	1706515
Anti-rabbit IgG	IF	Goat	Alexa 594	A-11012
Anti-mouse IgG	WB	Donkey	800CW	925-32212

Supplementary Table 2.

Detailed list of the top 25 differentially expressed genes (DEGs) identified in transient ZNF217 knockdown SJSA-1 OSA cells.

Ensembl gene ID	Gene name	Adjusted *P* value	Log2 (FC)
ENSG00000152766	ANKRD22	5.04E-18	6.47
ENSG00000000971	CFH	1.40E-13	3.66
ENSG00000118785	SPP1	5.25E-11	2.76
ENSG00000113083	LOX	1.19E-10	2.62
ENSG00000169429	CXCL8	8.03E-10	3.16
ENSG00000136244	IL6	1.21E-08	3.13
ENSG00000114698	PLSCR4	1.72E-08	3.42
ENSG00000154188	ANGPT1	2.23E-08	4.93
ENSG00000205426	KRT81	3.59E-08	-3.54
ENSG00000170323	FABP4	6.30E-08	3.22
ENSG00000044524	EPHA3	1.89E-07	3.90
ENSG00000171860	C3AR1	2.63E-07	4.46
ENSG00000150275	PCDH15	6.37E-07	3.28
ENSG00000184110	EIF3C	1.52E-06	2.45
ENSG00000163694	RBM47	1.57E-06	2.82
ENSG00000118503	TNFAIP3	4.41E-06	2.13
ENSG00000023445	BIRC3	5.01E-06	2.07
ENSG00000164211	STARD4	6.14E-06	2.11
ENSG00000081041	CXCL2	7.97E-06	2.44
ENSG00000100234	TIMP3	9.89E-06	-2.08
ENSG00000196754	S100A2	1.75E-05	-2.04
ENSG00000150995	ITPR1	2.46E-05	1.96
ENSG00000049249	TNFRSF9	2.64E-05	2.40
ENSG00000134363	FST	2.69E-05	-2.20
ENSG00000128567	PODXL	2.86E-05	-1.89

CHAPTER 6

CONCLUDING REMARKS

This thesis sought to explore the therapeutic potential of three novel OSA driver genes identified previously via the *Sleeping Beauty* (*SB*)-mutagenesis system in our laboratory, namely *SEMA4C*, *CSF1R*, and *ZNF217*. These three genes were selected as top candidates to pursue further given: 1) their high statistical prevalence found in our previous *SB* work, 2) that each gene represented a previously unappreciated candidate in OSA with therapeutic potential, and 3) the availability of existing therapeutics for preclinical studies in the context of each candidate.

Axonal guidance signaling molecules were previously identified in our *SB*-screen (Chapter 1, 2 and Moriarity et al., 2015). Immunohistochemical analyses of human patient samples demonstrated overexpression of SEMA4C staining in a subset of samples. Functional validation in SEMA4C-expressing OSA cells uncovered previously unappreciated roles for SEMA4C in cellular transformation, tumor progression, and metastasis in part through regulation of AKT survival signaling. Given the surface expression of SEMA4C in OSA patient samples and cell lines, this led to the trial of a commercially available monoclonal antibody (mAb) specific for SEMA4C as a therapeutic strategy. We confirmed mAb treatment could control OSA cellular proliferation, migration, and interrupted mitotic cell cycle regulation *in vitro*. Together, this work simultaneous uncovered novel functions for a previously unappreciated gene in OSA and posited a strategy for therapeutically inhibiting its function.

Chapter 4 of this thesis explored the signaling biology of the colony stimulating factor 1 receptor (*CSF1R*) gene in OSA and the evaluation of an FDA-approved small molecule inhibitor of active CSF1R signaling for treatment of CSF1R-expressing OSAs. Our studies demonstrated that ectopic expression of *CSF1R* in immortalized osteoblasts elicited properties of cellular transformation providing further evidence for its role in osteosarcomagenesis previously uncovered in our *SB* screen. Genetic studies using transient RNAi against CSF1R revealed a role for ERK signaling in transmitting CSF1R-induced oncogenic signaling. Pharmacological blockade (PLX3397) of autocrine CSF1R signaling reduced cell proliferation, colony formation, and active ERK signaling *in vitro*. When OSA-bearing animals were treated *in vivo*, CSF1R blockade produced modest reductions in tumor progression as well as the number of metastatic nodules present in the lungs.

The last chapter of this thesis (Chapter 5) focused on the Zinc Finger Protein 217 transcription factor (*ZNF217*) and characterizing its role in OSA biology. In human cancers, *ZNF217* amplification occurs frequently (Cohen et al., 2015) and has been previously found to be oncogenic in breast cancer (Littlepage et al., 2012). To understand ZNF217 in OSA, we first generated a new mouse model to study its role in OSA development and ultimately metastasis. Overexpression of *ZNF217* in the osteoblast lineage ($Sp7^{+}$) accelerated tumor development on a predisposing background using the $Trp53^{R270H}$ mutant allele. Knockdown and overexpression studies further confirmed the oncogenic potential of ZNF217 in OSA. RNA sequencing results

elucidated PI3K-AKT signaling as a major signaling pathway altered by reduction in *ZNF217* expression. With these findings, we evaluated a clinically relevant inhibitor of AKT signaling, triciribine (TCN) and found that TCN treatment drastically reduced tumor growth and metastasis in orthotopically-injected OSA tumors. In addition, TCN was combined with broad-spectrum chemotherapy agent doxorubicin and combinatorial studies were performed *in vitro*. Drug synergy between TCN and doxorubicin was observed in four independent OSA cell lines suggesting TCN may be an excellent candidate for neoadjuvant therapy in OSA patients.

Many questions were provoked from the results of these studies and remain to be explored. Highlighted below are a series of questions and future studies to be performed with respect to each gene explored throughout this thesis.

Chapter 3: *SEMA4C*

What role does SEMA4C play in osteosarcomagenesis?

What are the contribution(s) of the PLXNB2 receptor in transmitting SEMA4C-induced oncogenic signaling?

Does anti-SEMA4C monoclonal antibody treatment in *in vivo* orthotopic models of OSA effectively reduce tumor growth and metastasis?

Chapter 4: *CSF1R*

What role does CSF1R play in osteosarcomagenesis?

What are the specific functions of intracellular p-CSF1R^{Tyr723} and is its signaling redundant and/or distinct from that of membrane bound p-CSF1R^{Tyr723}?
What other downstream pathways beyond that of ERK can CSF1-CSF1R signaling activate?
How might these pathways be further explored for multimodal therapeutic opportunities?

Chapter 5: *ZNF217*

What are the direct gene targets of *ZNF217* in OSA?
Does PI3K-AKT signaling regulate *ZNF217* directly or indirectly and how?
Is there synergism between TCN and chemotherapy treatment *in vivo*?

In sum, further evaluation of top gene candidates identified via *SB* mutagenesis uncovered new knowledge on the signaling networks and cancer phenotypes associated with expression of *SEMA4C*, *CSF1R*, and *ZNF217 in vitro* and *in vivo*. Importantly, this thesis evaluated new therapeutic approaches for treatment of OSA patients and posited promising personalized therapies for eventual clinical trials in human OSA patients with abnormal expression of the genes discussed throughout this thesis.

Ultimately, these combined findings illustrate the use of personalized targeted therapy approaches that consider deeper understanding of important driver genes/pathways through mechanistic and functional study in conjunction with conventional treatment modalities as a strategy to enhance the dismal OSA survival rates which desperately need improvement.

BIBLIOGRAPHY

Abarrategi, A., Tornin, J., Martinez-Cruzado, L., Hamilton, A., Martinez-Campos, E., Rodrigo, J. P., . . . Rodriguez, R. (2016). Osteosarcoma: Cells-of-Origin, Cancer Stem Cells, and Targeted Therapies. *Stem Cells Int, 2016*, 3631764. doi:10.1155/2016/3631764

Abdeen, A., Chou, A. J., Healey, J. H., Khanna, C., Osborne, T. S., Hewitt, S. M., . . . Gorlick, R. (2009). Correlation between clinical outcome and growth factor pathway expression in osteogenic sarcoma. *Cancer, 115*(22), 5243-5250. doi:10.1002/cncr.24562

Ahmed, N., Salsman, V. S., Yvon, E., Louis, C. U., Perlaky, L., Wels, W. S., . . . Gottschalk, S. (2009). Immunotherapy for osteosarcoma: genetic modification of T cells overcomes low levels of tumor antigen expression. *Mol Ther, 17*(10), 1779-1787. doi:10.1038/mt.2009.133

Akatsuka, T., Wada, T., Kokai, Y., Kawaguchi, S., Isu, K., Yamashiro, K., . . . Ishii, S. (2002). ErbB2 expression is correlated with increased survival of patients with osteosarcoma. *Cancer, 94*(5), 1397-1404.

Al-Salihi, M. A., Ulmer, S. C., Doan, T., Nelson, C. D., Crotty, T., Prescott, S. M., . . . Topham, M. K. (2007). Cyclooxygenase-2 transactivates the epidermal growth factor receptor through specific E-prostanoid receptors and tumor necrosis factor-alpha converting enzyme. *Cell Signal, 19*(9), 1956-1963. doi:10.1016/j.cellsig.2007.05.003

Allison, D. C., Carney, S. C., Ahlmann, E. R., Hendifar, A., Chawla, S., Fedenko, A., . . . Menendez, L. R. (2012). A meta-analysis of osteosarcoma outcomes in the modern medical era. *Sarcoma, 2012*, 704872. doi:10.1155/2012/704872

Alto, L. T., & Terman, J. R. (2017). Semaphorins and their Signaling Mechanisms. *Methods in molecular biology (Clifton, N.J.), 1493*, 1-25. doi:10.1007/978-1-4939-6448-2_1

Ammar, I., Izsvak, Z., & Ivics, Z. (2012). The Sleeping Beauty transposon toolbox. *Methods Mol Biol, 859*, 229-240. doi:10.1007/978-1-61779-603-6_13

Anderson, H. C., Hsu, H. H., Raval, P., Hunt, T. R., Schwappach, J. R., Morris, D. C., & Schneider, D. J. (1995). The mechanism of bone induction and bone healing by human osteosarcoma cell extracts. *Clin Orthop Relat Res*(313), 129-134.

Ando, K., Heymann, M. F., Stresing, V., Mori, K., Redini, F., & Heymann, D. (2013). Current therapeutic strategies and novel approaches in osteosarcoma. *Cancers (Basel), 5*(2), 591-616. doi:10.3390/cancers5020591

Arihiro, K., & Inai, K. (2001). Expression of CD31, Met/hepatocyte growth factor receptor and bone morphogenetic protein in bone metastasis of osteosarcoma. *Pathol Int, 51*(2), 100-106.

Azzam, G., Wang, X., Bell, D., & Murphy, M. E. (2013). CSF1 is a novel p53 target gene whose protein product functions in a feed-forward manner to suppress apoptosis and enhance p53-mediated growth arrest. *PLoS One, 8*(9), e74297-e74297. doi:10.1371/journal.pone.0074297

Bacci, G., Briccoli, A., Ferrari, S., Saeter, G., Donati, D., Longhi, A., . . . Forni, C. (2000). Neoadjuvant chemotherapy for osteosarcoma of the extremities with synchronous lung metastases: treatment with cisplatin, adriamycin and high dose of methotrexate and ifosfamide. *Oncol Rep, 7*(2), 339-346. doi:10.3892/or.7.2.339

Ballas, S. K., Gupta, K., & Adams-Graves, P. (2012). Sickle cell pain: a critical reappraisal. *Blood, 120*(18), 3647-3656. doi:10.1182/blood-2012-04-383430

Barbetti, V., Morandi, A., Tusa, I., Digiacomo, G., Riverso, M., Marzi, I., . . . Rovida, E. (2013). Chromatin-associated CSF-1R binds to the promoter of proliferation-related genes in breast cancer cells. *Oncogene, 33*, 4359. doi:10.1038/onc.2013.542

Bencheikh, L., Diop, M. B. K., Rivière, J., Imanci, A., Pierron, G., Souquere, S., . . . Droin, N. (2019). Dynamic gene regulation by nuclear colony-stimulating factor 1 receptor in human monocytes and macrophages. *Nat Commun, 10*(1), 1935. doi:10.1038/s41467-019-09970-9

Bennett, J. H., Thomas, G., Evans, A. W., & Speight, P. M. (2000). Osteosarcoma of the jaws: a 30-year retrospective review. *Oral Surg Oral Med Oral Pathol Oral Radiol Endod, 90*(3), 323-332.

Bennett, M. I., Johnson, M. I., Brown, S. R., Radford, H., Brown, J. M., & Searle, R. D. (2010). Feasibility study of Transcutaneous Electrical Nerve Stimulation (TENS) for cancer bone pain. *J Pain, 11*(4), 351-359. doi:10.1016/j.jpain.2009.08.002

Berndt, N., Yang, H., Trinczek, B., Betzi, S., Zhang, Z., Wu, B., . . . Sebti, S. M. (2010). The Akt activation inhibitor TCN-P inhibits Akt phosphorylation by binding to the PH domain of Akt and blocking its recruitment to the plasma

membrane. *Cell Death Differ, 17*(11), 1795-1804. doi:10.1038/cdd.2010.63

Bimonte, S., Barbieri, A., Rea, D., Palma, G., Luciano, A., Cuomo, A., . . . Izzo, F. (2015). Morphine Promotes Tumor Angiogenesis and Increases Breast Cancer Progression. *Biomed Res Int, 2015*, 161508. doi:10.1155/2015/161508

Brett, B. T., Berquam-Vrieze, K. E., Nannapaneni, K., Huang, J., Scheetz, T. E., & Dupuy, A. J. (2011). Novel molecular and computational methods improve the accuracy of insertion site analysis in Sleeping Beauty-induced tumors. *PLoS One, 6*(9), e24668. doi:10.1371/journal.pone.0024668

Brett, M. E., Bomberger, H. E., Doak, G. R., Price, M. A., McCarthy, J. B., & Wood, D. K. (2018). In vitro elucidation of the role of pericellular matrix in metastatic extravasation and invasion of breast carcinoma cells. *Integr Biol (Camb), 10*(4), 242-252. doi:10.1039/c7ib00173h

Briscoe, J., & Therond, P. P. (2013). The mechanisms of Hedgehog signalling and its roles in development and disease. *Nat Rev Mol Cell Biol, 14*(7), 416-429. doi:10.1038/nrm3598

Brown, M. R., & Ramirez, J. D. (2015). Neuroimmune mechanisms in cancer pain. *Curr Opin Support Palliat Care, 9*(2), 103-111. doi:10.1097/spc.0000000000000140

Butti, R., Kumar, T. V., Nimma, R., & Kundu, G. C. (2018). Impact of semaphorin expression on prognostic characteristics in breast cancer. *Breast Cancer (Dove Med Press), 10*, 79-88. doi:10.2147/bctt.S135753

Campbell, V. T., Nadesan, P., Ali, S. A., Wang, C. Y., Whetstone, H., Poon, R., . . . Wunder, J. S. (2014). Hedgehog pathway inhibition in chondrosarcoma using the smoothened inhibitor IPI-926 directly inhibits sarcoma cell growth. *Mol Cancer Ther, 13*(5), 1259-1269. doi:10.1158/1535-7163.mct-13-0731

Caterina, M. J., Schumacher, M. A., Tominaga, M., Rosen, T. A., Levine, J. D., & Julius, D. (1997). The capsaicin receptor: a heat-activated ion channel in the pain pathway. *Nature, 389*(6653), 816-824. doi:10.1038/39807

Chan, C. K. F., Gulati, G. S., Sinha, R., Tompkins, J. V., Lopez, M., Carter, A. C., . . . Longaker, M. T. (2018). Identification of the Human Skeletal Stem Cell. *Cell, 175*(1), 43-56.e21. doi:10.1016/j.cell.2018.07.029

Chazan, S., Ekstein, M. P., Marouani, N., & Weinbroum, A. A. (2008). Ketamine for acute and subacute pain in opioid-tolerant patients. *J Opioid Manag, 4*(3), 173-180.

Chen, X., Bahrami, A., Pappo, A., Easton, J., Dalton, J., Hedlund, E., . . . Dyer, M. A. (2014). Recurrent somatic structural variations contribute to tumorigenesis in pediatric osteosarcoma. *Cell Rep, 7*(1), 104-112. doi:10.1016/j.celrep.2014.03.003

Chihara, T., Suzu, S., Hassan, R., Chutiwitoonchai, N., Hiyoshi, M., Motoyoshi, K., . . . Okada, S. (2010). IL-34 and M-CSF share the receptor Fms but are not identical in biological activity and signal activation. *Cell Death Differ, 17*, 1917. doi:10.1038/cdd.2010.60

Choo, S., Wang, P., Newbury, R., Roberts, W., & Yang, J. (2018). Reactivation of TWIST1 contributes to Ewing sarcoma metastasis. *Pediatr Blood Cancer, 65*(1). doi:10.1002/pbc.26721

Chou, T. C. (2006). Theoretical basis, experimental design, and computerized simulation of synergism and antagonism in drug combination studies. *Pharmacol Rev, 58*(3), 621-681. doi:10.1124/pr.58.3.10

Chou, T. C. (2010). Drug combination studies and their synergy quantification using the Chou-Talalay method. *Cancer Res, 70*(2), 440-446. doi:10.1158/0008-5472.Can-09-1947

Ciccarese, F., Bazzocchi, A., Ciminari, R., Righi, A., Rocca, M., Rimondi, E., . . . Vanel, D. (2015). The many faces of pulmonary metastases of osteosarcoma: Retrospective study on 283 lesions submitted to surgery. *Eur J Radiol, 84*(12), 2679-2685. doi:10.1016/j.ejrad.2015.09.022

Cioce, M., Canino, C., Goparaju, C., Yang, H., Carbone, M., & Pass, H. I. (2014). Autocrine CSF-1R signaling drives mesothelioma chemoresistance via AKT activation. *Cell Death &Amp; Disease, 5*, e1167. doi:10.1038/cddis.2014.136

Clavijo, P. E., Friedman, J., Robbins, Y., Moore, E. C., Smith, E. S., Zauderer, M., . . . Allen, C. T. (2018). Semaphorin4D inhibition improves response to immune checkpoint blockade via attenuation of MDSC recruitment and function. *Cancer Immunol Res*. doi:10.1158/2326-6066.Cir-18-0156

Cohen, P. A., Donini, C. F., Nguyen, N. T., Lincet, H., & Vendrell, J. A. (2015). The dark side of ZNF217, a key regulator of tumorigenesis with powerful biomarker value. *Oncotarget, 6*(39), 41566-41581. doi:10.18632/oncotarget.5893

Collier, L. S., Carlson, C. M., Ravimohan, S., Dupuy, A. J., & Largaespada, D. A. (2005). Cancer gene discovery in solid tumours using transposon-based

somatic mutagenesis in the mouse. *Nature, 436*(7048), 272-276. doi:10.1038/nature03681

Coniglio, S. J., Eugenin, E., Dobrenis, K., Stanley, E. R., West, B. L., Symons, M. H., & Segall, J. E. (2012). Microglial stimulation of glioblastoma invasion involves epidermal growth factor receptor (EGFR) and colony stimulating factor 1 receptor (CSF-1R) signaling. *Mol Med, 18*, 519-527. doi:10.2119/molmed.2011.00217

Copeland, N. G., & Jenkins, N. A. (2010). Harnessing transposons for cancer gene discovery. *Nat Rev Cancer, 10*(10), 696-706. doi:10.1038/nrc2916

Copray, J. C., Mantingh, I., Brouwer, N., Biber, K., Kust, B. M., Liem, R. S., . . . Boddeke, H. W. (2001). Expression of interleukin-1 beta in rat dorsal root ganglia. *J Neuroimmunol, 118*(2), 203-211.

Corli, O., Floriani, I., Roberto, A., Montanari, M., Galli, F., Greco, M. T., . . . Apolone, G. (2016). Are strong opioids equally effective and safe in the treatment of chronic cancer pain? A multicenter randomized phase IV 'real life' trial on the variability of response to opioids. *Ann Oncol, 27*(6), 1107-1115. doi:10.1093/annonc/mdw097

Cowger, J. J., Zhao, Q., Isovic, M., & Torchia, J. (2007). Biochemical characterization of the zinc-finger protein 217 transcriptional repressor complex: identification of a ZNF217 consensus recognition sequence. *Oncogene, 26*(23), 3378-3386. doi:10.1038/sj.onc.1210126

De Felice, M., Lambert, D., Holen, I., Escott, K. J., & Andrew, D. (2016). Effects of Src-kinase inhibition in cancer-induced bone pain. *Mol Pain, 12*. doi:10.1177/1744806916643725

Deng, S., Hirschberg, A., Worzfeld, T., Penachioni, J. Y., Korostylev, A., Swiercz, J. M., . . . Kuner, R. (2007). Plexin-B2, but not Plexin-B1, critically modulates neuronal migration and patterning of the developing nervous system in vivo. *J Neurosci, 27*(23), 6333-6347. doi:10.1523/jneurosci.5381-06.2007

Dhanani, N. M., Caruso, T. J., & Carinci, A. J. (2011). Complementary and alternative medicine for pain: an evidence-based review. *Curr Pain Headache Rep, 15*(1), 39-46. doi:10.1007/s11916-010-0158-y

Dupuy, A. J. (2010). Transposon-based screens for cancer gene discovery in mouse models. *Semin Cancer Biol, 20*(4), 261-268. doi:10.1016/j.semcancer.2010.05.003

Durfee, R. A., Mohammed, M., & Luu, H. H. (2016). Review of Osteosarcoma and Current Management. *Rheumatology and therapy, 3*(2), 221-243. doi:10.1007/s40744-016-0046-y

Evans, E. E., Jonason, A. S., Jr., Bussler, H., Torno, S., Veeraraghavan, J., Reilly, C., . . . Zauderer, M. (2015). Antibody Blockade of Semaphorin 4D Promotes Immune Infiltration into Tumor and Enhances Response to Other Immunomodulatory Therapies. *Cancer Immunol Res, 3*(6), 689-701. doi:10.1158/2326-6066.Cir-14-0171

Evans, E. E., Paris, M., Smith, E. S., & Zauderer, M. (2015). Immunomodulation of the tumor microenvironment by neutralization of Semaphorin 4D. *Oncoimmunology, 4*(12), e1054599. doi:10.1080/2162402x.2015.1054599

Fakhry, M., Hamade, E., Badran, B., Buchet, R., & Magne, D. (2013). Molecular mechanisms of mesenchymal stem cell differentiation towards osteoblasts. *World J Stem Cells, 5*(4), 136-148. doi:10.4252/wjsc.v5.i4.136

Falk, S., & Dickenson, A. H. (2014). Pain and nociception: mechanisms of cancer-induced bone pain. *J Clin Oncol, 32*(16), 1647-1654. doi:10.1200/jco.2013.51.7219

Fattori, V., Hohmann, M. S., Rossaneis, A. C., Pinho-Ribeiro, F. A., & Verri, W. A. (2016). Capsaicin: Current Understanding of Its Mechanisms and Therapy of Pain and Other Pre-Clinical and Clinical Uses. *Molecules, 21*(7). doi:10.3390/molecules21070844

Faustino-Rocha, A., Oliveira, P. A., Pinho-Oliveira, J., Teixeira-Guedes, C., Soares-Maia, R., da Costa, R. G., . . . Ginja, M. (2013). Estimation of rat mammary tumor volume using caliper and ultrasonography measurements. *Lab Anim (NY), 42*(6), 217-224. doi:10.1038/laban.254

Fazzari, J., Linher-Melville, K., & Singh, G. (2016). TUMOUR-DERIVED GLUTAMATE: LINKING ABERRANT CANCER CELL METABOLISM TO PERIPHERAL SENSORY PAIN PATHWAYS. *Curr Neuropharmacol*.

Feun, L. G., Blessing, J. A., Barrett, R. J., & Hanjani, P. (1993). A phase II trial of tricyclic nucleoside phosphate in patients with advanced squamous cell carcinoma of the cervix. A Gynecologic Oncology Group Study. *Am J Clin Oncol, 16*(6), 506-508. doi:10.1097/00000421-199312000-00010

Feun, L. G., Savaraj, N., Bodey, G. P., Lu, K., Yap, B. S., Ajani, J. A., . . . Krakoff, I. (1984). Phase I study of tricyclic nucleoside phosphate using a five-day continuous infusion schedule. *Cancer Res, 44*(8), 3608-3612.

Franchi, A. (2012). Epidemiology and classification of bone tumors. *Clin Cases Miner Bone Metab, 9*(2), 92-95.

Frietze, S., O'Geen, H., Littlepage, L. E., Simion, C., Sweeney, C. A., Farnham, P. J., & Krig, S. R. (2014). Global analysis of ZNF217 chromatin occupancy in the breast cancer cell genome reveals an association with ERalpha. *BMC Genomics, 15*(1), 520. doi:10.1186/1471-2164-15-520

García, Z., Kumar, A., Marqués, M., Cortés, I., & Carrera, A. C. (2006). Phosphoinositide 3-kinase controls early and late events in mammalian cell division. *Embo j, 25*(4), 655-661. doi:10.1038/sj.emboj.7600967

Garrett, C. R., Coppola, D., Wenham, R. M., Cubitt, C. L., Neuger, A. M., Frost, T. J., . . . Sebti, S. M. (2011). Phase I pharmacokinetic and pharmacodynamic study of triciribine phosphate monohydrate, a small-molecule inhibitor of AKT phosphorylation, in adult subjects with solid tumors containing activated AKT. *Invest New Drugs, 29*(6), 1381-1389. doi:10.1007/s10637-010-9479-2

Gelderblom, H., Jinks, R. C., Sydes, M., Bramwell, V. H., van Glabbeke, M., Grimer, R. J., . . . Whelan, J. (2011). Survival after recurrent osteosarcoma: data from 3 European Osteosarcoma Intergroup (EOI) randomized controlled trials. *Eur J Cancer, 47*(6), 895-902. doi:10.1016/j.ejca.2010.11.036

Gianferante, D. M., Mirabello, L., & Savage, S. A. (2017). Germline and somatic genetics of osteosarcoma - connecting aetiology, biology and therapy. *Nat Rev Endocrinol, 13*(8), 480-491. doi:10.1038/nrendo.2017.16

Giustini, N., Bernthal, N. M., Bukata, S. V., & Singh, A. S. (2018). Tenosynovial giant cell tumor: case report of a patient effectively treated with pexidartinib (PLX3397) and review of the literature. *Clin Sarcoma Res, 8*, 14. doi:10.1186/s13569-018-0101-2

Gorlick, R., Huvos, A. G., Heller, G., Aledo, A., Beardsley, G. P., Healey, J. H., & Meyers, P. A. (1999). Expression of HER2/erbB-2 correlates with survival in osteosarcoma. *J Clin Oncol, 17*(9), 2781-2788.

Gurrapu, S., Pupo, E., Franzolin, G., Lanzetti, L., & Tamagnone, L. (2018). Sema4C/PlexinB2 signaling controls breast cancer cell growth, hormonal dependence and tumorigenic potential. *Cell Death Differ, 25*(7), 1259-1275. doi:10.1038/s41418-018-0097-4

Hanahan, D., & Weinberg, R. A. (2000). The hallmarks of cancer. *Cell, 100*(1), 57-70. doi:10.1016/s0092-8674(00)81683-9

Hanahan, D., & Weinberg, R. A. (2011). Hallmarks of cancer: the next generation. *Cell, 144*(5), 646-674. doi:10.1016/j.cell.2011.02.013

Hara, A., Ikeda, T., Nomura, S., Yagita, H., Okumura, K., & Yamauchi, Y. (1996). In vivo implantation of human osteosarcoma cells in nude mice induces bones with human-derived osteoblasts and mouse-derived osteocytes. *Lab Invest, 75*(5), 707-717.

Harris, S. A., Enger, R. J., Riggs, B. L., & Spelsberg, T. C. (1995). Development and characterization of a conditionally immortalized human fetal osteoblastic cell line. *J Bone Miner Res, 10*(2), 178-186. doi:10.1002/jbmr.5650100203

Hassan, S. E., Bekarev, M., Kim, M. Y., Lin, J., Piperdi, S., Gorlick, R., & Geller, D. S. (2012). Cell surface receptor expression patterns in osteosarcoma. *Cancer, 118*(3), 740-749. doi:10.1002/cncr.26339

Hoffman, K., Holmes, F. A., Fraschini, G., Esparza, L., Frye, D., Raber, M. N., . . . Hortobagyi, G. N. (1996). Phase I-II study: triciribine (tricyclic nucleoside phosphate) for metastatic breast cancer. *Cancer Chemother Pharmacol, 37*(3), 254-258. doi:10.1007/bf00688325

Horvai, A. E., Roy, R., Borys, D., & O'Donnell, R. J. (2012). Regulators of skeletal development: a cluster analysis of 206 bone tumors reveals diagnostically useful markers. *Mod Pathol, 25*(11), 1452-1461. doi:10.1038/modpathol.2012.110

Houghton, P. J., Morton, C. L., Kolb, E. A., Gorlick, R., Lock, R., Carol, H., . . . Smith, M. A. (2008). Initial testing (stage 1) of the mTOR inhibitor rapamycin by the pediatric preclinical testing program. *Pediatr Blood Cancer, 50*(4), 799-805. doi:10.1002/pbc.21296

Huang, G., Krig, S., Kowbel, D., Xu, H., Hyun, B., Volik, S., . . . Collins, C. (2005). ZNF217 suppresses cell death associated with chemotherapy and telomere dysfunction. *Hum Mol Genet, 14*(21), 3219-3225. doi:10.1093/hmg/ddi352

Hung, J. Y., Horn, D., Woodruff, K., Prihoda, T., LeSaux, C., Peters, J., . . . Abboud-Werner, S. L. (2014). Colony-stimulating factor 1 potentiates lung cancer bone metastasis. *Lab Invest, 94*(4), 371-381. doi:10.1038/labinvest.2014.1

Iadarola, M. J., & Gonnella, G. L. (2013). Resiniferatoxin for Pain Treatment: An Interventional Approach to Personalized Pain Medicine. *Open Pain J, 6*, 95-107. doi:10.2174/1876386301306010095

Ivanovska V, Rademaker CM, van Dijk L, Mantel-Teeuwisse AK. Pediatric drug formulations: a review of challenges and progress. Pediatrics 2014;134:361-72

Ivics, Z., Hackett, P. B., Plasterk, R. H., & Izsvak, Z. (1997). Molecular reconstruction of Sleeping Beauty, a Tc1-like transposon from fish, and its transposition in human cells. *Cell, 91*(4), 501-510.

Izsvak, Z., & Ivics, Z. (2005). Sleeping Beauty hits them all: transposon-mediated saturation mutagenesis in the mouse germline. *Nat Methods, 2*(10), 735-736. doi:10.1038/nmeth1005-735

Jaffe, N., Puri, A., & Gelderblom, H. (2013). Osteosarcoma: evolution of treatment paradigms. *Sarcoma, 2013*, 203531. doi:10.1155/2013/203531

Jiang, W. G., Sanders, A. J., Katoh, M., Ungefroren, H., Gieseler, F., Prince, M., . . . Santini, D. (2015). Tissue invasion and metastasis: Molecular, biological and clinical perspectives. *Semin Cancer Biol, 35 Suppl*, S244-s275. doi:10.1016/j.semcancer.2015.03.008

Jimenez-Andrade, J. M., Ghilardi, J. R., Castaneda-Corral, G., Kuskowski, M. A., & Mantyh, P. W. (2011). Preventive or late administration of anti-NGF therapy attenuates tumor-induced nerve sprouting, neuroma formation, and cancer pain. *Pain, 152*(11), 2564-2574. doi:10.1016/j.pain.2011.07.020

Johnson, J. R., Burnell-Nugent, M., Lossignol, D., Ganae-Motan, E. D., Potts, R., & Fallon, M. T. (2010). Multicenter, double-blind, randomized, placebo-controlled, parallel-group study of the efficacy, safety, and tolerability of THC:CBD extract and THC extract in patients with intractable cancer-related pain. *J Pain Symptom Manage, 39*(2), 167-179. doi:10.1016/j.jpainsymman.2009.06.008

Kager, L., Zoubek, A., Potschger, U., Kastner, U., Flege, S., Kempf-Bielack, B., . . . Bielack, S. S. (2003). Primary metastatic osteosarcoma: presentation and outcome of patients treated on neoadjuvant Cooperative Osteosarcoma Study Group protocols. *J Clin Oncol, 21*(10), 2011-2018. doi:10.1200/jco.2003.08.132

Kansara, M., & Thomas, D. M. (2007). Molecular pathogenesis of osteosarcoma. *DNA Cell Biol, 26*(1), 1-18. doi:10.1089/dna.2006.0505

Kansara, M., Teng, M. W., Smyth, M. J., & Thomas, D. M. (2014). Translational biology of osteosarcoma. *Nat Rev Cancer, 14*(11), 722-735. doi:10.1038/nrc3838

Khanna, C., Prehn, J., Yeung, C., Caylor, J., Tsokos, M., & Helman, L. (2000). An orthotopic model of murine osteosarcoma with clonally related variants differing in pulmonary metastatic potential. *Clin Exp Metastasis, 18*(3), 261-271.

Kim, S., Lewis, C., & Nadel, J. A. (2011). Epidermal growth factor receptor reactivation induced by E-prostanoid-3 receptor- and tumor necrosis factor-alpha-converting enzyme-dependent feedback exaggerates interleukin-8 production in airway cancer (NCI-H292) cells. *Exp Cell Res, 317*(18), 2650-2660. doi:10.1016/j.yexcr.2011.08.023

King, T., Vardanyan, A., Majuta, L., Melemedjian, O., Nagle, R., Cress, A. E., . . . Porreca, F. (2007). Morphine treatment accelerates sarcoma-induced bone pain, bone loss, and spontaneous fracture in a murine model of bone cancer. *Pain, 132*(1-2), 154-168. doi:10.1016/j.pain.2007.06.026

Kohli, D. R., Li, Y., Khasabov, S. G., Gupta, P., Kehl, L. J., Ericson, M. E., . . . Gupta, K. (2010). Pain-related behaviors and neurochemical alterations in mice expressing sickle hemoglobin: modulation by cannabinoids. *Blood, 116*(3), 456-465. doi:10.1182/blood-2010-01-260372

Kool, J., & Berns, A. (2009). High-throughput insertional mutagenesis screens in mice to identify oncogenic networks. *Nat Rev Cancer, 9*(6), 389-399. doi:10.1038/nrc2647

Krig, S. R., Miller, J. K., Frietze, S., Beckett, L. A., Neve, R. M., Farnham, P. J., . . . Sweeney, C. A. (2010). ZNF217, a candidate breast cancer oncogene amplified at 20q13, regulates expression of the ErbB3 receptor tyrosine kinase in breast cancer cells. *Oncogene, 29*(40), 5500-5510. doi:10.1038/onc.2010.289

Kuijjer, M. L., Hogendoorn, P. C., & Cleton-Jansen, A. M. (2013). Genome-wide analyses on high-grade osteosarcoma: making sense of a genomically most unstable tumor. *Int J Cancer, 133*(11), 2512-2521. doi:10.1002/ijc.28124

Kumar, S., Das, A., & Sen, S. (2014). Extracellular matrix density promotes EMT by weakening cell-cell adhesions. *Mol Biosyst, 10*(4), 838-850. doi:10.1039/c3mb70431a

Lam, D. K. (2016). Emerging factors in the progression of cancer-related pain. *Pain Manag*. doi:10.2217/pmt-2015-0003

Lambert, M., Jambon, S., Depauw, S., & David-Cordonnier, M. H. (2018). Targeting Transcription Factors for Cancer Treatment. *Molecules, 23*(6). doi:10.3390/molecules23061479

Lamouille, S., Xu, J., & Derynck, R. (2014). Molecular mechanisms of epithelial-mesenchymal transition. *Nat Rev Mol Cell Biol, 15*(3), 178-196. doi:10.1038/nrm3758

Lau, C. H., Wu, X., Chung, V. C., Liu, X., Hui, E. P., Cramer, H., . . . Wu, J. C. (2016). Acupuncture and Related Therapies for Symptom Management in Palliative Cancer Care: Systematic Review and Meta-Analysis. *Medicine (Baltimore), 95*(9), e2901. doi:10.1097/md.0000000000002901

Le, A. P., Huang, Y., Pingle, S. C., Kesari, S., Wang, H., Yong, R. L., . . . Friedel, R. H. (2015). Plexin-B2 promotes invasive growth of malignant glioma. *Oncotarget, 6*(9), 7293-7304. doi:10.18632/oncotarget.3421

Leary, S. E., Wozniak, A. W., Billups, C. A., Wu, J., McPherson, V., Neel, M. D., . . . Daw, N. C. (2013). Survival of pediatric patients after relapsed osteosarcoma: the St. Jude Children's Research Hospital experience. *Cancer, 119*(14), 2645-2653. doi:10.1002/cncr.28111

Leder, K., Holland, E. C., & Michor, F. (2010). The therapeutic implications of plasticity of the cancer stem cell phenotype. *PLoS One, 5*(12), e14366. doi:10.1371/journal.pone.0014366

Lee, K. W., Lee, N. K., Ham, S., Roh, T. Y., & Kim, S. H. (2014). Twist1 is essential in maintaining mesenchymal state and tumor-initiating properties in synovial sarcoma. *Cancer Lett, 343*(1), 62-73. doi:10.1016/j.canlet.2013.09.013

Lemmon, M. A., & Schlessinger, J. (2010). Cell signaling by receptor tyrosine kinases. *Cell, 141*(7), 1117-1134. doi:10.1016/j.cell.2010.06.011

Levine, R. A., Forest, T., & Smith, C. (2002). Tumor suppressor PTEN is mutated in canine osteosarcoma cell lines and tumors. *Vet Pathol, 39*(3), 372-378. doi:10.1354/vp.39-3-372

Li, J., Song, L., Qiu, Y., Yin, A., & Zhong, M. (2014). ZNF217 is associated with poor prognosis and enhances proliferation and metastasis in ovarian cancer. *Int J Clin Exp Pathol, 7*(6), 3038-3047.

Li, N. F., Kocher, H. M., Salako, M. A., Obermueller, E., Sandle, J., & Balkwill, F. (2009). A novel function of colony-stimulating factor 1 receptor in hTERT immortalization of human epithelial cells. *Oncogene, 28*(5), 773-780. doi:10.1038/onc.2008.412

Li, Z., Du, L., Dong, Z., Yang, Y., Zhang, X., Wang, L., . . . Wang, C. (2015). MiR-203 suppresses ZNF217 upregulation in colorectal cancer and its

oncogenicity. *PLoS One, 10*(1), e0116170. doi:10.1371/journal.pone.0116170

Littlepage, L. E., Adler, A. S., Kouros-Mehr, H., Huang, G., Chou, J., Krig, S. R., . . . Werb, Z. (2012). The transcription factor ZNF217 is a prognostic biomarker and therapeutic target during breast cancer progression. *Cancer Discov, 2*(7), 638-651. doi:10.1158/2159-8290.Cd-12-0093

Long, F. (2012). Building strong bones: molecular regulation of the osteoblast lineage. *Nat Rev Mol Cell Biol, 13*(1), 27-38. doi:10.1038/nrm3254

Lu, J., Lin, Y., Li, F., Ye, H., Zhou, R., Jin, Y., . . . Cheng, N. (2018). MiR-205 suppresses tumor growth, invasion, and epithelial-mesenchymal transition by targeting SEMA4C in hepatocellular carcinoma. *Faseb j*, fj201800113R. doi:10.1096/fj.201800113R

Lum, L., & Beachy, P. A. (2004). The Hedgehog response network: sensors, switches, and routers. *Science, 304*(5678), 1755-1759. doi:10.1126/science.1098020

Lv, Z., Yang, D., Li, J., Hu, M., Luo, M., Zhan, X., . . . Weng, Y. (2013). Bone morphogenetic protein 9 overexpression reduces osteosarcoma cell migration and invasion. *Mol Cells, 36*(2), 119-126. doi:10.1007/s10059-013-0043-8

Mantyh, P. W., Clohisy, D. R., Koltzenburg, M., & Hunt, S. P. (2002). Molecular mechanisms of cancer pain. *Nat Rev Cancer, 2*(3), 201-209. doi:10.1038/nrc747

Mantyh, W. G., Jimenez-Andrade, J. M., Stake, J. I., Bloom, A. P., Kaczmarska, M. J., Taylor, R. N., . . . Mantyh, P. W. (2010). Blockade of nerve sprouting and neuroma formation markedly attenuates the development of late stage cancer pain. *Neuroscience, 171*(2), 588-598. doi:10.1016/j.neuroscience.2010.08.056

Marko, T. A., Shamsan, G. A., Edwards, E. N., Hazelton, P. E., Rathe, S. K., Cornax, I., . . . Largaespada, D. A. (2016). Slit-Robo GTPase-Activating Protein 2 as a metastasis suppressor in osteosarcoma. *Sci Rep, 6*, 39059. doi:10.1038/srep39059

Martin, J. W., Squire, J. A., & Zielenska, M. (2012). The Genetics of Osteosarcoma. *Sarcoma, 2012*.

Matthews, H., Deakin, J., Rajab, M., Idris-Usman, M., & Nirmalan, N. J. (2017). Investigating antimalarial drug interactions of emetine dihydrochloride

hydrate using CalcuSyn-based interactivity calculations. *PLoS One, 12*(3), e0173303. doi:10.1371/journal.pone.0173303

Meazza, C., & Scanagatta, P. (2016). Metastatic osteosarcoma: a challenging multidisciplinary treatment. *Expert Rev Anticancer Ther, 16*(5), 543-556. doi:10.1586/14737140.2016.1168697

Meng, F. F., Xu, Y., Dan, Q. Q., Wei, L., Deng, Y. J., Liu, J., . . . Wang, X. Y. (2015). Intrathecal injection of lentivirus-mediated glial cell line-derived neurotrophic factor RNA interference relieves bone cancer-induced pain in rats. *Cancer Sci, 106*(4), 430-437. doi:10.1111/cas.12609

Messana, M. J., Yang, C., & Littlepage, L. E. (2014). Abstract 4252: Regulation of the oncogene ZNF217 by localization in breast cancer. *Cancer Research, 74*(19 Supplement), 4252. doi:10.1158/1538-7445.AM2014-4252

Meuser, T., Pietruck, C., Radbruch, L., Stute, P., Lehmann, K. A., & Grond, S. (2001). Symptoms during cancer pain treatment following WHO-guidelines: a longitudinal follow-up study of symptom prevalence, severity and etiology. *Pain, 93*(3), 247-257.

Meyer, L. A., Fritz, J., Pierdant-Mancera, M., & Bagnard, D. (2016). Current drug design to target the Semaphorin/Neuropilin/Plexin complexes. *Cell Adh Migr, 10*(6), 700-708. doi:10.1080/19336918.2016.1261785

Meyers, P. A., Heller, G., Healey, J. H., Huvos, A., Applewhite, A., Sun, M., & LaQuaglia, M. (1993). Osteogenic sarcoma with clinically detectable metastasis at initial presentation. *J Clin Oncol, 11*(3), 449-453.

Mirabello, L., Troisi, R. J., & Savage, S. A. (2009). Osteosarcoma incidence and survival rates from 1973 to 2004: data from the Surveillance, Epidemiology, and End Results Program. *Cancer, 115*(7), 1531-1543. doi:10.1002/cncr.24121

Misaghi, A., Goldin, A., Awad, M., & Kulidjian, A. A. (2018). Osteosarcoma: a comprehensive review. *SICOT-J, 4*, 12-12. doi:10.1051/sicotj/2017028

Misaghi, A., Goldin, A., Awad, M., & Kulidjian, A. A. (2018). Osteosarcoma: a comprehensive review. *SICOT-J, 4*, 12. doi:10.1051/sicotj/2017028

Montell, C. (2011). The history of TRP channels, a commentary and reflection. *Pflugers Arch, 461*(5), 499-506. doi:10.1007/s00424-010-0920-3

Morandi, A., Barbetti, V., Riverso, M., Dello Sbarba, P., & Rovida, E. (2011). The colony-stimulating factor-1 (CSF-1) receptor sustains ERK1/2 activation

and proliferation in breast cancer cell lines. *PLoS One, 6*(11), e27450-e27450. doi:10.1371/journal.pone.0027450

Mori, S., Chang, J. T., Andrechek, E. R., Matsumura, N., Baba, T., Yao, G., . . . Nevins, J. R. (2009). Anchorage-independent cell growth signature identifies tumors with metastatic potential. *Oncogene, 28*(31), 2796-2805. doi:10.1038/onc.2009.139

Moriarity, B. S., & Largaespada, D. A. (2015). Sleeping Beauty transposon insertional mutagenesis based mouse models for cancer gene discovery. *Curr Opin Genet Dev, 30*, 66-72. doi:10.1016/j.gde.2015.04.007

Moriarity, B. S., Otto, G. M., Rahrmann, E. P., Rathe, S. K., Wolf, N. K., Weg, M. T., . . . Largaespada, D. A. (2015). A Sleeping Beauty forward genetic screen identifies new genes and pathways driving osteosarcoma development and metastasis. *Nat Genet, 47*(6), 615-624. doi:10.1038/ng.3293

Moriarity, B. S., Rahrmann, E. P., Beckmann, D. A., Conboy, C. B., Watson, A. L., Carlson, D. F., . . . Largaespada, D. A. (2014). Simple and efficient methods for enrichment and isolation of endonuclease modified cells. *PLoS One, 9*(5), e96114. doi:10.1371/journal.pone.0096114

Morrow, J. J., & Khanna, C. (2015). Osteosarcoma Genetics and Epigenetics: Emerging Biology and Candidate Therapies. *Crit Rev Oncog, 20*(3-4), 173-197.

Mu, X., Brynien, D., & Weiss, K. R. (2015). The HDAC inhibitor Vorinostat diminishes the in vitro metastatic behavior of Osteosarcoma cells. *Biomed Res Int, 2015*, 290368. doi:10.1155/2015/290368

Mu, X., Isaac, C., Schott, T., Huard, J., & Weiss, K. (2013). Rapamycin Inhibits ALDH Activity, Resistance to Oxidative Stress, and Metastatic Potential in Murine Osteosarcoma Cells. *Sarcoma, 2013*, 480713. doi:10.1155/2013/480713

Mu, X., Sultankulov, B., Agarwal, R., Mahjoub, A., Schott, T., Greco, N., . . . Weiss, K. (2014). Chick embryo extract demethylates tumor suppressor genes in osteosarcoma cells. *Clin Orthop Relat Res, 472*(3), 865-873. doi:10.1007/s11999-013-3104-6

Muñoz-López, M., & García-Pérez, J. L. (2010). DNA Transposons: Nature and Applications in Genomics. *Curr Genomics, 11*(2), 115-128. doi:10.2174/138920210790886871

Murga-Zamalloa, C., Rolland, D. C. M., Polk, A., Wolfe, A., Dewar, H., Chowdhury, P., . . . Wilcox, R. A. (2019). Colony-Stimulating Factor 1 Receptor (CSF1R) Activates AKT/mTOR Signaling and Promotes T-Cell Lymphoma Viability. *Clin Cancer Res*. doi:10.1158/1078-0432.Ccr-19-1486

Nair AB, Jacob S. A simple practice guide for dose conversion between animals and human. J Basic Clin Pharm 2016;7:27-31

Negishi-Koga, T., Shinohara, M., Komatsu, N., Bito, H., Kodama, T., Friedel, R. H., & Takayanagi, H. (2011). Suppression of bone formation by osteoclastic expression of semaphorin 4D. *Nat Med, 17*(11), 1473-1480. doi:10.1038/nm.2489

Nguyen, A., Scott, M. A., Dry, S. M., & James, A. W. (2014). Roles of bone morphogenetic protein signaling in osteosarcoma. *Int Orthop, 38*(11), 2313-2322. doi:10.1007/s00264-014-2512-x

Nguyen, N. T., Vendrell, J. A., Poulard, C., Győrffy, B., Goddard-Léon, S., Bièche, I., . . . Cohen, P. A. (2014). A functional interplay between ZNF217 and estrogen receptor alpha exists in luminal breast cancers. *Mol Oncol, 8*(8), 1441-1457. doi:10.1016/j.molonc.2014.05.013

Niu, D. G., Peng, F., Zhang, W., Guan, Z., Zhao, H. D., Li, J. L., . . . Liu, Q. (2015). Morphine promotes cancer stem cell properties, contributing to chemoresistance in breast cancer. *Oncotarget, 6*(6), 3963-3976. doi:10.18632/oncotarget.2894

Ogose, A., Motoyama, T., Hotta, T., Watanabe, H., & Takahashi, H. E. (1995). Bone formation in vitro and in nude mice by human osteosarcoma cells. *Virchows Arch, 426*(2), 117-125.

O'Hara K. Paediatric pharmacokinetics and drug doses. Aust Prescr 2016;39:208-10

Oliveira, A., Dinis-Oliveira, R. J., Nogueira, A., Goncalves, F., Silva, P., Vieira, C., . . . Medeiros, R. (2014). Interleukin-1beta genotype and circulating levels in cancer patients: metastatic status and pain perception. *Clin Biochem, 47*(13-14), 1209-1213. doi:10.1016/j.clinbiochem.2014.04.009

Ottaviano, L., Schaefer, K. L., Gajewski, M., Huckenbeck, W., Baldus, S., Rogel, U., . . . Poremba, C. (2010). Molecular characterization of commonly used cell lines for bone tumor research: a trans-European EuroBoNet effort. *Genes Chromosomes Cancer, 49*(1), 40-51. doi:10.1002/gcc.20717

Paget, C., Duret, H., Ngiow, S. F., Kansara, M., Thomas, D. M., & Smyth, M. J. (2012). Studying the role of the immune system on the antitumor activity of a Hedgehog inhibitor against murine osteosarcoma. *Oncoimmunology, 1*(8), 1313-1322. doi:10.4161/onci.21680

Paldy, E., Simonetti, M., Worzfeld, T., Bali, K. K., Vicuna, L., Offermanns, S., & Kuner, R. (2017). Semaphorin 4C Plexin-B2 signaling in peripheral sensory neurons is pronociceptive in a model of inflammatory pain. *Nat Commun, 8*(1), 176. doi:10.1038/s41467-017-00341-w

Paley, C. A., Johnson, M. I., Tashani, O. A., & Bagnall, A. M. (2015). Acupuncture for cancer pain in adults. *Cochrane Database Syst Rev*(10), CD007753. doi:10.1002/14651858.CD007753.pub3

Pass, H. I., Lavilla, C., Canino, C., Goparaju, C., Preiss, J., Noreen, S., . . . Cioce, M. (2016). Inhibition of the colony-stimulating-factor-1 receptor affects the resistance of lung cancer cells to cisplatin. *Oncotarget, 7*(35), 56408-56421. doi:10.18632/oncotarget.10895

Patane, S., Avnet, S., Coltella, N., Costa, B., Sponza, S., Olivero, M., . . . Di Renzo, M. F. (2006). MET overexpression turns human primary osteoblasts into osteosarcomas. *Cancer Res, 66*(9), 4750-4757. doi:10.1158/0008-5472.Can-05-4422

Perry, J. A., Kiezun, A., Tonzi, P., Van Allen, E. M., Carter, S. L., Baca, S. C., . . . Janeway, K. A. (2014). Complementary genomic approaches highlight the PI3K/mTOR pathway as a common vulnerability in osteosarcoma. *Proceedings of the National Academy of Sciences, 111*(51), E5564. doi:10.1073/pnas.1419260111

Pevida, M., Gonzalez-Rodriguez, S., Lastra, A., Garcia-Suarez, O., Hidalgo, A., Menendez, L., & Baamonde, A. (2014). Involvement of spinal chemokine CCL2 in the hyperalgesia evoked by bone cancer in mice: a role for astroglia and microglia. *Cell Mol Neurobiol, 34*(1), 143-156. doi:10.1007/s10571-013-9995-7

Plasterk, R. H. (1996). The Tc1/mariner transposon family. *Curr Top Microbiol Immunol, 204*, 125-143.

Poleszczuk, J., & Enderling, H. (2016). Cancer Stem Cell Plasticity as Tumor Growth Promoter and Catalyst of Population Collapse. *Stem Cells Int, 2016*, 3923527. doi:10.1155/2016/3923527

Portenoy, R. K., & Hagen, N. A. (1990). Breakthrough pain: definition, prevalence and characteristics. *Pain, 41*(3), 273-281.

Porter, D. E., Holden, S. T., Steel, C. M., Cohen, B. B., Wallace, M. R., & Reid, R. (1992). A significant proportion of patients with osteosarcoma may belong to Li-Fraumeni cancer families. *J Bone Joint Surg Br, 74*(6), 883-886.

Przewlocki, R., & Przewlocka, B. (2001). Opioids in chronic pain. *Eur J Pharmacol, 429*(1-3), 79-91.

Qi, H., Aguiar, D. J., Williams, S. M., La Pean, A., Pan, W., & Verfaillie, C. M. (2003). Identification of genes responsible for osteoblast differentiation from human mesodermal progenitor cells. *Proc Natl Acad Sci U S A, 100*(6), 3305-3310. doi:10.1073/pnas.0532693100

Quinlan, K. G., Nardini, M., Verger, A., Francescato, P., Yaswen, P., Corda, D., . . . Crossley, M. (2006). Specific recognition of ZNF217 and other zinc finger proteins at a surface groove of C-terminal binding proteins. *Mol Cell Biol, 26*(21), 8159-8172. doi:10.1128/mcb.00680-06

Quinlan, K. G., Verger, A., Yaswen, P., & Crossley, M. (2007). Amplification of zinc finger gene 217 (ZNF217) and cancer: when good fingers go bad. *Biochim Biophys Acta, 1775*(2), 333-340. doi:10.1016/j.bbcan.2007.05.001

Quist, T., Jin, H., Zhu, J. F., Smith-Fry, K., Capecchi, M. R., & Jones, K. B. (2015). The impact of osteoblastic differentiation on osteosarcomagenesis in the mouse. *Oncogene, 34*(32), 4278-4284. doi:10.1038/onc.2014.354

Ragland, B. D., Bell, W. C., Lopez, R. R., & Siegal, G. P. (2002). Cytogenetics and molecular biology of osteosarcoma. *Lab Invest, 82*(4), 365-373.

Rahrmann, E. P., Watson, A. L., Keng, V. W., Choi, K., Moriarity, B. S., Beckmann, D. A., . . . Largaespada, D. A. (2013). Forward genetic screen for malignant peripheral nerve sheath tumor formation identifies new genes and pathways driving tumorigenesis. *Nat Genet, 45*(7), 756-766. doi:10.1038/ng.2641

Raymond, A. K., & Jaffe, N. (2009). Osteosarcoma multidisciplinary approach to the management from the pathologist's perspective. *Cancer Treat Res, 152*, 63-84. doi:10.1007/978-1-4419-0284-9_4

Remeniuk, B., Sukhtankar, D., Okun, A., Navratilova, E., Xie, J. Y., King, T., & Porreca, F. (2015). Behavioral and neurochemical analysis of ongoing bone cancer pain in rats. *Pain, 156*(10), 1864-1873. doi:10.1097/j.pain.0000000000000218

Ren, B. X., Gu, X. P., Zheng, Y. G., Liu, C. L., Wang, D., Sun, Y. E., & Ma, Z. L. (2012). Intrathecal injection of metabotropic glutamate receptor subtype 3

and 5 agonist/antagonist attenuates bone cancer pain by inhibition of spinal astrocyte activation in a mouse model. *Anesthesiology, 116*(1), 122-132. doi:10.1097/ALN.0b013e31823de68d

Rickel, K., Fang, F., & Tao, J. (2017). Molecular genetics of osteosarcoma. *Bone, 102*, 69-79. doi:10.1016/j.bone.2016.10.017

Roche, J. (2018). The Epithelial-to-Mesenchymal Transition in Cancer. *Cancers (Basel), 10*(2). doi:10.3390/cancers10020052

Rooney, P. H., Boonsong, A., McFadyen, M. C., McLeod, H. L., Cassidy, J., Curran, S., & Murray, G. I. (2004). The candidate oncogene ZNF217 is frequently amplified in colon cancer. *J Pathol, 204*(3), 282-288. doi:10.1002/path.1632

Roussel, M. F. (1994). Signal transduction by the macrophage-colony-stimulating factor receptor (CSF-1R). *J Cell Sci Suppl, 18*, 105-108.

Roussel, M. F., Dull, T. J., Rettenmier, C. W., Ralph, P., Ullrich, A., & Sherr, C. J. (1987). Transforming potential of the c-fms proto-oncogene (CSF-1 receptor). *Nature, 325*(6104), 549-552. doi:10.1038/325549a0

Rudin, C. M., Hann, C. L., Laterra, J., Yauch, R. L., Callahan, C. A., Fu, L., . . . Low, J. A. (2009). Treatment of medulloblastoma with hedgehog pathway inhibitor GDC-0449. *N Engl J Med, 361*(12), 1173-1178. doi:10.1056/NEJMoa0902903

Russell, D. S., Jaworski, L., & Kisseberth, W. C. (2018). Immunohistochemical detection of p53, PTEN, Rb, and p16 in canine osteosarcoma using tissue microarray. *J Vet Diagn Invest, 30*(4), 504-509. doi:10.1177/1040638718770239

Ryu, H. K., Baek, Y. H., Park, Y. C., & Seo, B. K. (2014). Current studies of acupuncture in cancer-induced bone pain animal models. *Evid Based Complement Alternat Med, 2014*, 191347. doi:10.1155/2014/191347

Sadikovic, B., Yoshimoto, M., Al-Romaih, K., Maire, G., Zielenska, M., & Squire, J. A. (2008). In vitro analysis of integrated global high-resolution DNA methylation profiling with genomic imbalance and gene expression in osteosarcoma. *PLoS One, 3*(7), e2834. doi:10.1371/journal.pone.0002834

Saraf, A. J., Fenger, J. M., & Roberts, R. D. (2018). Osteosarcoma: Accelerating Progress Makes for a Hopeful Future. *Frontiers in Oncology, 8*, 4.

Sayles, L. C., Breese, M. R., Koehne, A. L., Leung, S. G., Lee, A. G., Liu, H. Y., . . . Sweet-Cordero, E. A. (2019). Genome-Informed Targeted Therapy for

Osteosarcoma. *Cancer Discov, 9*(1), 46-63. doi:10.1158/2159-8290.Cd-17-1152

Schilcher, R. B., Haas, C. D., Samson, M. K., Young, J. D., & Baker, L. H. (1986). Phase I evaluation and clinical pharmacology of tricyclic nucleoside 5'-phosphate using a weekly intravenous regimen. *Cancer Res, 46*(6), 3147-3151.

Schmittgen, T. D., & Livak, K. J. (2008). Analyzing real-time PCR data by the comparative C(T) method. *Nat Protoc, 3*(6), 1101-1108.

Scott, M. C., Temiz, N. A., Sarver, A. E., LaRue, R. S., Rathe, S. K., Varshney, J., . . . Sarver, A. L. (2018). Comparative Transcriptome Analysis Quantifies Immune Cell Transcript Levels, Metastatic Progression, and Survival in Osteosarcoma. *Cancer Res, 78*(2), 326-337. doi:10.1158/0008-5472.Can-17-0576

Segaliny, A. I., Mohamadi, A., Dizier, B., Lokajczyk, A., Brion, R., Lanel, R., . . . Heymann, D. (2015). Interleukin-34 promotes tumor progression and metastatic process in osteosarcoma through induction of angiogenesis and macrophage recruitment. *Int J Cancer, 137*(1), 73-85. doi:10.1002/ijc.29376

Sehrawat, A., Gao, L., Wang, Y., Bankhead, A., 3rd, McWeeney, S. K., King, C. J., . . . Alumkal, J. J. (2018). LSD1 activates a lethal prostate cancer gene network independently of its demethylase function. *Proc Natl Acad Sci U S A, 115*(18), E4179-e4188. doi:10.1073/pnas.1719168115

Sharma, N., Wesolowski, R., Reebel, L., Rodal, M. B., Peck, A., West, B., . . . Rugo, H. S. (2014). A phase 1b study to assess the safety of PLX3397, a CSF-1 receptor inhibitor, and paclitaxel in patients with advanced solid tumors. *Journal of Clinical Oncology, 32*(15_suppl), TPS3127-TPS3127. doi:10.1200/jco.2014.32.15_suppl.tps3127

She, Q. B., Halilovic, E., Ye, Q., Zhen, W., Shirasawa, S., Sasazuki, T., . . . Rosen, N. (2010). 4E-BP1 is a key effector of the oncogenic activation of the AKT and ERK signaling pathways that integrates their function in tumors. *Cancer Cell, 18*(1), 39-51. doi:10.1016/j.ccr.2010.05.023

Shor, S., Fadl-Alla, B. A., Pondenis, H. C., Zhang, X., Wycislo, K. L., Lezmi, S., & Fan, T. M. (2015). Expression of nociceptive ligands in canine osteosarcoma. *J Vet Intern Med, 29*(1), 268-275. doi:10.1111/jvim.12511

Siddiqui, R., Onel, K., Facio, F., Nafa, K., Diaz, L. R., Kauff, N., . . . Offit, K. (2005). The TP53 mutational spectrum and frequency of CHEK2*1100delC in Li-Fraumeni-like kindreds. *Fam Cancer, 4*(2), 177-181. doi:10.1007/s10689-004-1946-5

Sims, N. A., & Martin, T. J. (2014). Coupling the activities of bone formation and resorption: a multitude of signals within the basic multicellular unit. *Bonekey Rep, 3*, 481. doi:10.1038/bonekey.2013.215

Smeester, B. A., Al-Gizawiy, M., & Beitz, A. J. (2012). Effects of different electroacupuncture scheduling regimens on murine bone tumor-induced hyperalgesia: sex differences and role of inflammation. *Evid Based Complement Alternat Med, 2012*, 671386. doi:10.1155/2012/671386

Smeester, B. A., Al-Gizawiy, M., O'Brien, E. E., Ericson, M. E., Triemstra, J. L., & Beitz, A. J. (2013). The effect of electroacupuncture on osteosarcoma tumor growth and metastasis: analysis of different treatment regimens. *Evid Based Complement Alternat Med, 2013*, 387169. doi:10.1155/2013/387169

Smeester, B. A., Lunzer, M. M., Akgun, E., Beitz, A. J., & Portoghese, P. S. (2014). Targeting putative mu opioid/metabotropic glutamate receptor-5 heteromers produces potent antinociception in a chronic murine bone cancer model. *Eur J Pharmacol, 743*, 48-52. doi:10.1016/j.ejphar.2014.09.008

Smeester, B. A., Slipek, N. J., Pomeroy, E. J., Bomberger, H. E., Shamsan, G. A., Peterson, J. J., . . . Moriarity, B. S. (2019). SEMA4C is a novel target to limit osteosarcoma growth, progression, and metastasis. *bioRxiv*, 520452. doi:10.1101/520452

Sottnik, J. L., Hall, C. L., Zhang, J., & Keller, E. T. (2012). Wnt and Wnt inhibitors in bone metastasis. *Bonekey Rep, 1*, 101. doi:10.1038/bonekey.2012.101

Stanley, E. R., & Chitu, V. (2014). CSF-1 receptor signaling in myeloid cells. *Cold Spring Harbor perspectives in biology, 6*(6), a021857. doi:10.1101/cshperspect.a021857

Stone, J. A., & Johnstone, P. A. (2010). Mechanisms of action for acupuncture in the oncology setting. *Curr Treat Options Oncol, 11*(3-4), 118-127. doi:10.1007/s11864-010-0128-y

Sueyoshi, T., Jono, H., Shinriki, S., Ota, K., Ota, T., Tasaki, M., . . . Ando, Y. (2012). Therapeutic approaches targeting midkine suppress tumor growth and lung metastasis in osteosarcoma. *Cancer Lett, 316*(1), 23-30. doi:10.1016/j.canlet.2011.10.013

Sulzbacher, I., Birner, P., Trieb, K., Pichlbauer, E., & Lang, S. (2002). The expression of bone morphogenetic proteins in osteosarcoma and its relevance as a prognostic parameter. *J Clin Pathol, 55*(5), 381-385.

Swiercz, J. M., Worzfeld, T., & Offermanns, S. (2008). ErbB-2 and met reciprocally regulate cellular signaling via plexin-B1. *J Biol Chem, 283*(4), 1893-1901. doi:10.1074/jbc.M706822200

Tamagnone, L. (2012). Emerging role of semaphorins as major regulatory signals and potential therapeutic targets in cancer. *Cancer Cell, 22*(2), 145-152. doi:10.1016/j.ccr.2012.06.031

Tarkkanen, M., Karhu, R., Kallioniemi, A., Elomaa, I., Kivioja, A. H., Nevalainen, J., . . . et al. (1995). Gains and losses of DNA sequences in osteosarcomas by comparative genomic hybridization. *Cancer Res, 55*(6), 1334-1338.

Temiz, N. A., Moriarity, B. S., Wolf, N. K., Riordan, J. D., Dupuy, A. J., Largaespada, D. A., & Sarver, A. L. (2016). RNA sequencing of Sleeping Beauty transposon-induced tumors detects transposon-RNA fusions in forward genetic cancer screens. *Genome Res, 26*(1), 119-129. doi:10.1101/gr.188649.114

Thollet, A., Vendrell, J. A., Payen, L., Ghayad, S. E., Ben Larbi, S., Grisard, E., . . . Cohen, P. A. (2010). ZNF217 confers resistance to the pro-apoptotic signals of paclitaxel and aberrant expression of Aurora-A in breast cancer cells. *Mol Cancer, 9*, 291. doi:10.1186/1476-4598-9-291

Tiet, T. D., Hopyan, S., Nadesan, P., Gokgoz, N., Poon, R., Lin, A. C., . . . Wunder, J. S. (2006). Constitutive hedgehog signaling in chondrosarcoma up-regulates tumor cell proliferation. *Am J Pathol, 168*(1), 321-330. doi:10.2353/ajpath.2006.050001

Tsubaki, M., Satou, T., Itoh, T., Imano, M., Ogaki, M., Yanae, M., & Nishida, S. (2012). Reduction of metastasis, cell invasion, and adhesion in mouse osteosarcoma by YM529/ONO-5920-induced blockade of the Ras/MEK/ERK and Ras/PI3K/Akt pathway. *Toxicol Appl Pharmacol, 259*(3), 402-410. doi:10.1016/j.taap.2012.01.024

Tsuchiya, T., Sekine, K., Hinohara, S., Namiki, T., Nobori, T., & Kaneko, Y. (2000). Analysis of the p16INK4, p14ARF, p15, TP53, and MDM2 genes and their prognostic implications in osteosarcoma and Ewing sarcoma. *Cancer Genet Cytogenet, 120*(2), 91-98.

Twine, N. A., Harkness, L., Kassem, M., & Wilkins, M. R. (2016). Transcription factor ZNF25 is associated with osteoblast differentiation of human skeletal stem cells. *BMC Genomics, 17*(1), 872. doi:10.1186/s12864-016-3214-0

Ueno, A., & Oh-ishi, S. (2002). Critical roles for bradykinin and prostanoids in acute inflammatory reactions: a search using experimental animal models. *Curr Drug Targets Inflamm Allergy, 1*(4), 363-376.

Varilla, V., Schneiderman, H., & Keefe, S. (2015). No Ceiling Dose: Effective Pain Control with Extraordinary Opiate Dosing in Cancer. *Conn Med, 79*(9), 521-524.

Vendrell, J. A., Thollet, A., Nguyen, N. T., Ghayad, S. E., Vinot, S., Bieche, I., . . . Cohen, P. A. (2012). ZNF217 is a marker of poor prognosis in breast cancer that drives epithelial-mesenchymal transition and invasion. *Cancer Res, 72*(14), 3593-3606. doi:10.1158/0008-5472.Can-11-3095

Von Hoff, D. D., LoRusso, P. M., Rudin, C. M., Reddy, J. C., Yauch, R. L., Tibes, R., . . . Low, J. A. (2009). Inhibition of the hedgehog pathway in advanced basal-cell carcinoma. *N Engl J Med, 361*(12), 1164-1172. doi:10.1056/NEJMoa0905360

von Tresckow, B., Morschhauser, F., Ribrag, V., Topp, M. S., Chien, C., Seetharam, S., . . . Engert, A. (2015). An Open-Label, Multicenter, Phase I/II Study of JNJ-40346527, a CSF-1R Inhibitor, in Patients with Relapsed or Refractory Hodgkin Lymphoma. *Clin Cancer Res, 21*(8), 1843-1850. doi:10.1158/1078-0432.Ccr-14-1845

Walkley, C. R., Qudsi, R., Sankaran, V. G., Perry, J. A., Gostissa, M., Roth, S. I., . . . Orkin, S. H. (2008). Conditional mouse osteosarcoma, dependent on p53 loss and potentiated by loss of Rb, mimics the human disease. *Genes Dev, 22*(12), 1662-1676. doi:10.1101/gad.1656808

Wan, X., Mendoza, A., Khanna, C., & Helman, L. J. (2005). Rapamycin inhibits ezrin-mediated metastatic behavior in a murine model of osteosarcoma. *Cancer Res, 65*(6), 2406-2411. doi:10.1158/0008-5472.can-04-3135

Wang, D., Niu, X., Wang, Z., Song, C. L., Huang, Z., Chen, K. N., . . . Wang, J. (2019). Multiregion Sequencing Reveals the Genetic Heterogeneity and Evolutionary History of Osteosarcoma and Matched Pulmonary Metastases. *Cancer Res, 79*(1), 7-20. doi:10.1158/0008-5472.Can-18-1086

Wang, L., Park, P., La Marca, F., Than, K., Rahman, S., & Lin, C. Y. (2013). Bone formation induced by BMP-2 in human osteosarcoma cells. *Int J Oncol, 43*(4), 1095-1102. doi:10.3892/ijo.2013.2030

Wang, Z., Jensen, M. A., & Zenklusen, J. C. (2016). A Practical Guide to The Cancer Genome Atlas (TCGA). *Methods Mol Biol, 1418*, 111-141. doi:10.1007/978-1-4939-3578-9_6

Wei, J. C., Yang, J., Liu, D., Wu, M. F., Qiao, L., Wang, J. N., . . . Gao, Q. L. (2017). Tumor-associated Lymphatic Endothelial Cells Promote Lymphatic Metastasis By Highly Expressing and Secreting SEMA4C. *Clin Cancer Res, 23*(1), 214-224. doi:10.1158/1078-0432.Ccr-16-0741

Wen, Z.-Q., Li, X.-G., Zhang, Y.-J., Ling, Z.-H., & Lin, X.-J. (2017). Osteosarcoma cell-intrinsic colony stimulating factor-1 receptor functions to promote tumor cell metastasis through JAG1 signaling. *American journal of cancer research, 7*(4), 801-815.

Wesolowski, R., Sharma, N., Reebel, L., Rodal, M. B., Peck, A., West, B. L., . . . Rugo, H. S. (2019). Phase Ib study of the combination of pexidartinib (PLX3397), a CSF-1R inhibitor, and paclitaxel in patients with advanced solid tumors. *Ther Adv Med Oncol, 11*, 1758835919854238. doi:10.1177/1758835919854238

Wesolowski, R., Sharma, N., West, B., Coussens, L., Marimuthu, A., Pelayo, M., . . . Rugo, H. S. (2016). A phase Ib study of pexidartinib (PLX3397) and weekly paclitaxel in patients with advanced solid tumors including an ovarian cancer subset. *Gynecologic Oncology, 141*, 121. doi:10.1016/j.ygyno.2016.04.325

Wittrant, Y., Gorin, Y., Mohan, S., Wagner, B., & Abboud-Werner, S. L. (2009). Colony-stimulating factor-1 (CSF-1) directly inhibits receptor activator of nuclear factor-{kappa}B ligand (RANKL) expression by osteoblasts. *Endocrinology, 150*(11), 4977-4988. doi:10.1210/en.2009-0248

Worzfeld, T., & Offermanns, S. (2014). Semaphorins and plexins as therapeutic targets. *Nat Rev Drug Discov, 13*(8), 603-621. doi:10.1038/nrd4337

Wrobel, C. N., Debnath, J., Lin, E., Beausoleil, S., Roussel, M. F., & Brugge, J. S. (2004). Autocrine CSF-1R activation promotes Src-dependent disruption of mammary epithelial architecture. *The Journal of cell biology, 165*(2), 263-273. doi:10.1083/jcb.200309102

Xi, Y., & Chen, Y. (2017). PTEN Plays Dual Roles As a Tumor Suppressor in Osteosarcoma Cells. *J Cell Biochem, 118*(9), 2684-2692. doi:10.1002/jcb.25888

Xi, Y., Qi, Z., Ma, J., & Chen, Y. (2020). PTEN loss activates a functional AKT/CXCR4 signaling axis to potentiate tumor growth and lung metastasis in human osteosarcoma cells. *Clin Exp Metastasis, 37*(1), 173-185. doi:10.1007/s10585-019-09998-7

Xue, D., Desjardins, M., Kaufman, G. N., Béland, M., Al-Tamemi, S., Ahmed, E., . . . Mazer, B. D. (2016). Semaphorin 4C: A Novel Component of B-Cell Polarization in Th2-Driven Immune Responses. *Front Immunol, 7*, 558. doi:10.3389/fimmu.2016.00558

Yan, G. N., Lv, Y. F., & Guo, Q. N. (2016). Advances in osteosarcoma stem cell research and opportunities for novel therapeutic targets. *Cancer Lett, 370*(2), 268-274. doi:10.1016/j.canlet.2015.11.003

Yang, C., Huang, D., Ma, C., Ren, J., Fu, L., Cheng, C., . . . Shi, X. (2019). Identification of Pathogenic Genes and Transcription Factors in Osteosarcoma. *Pathol Oncol Res*. doi:10.1007/s12253-019-00645-w

Yang, L., Dan, H. C., Sun, M., Liu, Q., Sun, X. M., Feldman, R. I., . . . Cheng, J. Q. (2004). Akt/protein kinase B signaling inhibitor-2, a selective small molecule inhibitor of Akt signaling with antitumor activity in cancer cells overexpressing Akt. *Cancer Res, 64*(13), 4394-4399. doi:10.1158/0008-5472.Can-04-0343

Yang, Q., Wang, Y., Lu, X., Zhao, Z., Zhu, L., Chen, S., . . . Wang, Z. (2015). MiR-125b regulates epithelial-mesenchymal transition via targeting Sema4C in paclitaxel-resistant breast cancer cells. *Oncotarget, 6*(5), 3268-3279. doi:10.18632/oncotarget.3065

Yao, G. Q., Sun, B. H., Weir, E. C., & Insogna, K. L. (2002). A role for cell-surface CSF-1 in osteoblast-mediated osteoclastogenesis. *Calcif Tissue Int, 70*(4), 339-346. doi:10.1007/s00223-001-1079-x

Yavropoulou, M. P., & Yovos, J. G. (2008). Osteoclastogenesis--current knowledge and future perspectives. *J Musculoskelet Neuronal Interact, 8*(3), 204-216.

Ye, X., & Weinberg, R. A. (2015). Epithelial-Mesenchymal Plasticity: A Central Regulator of Cancer Progression. *Trends Cell Biol, 25*(11), 675-686. doi:10.1016/j.tcb.2015.07.012

Yin, K., Liao, Q., He, H., & Zhong, D. (2012). Prognostic value of Twist and E-cadherin in patients with osteosarcoma. *Med Oncol, 29*(5), 3449-3455. doi:10.1007/s12032-012-0317-6

Zarogoulidis, P., Lampaki, S., Turner, J. F., Huang, H., Kakolyris, S., Syrigos, K., & Zarogoulidis, K. (2014). mTOR pathway: A current, up-to-date mini-review (Review). *Oncol Lett, 8*(6), 2367-2370. doi:10.3892/ol.2014.2608

Zhang, J., Yu, X. H., Yan, Y. G., Wang, C., & Wang, W. J. (2015). PI3K/Akt signaling in osteosarcoma. *Clin Chim Acta, 444*, 182-192. doi:10.1016/j.cca.2014.12.041

Zhang, R. X., Li, A., Liu, B., Wang, L., Ren, K., Qiao, J. T., . . . Lao, L. (2007). Electroacupuncture attenuates bone cancer pain and inhibits spinal interleukin-1 beta expression in a rat model. *Anesth Analg, 105*(5), 1482-1488, table of contents. doi:10.1213/01.ane.0000284705.34629.c5

Zhang, Y. K., Huang, Z. J., Liu, S., Liu, Y. P., Song, A. A., & Song, X. J. (2013). WNT signaling underlies the pathogenesis of neuropathic pain in rodents. *J Clin Invest, 123*(5), 2268-2286. doi:10.1172/jci65364

Zhang, Y., Yang, J., Zhao, N., Wang, C., Kamar, S., Zhou, Y., . . . Yang, Z. (2018). Progress in the chemotherapeutic treatment of osteosarcoma. *Oncology letters, 16*(5), 6228-6237. doi:10.3892/ol.2018.9434

Zhou, H., Binmadi, N. O., Yang, Y. H., Proia, P., & Basile, J. R. (2012). Semaphorin 4D cooperates with VEGF to promote angiogenesis and tumor progression. *Angiogenesis, 15*(3), 391-407. doi:10.1007/s10456-012-9268-y

Zhou, J., Xiao, X., Wang, W., & Luo, Y. (2019). Association between PTEN and clinical-pathological features of osteosarcoma. *Biosci Rep, 39*(7). doi:10.1042/bsr20190954

Zhou, Q. D., Ning, Y., Zeng, R., Chen, L., Kou, P., Xu, C. O., . . . Xu, G. (2013). Erbin interacts with Sema4C and inhibits Sema4C-induced epithelial-mesenchymal transition in HK2 cells. *J Huazhong Univ Sci Technolog Med Sci, 33*(5), 672-679. doi:10.1007/s11596-013-1179-7

Zhou, Q., Deng, Z., Zhu, Y., Long, H., Zhang, S., & Zhao, J. (2010). mTOR/p70S6K signal transduction pathway contributes to osteosarcoma progression and patients' prognosis. *Med Oncol, 27*(4), 1239-1245. doi:10.1007/s12032-009-9365-y

Zhou, W., Hao, M., Du, X., Chen, K., Wang, G., & Yang, J. (2014). Advances in targeted therapy for osteosarcoma. *Discov Med, 17*(96), 301-307.

Zhu, J., Liu, Y., Zhu, Y., Zeng, M., Xie, J., Lei, P., . . . Hu, Y. (2017). Role of RANK and Akt1 activation in human osteosarcoma progression: A clinicopathological study. *Exp Ther Med, 13*(6), 2862-2866. doi:10.3892/etm.2017.4360

Zhu, X. C., Zhang, J. L., Ge, C. T., Yu, Y. Y., Wang, P., Yuan, T. F., & Fu, C. Y. (2015). Advances in cancer pain from bone metastasis. *Drug Des Devel Ther, 9*, 4239-4245. doi:10.2147/dddt.s87568

Zhu, Y., Zhou, J., Ji, Y., & Yu, B. (2014). Elevated expression of AKT2 correlates with disease severity and poor prognosis in human osteosarcoma. *Mol Med Rep, 10*(2), 737-742. doi:10.3892/mmr.2014.2314